1-1-2016

Anatomy, Implant Selection and Placement Influence Spine Mechanics Associated with Total Disc Replacement

Justin F.M. Hollenbeck
University of Denver

Recommended Citation

ANATOMY, IMPLANT SELECTION AND PLACEMENT

INFLUENCE SPINE MECHANICS ASSOCIATED WITH

TOTAL DISC REPLACEMENT

_____

A Thesis

Presented to

the Faculty of the Daniel Felix Ritchie School of Engineering and Computer Science

University of Denver

_____

In Partial Fulfillment

of the Requirements for the Degree

Master of Science

_____

by

Justin F.M. Hollenbeck

June 2016

Advisor: Peter J. Laz

Author: Justin F.M. Hollenbeck
Title: Anatomy, Implant Selection and Placement Influence Spine Mechanics Associated
with Total Disc Replacement
Advisor: Peter J. Laz
Degree date: June 2016

ABSTRACT

Through aging and injury, the intervertebral disc of the lumbar spine can undergo

degeneration, leading to collapse of the vertebrae and low back pain, a symptom that

affects half the adult population in any given year. In an effort to reduce low back pain,

total disc replacement treatment removes the degenerated disc, restores natural height and

lordosis of the segment, and preserves motion at the joint. Patient anatomy, implant

selection, and implant placement play significant roles in a patient's outcomes after total

disc replacement surgery. Thus, the objective of the work presented in this thesis was to

develop a suite of statistical and computational tools describe population-based anatomy

and to support component selection and placement in TDR surgical procedures with the

goal of improving implant design and patient outcomes.

The statistical modeling approach quantified shape and alignment variation of the

lumbar spine by characterizing variability of shape and size of individual vertebra,

relative alignment of relevant segments, and overall anatomy of the lumbar spine.

Statistical shape models of single vertebrae revealed that the primary mode of variation

correlated to vertebral body size variation (average $R^2 = 0.82$ across vertebrae), which can

inform sizing lines for total disc replacements. Strong correlations of disc height to the

second ($R^2 = 0.82$) and third ($R^2 = 0.88$) principal components of the shape-alignment

models of the L4-L5 and L5-S1 segments are useful in assisting clinicians diagnose

pathologies, screening patients for treatment options, and pre-operatively planning for surgical treatment. Statistical models of the entire spine reveal how vertebral shape changes influence the spine as a whole.

The subject-specific templating approach of total disc replacement surgeries accurately predicted ROM in a cohort of twenty two patients implanted with the ProDisc-L device and suggested changes to total disc replacement size selection and alignment to improve ROM. Predicted ROM was 11.8% different to actual ROM. Improvements in ROM could have been achieved in over 85% of the cases had the proposed templating process been employed, which showed that pre-operative templating can be an important tool to achieve maximum ROM and optimal clinical outcomes.

Computational pilot evaluations of subjects implanted with the Activ-L device provided insight into the mechanical behavior of a total disc replacement featuring a center inlay that can translate within the inferior end plate. Results indicated that greater translation of the inlay related to greater overall ROM. Subjects implanted with the Activ-L achieved greater ideal range of motion than subjects with a ProDisc-L, a device featuring an inlay that is fixed within the inferior end plate. Further investigations into this work can reveal design considerations that significantly influence ROM and patient outcomes.

ACKNOWLEDGEMENTS

This document represents a milestone in almost five years of work at the Computational Biomechanics Laboratory at the University of Denver. I have felt home in this laboratory and with the people who work here.

First and foremost I wish to thank my advisors, Dr. Peter Laz and Dr. Paul Rullkoetter. They have given me freedom to explore on my own, yet provided guidance and instruction when my steps faltered. I have learned much from Dr. Laz's unique research perspectives, his exceptional teaching ability, his personal integrity, and his expectations of excellence. Dr. Rullkoetter introduced me to the wonders and frustrations of scientific research.

I owe deep appreciation to our clinical partners, Dr. Christopher Cain, Jill Fattor, and the Anschutz Foundation who have been exceptionally supportive in driving these projects forward. Thank you to DePuy Synthes for providing geometry for the ProDisc-L.

I am indebted to the other members of my thesis committee, Dr. Yun-Bo Yi and Dr. Dinah Loerke for their constant support, advice, and guidance. I am grateful Dr. Matt Gordon, Yvonne Petit, Renee Carvalho, Tim Sheu, and John Buckley for their assistance and advice, and I thank my coworkers who have been unwavering in their support, valuable advice, and eagerness to share a laugh.

Life would not be so colorful without my family and my friends. I am thankful for their big hearts, deep souls, and wild minds.

TABLE OF CONTENTS

LIST OF FIGURES

LIST OF TABLES

CHAPTER 1. INTRODUCTION

1.1 Motivation

Low back pain is experienced by half the adult population in any given year and by two thirds of the population at least once over his or her lifetime (Andersson 1999, Deyo et al. 2002, Bressler et al. 1999). Health care expenditures associated with LBP remain significantly high (Martin et al. 2009, Dagenais et al. 2008) with the total estimated cost of spinal medical treatment eclipsing 100 billion dollars per year (Martin et al. 2008). Under existing treatment patterns, trends indicate that the frequency of adult LBP and the associated costs will likely accelerate in the coming decades (Smith et al. 2013). Multiple clinical studies have identified discogenic LBP, or pain without disc herniation or facet joint pain, as the primary source of pain in the lumbar region. Discogenic LBP originates in the intervertebral disc as pathologies, such as degenerative disc disease, scoliosis, and spondylolisthesis, mechanically and chemically break down the structure of the disc and compress the surrounding neural structures.

To mitigate LBP symptoms, patients typically undergo a series of passive treatment options beginning with conservative treatments, like segmental realignment and physical therapy, and progressing to more non-operative pain management methods, such as electrotherapy and corticosteroid epidural injections, that offer non-invasive, short-term pain relief. If unresponsive to passive treatment, treatment progresses to operative

methods, like lumbar arthrodesis and arthroplasty, which look to eliminate discogenic LBP by removing the diseased disc and stabilizing the segment.

With over 122,000 surgeries performed in 2001 (Deyo et al. 2005), lumbar arthrodesis or fusion is the gold standard of surgical treatment that eliminates motion and instability at the symptomatic degenerated segments, thereby reducing LBP at that level. Lumbar interbody fusion methods utilize different combinations of rods, interbody spacers, and pedicle screw systems to maintain segmental disc height and natural lordosis. Instrumentation is typically coupled with a discectomy or laminectomy to remove diseased elements in the intervertebral disc space and facet joint. Despite clinical success rates exceeding 80% (Zeilstra et al. 2013), continuing evaluations of lumbar fusion procedures report development of adjacent segment disease (ASD) over the long term.

Development of the total disc replacement (TDR) has aimed to avert the negative effects of fusion by eliminating pain at the offending joint, restoring natural spinal lordosis, and preserving ROM. Most TDR procedures include partial removal of the degenerated disc, vertebral distraction, and insertion of the TDR device, which is typically a modular ball-and-socket-based design. Though post-operative Oswestry Disability Index (ODI) scores, Visual Analog Scale (VAS) scores, and complication rates are reported to be similar for patients with both fusion and TDR devices, long-term follow-ups indicate reoperation rates attributed to ASD is significantly lower in the TDR group than the fusion group (Zigler et al. 2012). Additionally, clinical studies report TDR cohorts as having higher patient satisfaction scores, higher employment status, and lower

re-operation rates than the fusion cohorts (Lemaire et al. 2005, David et al. 2007). In spite of these findings, most U.S. health insurance companies refuse coverage for TDR surgery and argue that many studies lack sufficient sample sizes, long-term follow-ups, randomization, or a control group, and that continuing evaluations report similar long-term complications to fusion procedures. Many groups including the International Society of the Advancement of Spinal Surgery (ISASS) assert that reasons against TDR coverage are debatable, that long-term efficacy of TDRs has already been established, and that continuing advancements in design and surgical protocol can lead to more-consistent improvements in clinical outcomes (Zigler et al.).

Prior clinical studies reveal that after TDR surgery, higher segmental ROM at the operative level is statistically correlated to factors related to better clinical outcomes (Siepe et al. 2009) and lower prevalence of degeneration at the adjacent levels (Siepe et al. 2014). Prior investigations report that variable features of patient vertebral anatomy, such as the transverse orientation of the facet structures, can significantly influence segmental motion. Additionally, the spherical articular surfaces of the Activ-L and ProDisc-L more accurately reproduce natural segmental motion compared to fusion, and placement of the spherical center of the implant as close as possible to the anatomical center of rotation (COR) of the segment is essential in distributing forces across the vertebra and maximizing ROM. Therefore, an understanding of patient anatomical variability coupled with patient-specific optimization of implant position has the potential to maximize ROM and improve patient outcomes.

1.2 Objectives

The objectives of this thesis were to 1) characterize variation of lumbar spine anatomy across a variable population and to 2) develop computational templating tools used to identify optimal device selection and placement in contemporary implants to maximize ROM and optimize patient outcome. A comprehensive set of statistical shape-alignment models were developed for the vertebrae of the entire lumbar spine, the bones of relevant functional spinal units (FSUs), and each individual vertebra to quantify anatomical variation of the vertebrae of the lumbar spine. Explicit finite element methods were employed to predict flexion and extensions motions at the operative levels of patients implanted with the ProDisc-L and Activ-L devices, and computational templating procedures identified optimal device placement to maximize patient ROM. Overall, the goal of this work was to develop a suite of statistical and computational tools that provide an understanding of population-based anatomy and that may assist TDR surgical procedures to improve implant performance and patient outcomes.

1.3 Organization

Chapter 2 provides an overview of the relevant clinical terminology and lumbar spine anatomy that is used in the subsequent chapters. Contributing factors to discogenic LBP are considered. Details of the relevant TDR implants are examined, and there is a discussion on the key methods utilized in this study, particularly statistical shape and alignment modeling and explicit finite element analysis.

Chapter 3 discusses the statistical shape modeling approach to characterize anatomic variability and evaluates findings of the set of statistical shape and alignment

models developed in this study to evaluate variation in shape and alignment variability between bones of the lumbar spine.

Chapter 4 and 5 discuss the predictive capabilities of templating for TDR surgery as well as suggest optimal TDR placement to optimize patient outcome for two contemporary TDR implants, the DePuy Synthes ProDisc-L (Chapter 4) and the Aesculap Activ-L (Chapter 5). Chapters 4 and 5 present studies verifying model ROM predictions to post-operative lateral flexion-extension radiographs. The study employed explicit finite element analysis to optimize intervertebral implant placement and to provide insight into implant mechanical behavior during flexion and extension exercises. Chapter 4 presents the capabilities of a proposed templating process to predict post-operative ROM from ProDisc-L implant placement and suggests how modifications to implant placement can influence post-operative ROM. Chapter 5 presents methods to understand implant behavior and post-operative ROM in patients implanted with the Activ-L device. The study provides insight into the mechanical behavior of the partially-constrained center polyethylene inlay during flexion and extension motions. Post-operative ROM of patients implanted with the Activ-L is compared to ROM of patients implanted with the ProDisc-L.

Chapter 6 presents a summary of the work, discusses limitations, and makes recommendations for future research.

CHAPTER 2: LITERATURE REVIEW

This chapter presents an overview of the background information and literature that are pertinent to quantifying variation of anatomy and computational evaluation of spine mechanics. The first section describes relevant clinical terminology, the second describes relevant natural anatomy of the lumbar spine, the third provides an overview of lumbar pathology and treatment, the fourth outlines the statistical shape and alignment method employed in Chapter 3, and the fifth presents the technical aspects of the explicit finite element method used in Chapters 4 and 5. Clinical terminology and anatomy provided by Dr. Robert McClintic's "Basic Anatomy and Physiology of the Human Body" (McClintic 1978) and Henry Gray's "Anatomy of the Human Body." (Gray 1918).

2.1 Clinical Terminology

The biomechanics of the joints of the body are complex and variable. Universal clinical terminology apply to a standard orientation of the human body and are useful in describing basic positions, directions, and movements of structures within the human body. When the body is oriented in its anatomical position, with the body in an upright posture, the head level, the arms straight and to the sides, and the feet directed forward, it can be divided by imaginary planes coined cardinal orientation planes. The three cardinal planes relate to the three dimensions of space, each plane being orthogonal to the other

6

two. The sagittal plane is the vertical plane that divides the body into left and right regions; the coronal plane is the vertical plane that divides the body into front and back regions; and the transverse plane is the horizontal plane that divides the body into upper and lower regions. Other anatomical terms denote general position of a structure relative to other structures. Anterior refers to the front of the body; posterior to the back; superior to the head; inferior to the tail or lower end of the body; lateral to the sides; and medial to the middle (Figure 2.1).

While the movement capabilities of the joints of the body are numerous and complex, the movements associated to the spinal column are described here. Flexion and extension are movements in the sagittal plane, or about the transverse axis. Flexion is rotation towards the anterior side of the body (touching toes), and extension is rotation towards the posterior side (leaning back). Lateral bending refers to rotation in the coronal plane, or about the anteroposterior axis (leaning left or right), and axial rotation refers to rotation in the transverse plane, or about the longitudinal axis. Flexion, extension, and lateral bending are not pure rotations but a complex combination of translations and rotations. The location of the instantaneous center of rotation varies (Liu et al. 2016), and vertebral translations occur as compressive and shear loads are applied to the segment (Schultz et al. 1982, Anderson et al. 1980). To describe complex spinal motion pathways, an instantaneous helical axis can be computed at each segment. Motion of a joint can be characterized by the position and direction of an axis of motion, the helical axis, with a scalar translation along this axis and a scalar rotation about it (Wu et al. 2002). The helical axis has been employed to qualitatively describe normal motions in the knee (van

den Bogert et al. 2008, Grip and Hager 2013) and the spine (Kettler et al. 2004, Schmidt et al. 2008). For purposes of this study, only range of motion values, not motion pathways, are reported.

2.2 Natural Anatomy of the Lumbar Spine

The skeletal and muscular elements of the spine transmit body forces through the pelvis to the lower limbs, encase and protect the spinal cord, and facilitate motion of the trunk. The spine is divided into the cervical, thoracic, and lumbar regions, which each play a role in maintaining posture and bipedal locomotion. The column is loaded cumulatively from the superior to the inferior end with the lumbar region bearing the majority of the weight of trunk. An array of muscles including the erector spinae, internal abdominal obliques, and external abdominal obliques, act to stabilize the trunk and actuate movements. The average compressive, or axial, loads experienced by the motion segments of the lumbar spine during a relaxed, standing posture is 470 N. Compressive loads of 1390 N, 690 N, 880 N, 970 N are exerted when performing flexion, extension, lateral bend, and axial rotation movements, respectively. Lateral and anterior-posterior shear loads do not exceed 160 N for all movements (Schultz et al. 1982, Anderson et al. 1980). The lumbar region consists of five lumbar bones, or vertebrae, and a sacral bone. Two vertebrae make up a spinal joint, which articulates through an intervertebral fibrous disc and is passively supported by ligamentous structures. Other names for the lumbar joint include the functional spinal unit (FSU), segment, or level. Lordotic curvature is the posteriorly concave curvature of the lumbar that allows the body's weight to be balanced on the vertebral column in a way that expends the least amount of muscular energy to

maintain an upright, bipedal stance. Lordosis occurs when the lordotic curvature of the lumbar is exaggerated.

2.2.1 Bony structures

There are six major bones, or vertebrae, in the lumbar spine numbered L1 through L5 from the superior to inferior end. The lumbosacral joint is the segment that incorporates both the sacrum, which will be included as part of the lumbar spine when referenced in this paper, and the L5 vertebrae. A typical vertebrae consists of a vertebral body and a posterior neural arch. Though the articular processes are partially weight-bearing, the vertebral body bears most of the load and is linked to the adjacent vertebral bodies by an intervertebral disc and ligaments. End plates on the superior and inferior sides of the vertebral body provide a bone-to-soft-tissue interface which helps facilitate nutrient transport to the disc. The vertebral body forms the anterior side and the neural arch, consisting of two pedicles and two laminae, forms the lateral and posterior sides of the foramina. Collectively, the foramen of all vertebrae in the column form the spinal canal, which protects the spinal cord. Bony pedicles attach the neural arch to the vertebral body, continue as laminae on either side, and meet in the midline of the posterior side of the vertebral foramina. A number of processes, including the left and right transverse processes, superior and inferior articular processes, and the spinous process, extend from the neural arch and provide sites for muscle attachment and articulation surfaces for adjacent bones. A transverse process projects posterolaterally from each pedicle, and provides an attachment site for muscles and ligaments. The spinous process extends posteriorially from the junction of the two sides of the laminae and also provides

ligament and muscle attachment sites. The inferior and superior articular processes project in the superior and inferior directions, respectively, from the pedicle and provide a surface on which the vertebra can articulate with adjacent vertebrae (Figure 2.2).

2.2.2 Intervertebral Disc

Between each vertebral body exists a cartilaginous intervertebral disc that mediates the pressures within the load-bearing segment and allows relative movement to occur. The intervertebral disc is composed of an annulus fibrosus, an outer fibrous structure, and a nucleus pulposus, a fluid-like core. Due to the high water content within the nucleus pulposus, large loads transmitted from the superior vertebra can be sustained, distributed to the annulus fibrosus through hydrostatic pressure, and evenly transmitted to the inferior vertebra. The approximate 30° fiber orientation of the annulus fibrosus is suitable to resist hoop stresses generated by the hydrostatic pressure. The anterior and posterior longitudinal ligaments ensure that any loads within the intervertebral space other than compression and decompression are resisted. Loss of height due to disc degeneration is a primary indicator of lumbar pathologies, and can lead to disc herniation and chronic LBP. Surgical treatment options attempt to alleviate LBP by distracting the intervertebral space to the original disc height. Healthy anterior disc heights averaged 11 ± 2.2 millimeters for the L4-L5 and L5-S1 FSUs, and healthy posterior disc heights averaged 6 ± 1.8 millimeters and 5 ± 1.6 for the L4-L5 and L5-S1 FSUs, respectively (Albietz et al. 2012).

2.2.3 Zygapophysial Joints

The synovial joints between the superior and inferior articular processes on adjacent vertebrae are called the zygapophysial joints, or facet joints, and are enclosed by a thin articular capsule. A series of ligaments that pass between vertebral bodies and interconnect components of the neural arches discourage joint over-articulation and support the facets. The facet joint is stabilized during flexion-extension movements by the ligamentum flavum, which connects the laminae of adjacent neural arches, and the interspinous and supraspinous ligaments, which bind adjacent spinous processes together. During lateral bending or axial rotation, the facet joint is supported by intertransverse ligaments, which connect the adjacent transverse processes. As segmental motion can be limited by bony impingement, orientation of the facets play an important role in defining flexion-extension ROM within a segment. In flexion, smaller facet angles in the transverse plane yield earlier impingement and a lesser range of motion, whereas larger facet angles in the transverse plane yield later impingement and a greater range of motion. In a similar fashion, smaller angles of the articular process in the sagittal plane yield earlier impingement and a lesser range of motion, whereas larger angles of the articular process in the sagittal plane yield later impingement and a greater range of motion (Masharawi et al. 2004).

2.3 Lumbar Pathology and Treatment

Onset of pathologies of the intervertebral disc, including degenerative disc disease (DDD), are typically age-related, and associated to LBP (Bendix et al. 2008, Cheung et al. 2009, de Schepper et al. 2010). Etiology associated with DDD include heredity (Battie

et al. 2008), age (Miller et al. 1988), frequency of smoking (Battie et al. 1991), and heavy

lifting (Videman et al. 1995). Features of pain-related disc degeneration include changes

to the structure of the vertebral body, the existence of fissures in the annulus fibrosus, and

nerve sensitisation. Though there is little association that biochemical changes influence

LBP (Boos et al. 1995, Jensen et al. 1994), there still exists a positive correlation of DDD

to disc dehydration and proteoglycan loss, which can lead to disc collapse or disc

herniation. Collapse of a degenerated disc, identified by a reduction in disc height,

narrows neural passageways and compresses nerves, inducing pain in the back and legs

(Videman et al. 2003, Cheung et al. 2009, de Schepper et al. 2010).

Acceleration of disc degeneration can occur as a result of anatomical

abnormalities of the spine, including scoliosis and spondylolisthesis. Scoliosis, a three-

dimensional deviation of the spinal axis, is primarily diagnosed by identifying if spinal

curvature in the coronal plane exceeds 10 degrees (Kyu-Jung et al. 2014). Incidence rates

of scoliosis in exceeds 8% in adults aged 25 and older and 68% in persons 60 and older.

Severity of cases typically progress until long term, complex treatment is required (Carter

et al. 1987). LBP is prevalent in 60% to 80% of scoliosis instances and is associated to

degenerative changes in the disc and facet joint on the convex side of the curvature

(Daffner et al. 2003). Primary indicators for surgical intervention include foraminal

stenosis, or narrowing of the disc space on the concave side, reduced disc height on the

concave side, and muscle fatigue (Kyu-Jung et al. 2014). Degenerative lumbar

spondylolisthesis, or anterior migration of a vertebra relative to its inferior vertebra, is

often correlated to scoliosis (Crostelli et al. 2013). With incidence among middle-aged

12

and elderly adults ranging from 14% to 30%, spondylolisthesis presumably results from age-related degeneration of the facet joints and intervertebral discs and anatomical abnormalities of the laminae (Kalichman et al. 2009, Kauppila et al. 1998). LBP is a common symptom in patients suffering from spondylolisthesis, as segmental instability often leads to the narrowing of neural passageways and compression of nerve roots, and it typically leads to surgical intervention. In the United States, over 300,000 lumbar fusion surgeries are performed every year to treat degenerative spondylolisthesis, spinal stenosis, and scoliosis (Denard et al. 2010).

2.3.1 Lumbar Arthrodesis

In an effort to relieve discogenic LBP from disorders such as DDD, scoliosis, or spondylolisthesis, arthrodesis or fusion stabilizes the offending segment and reduces painful motions at that level. An anterior lumbar interbody fusion (ALIF) or posterior lumbar interbody fusion (PLIF) surgery typically involves a discectomy, where diseased soft tissue including sensitized neural structures are removed, segment distraction to open neural passageways and decompress nerves, and fixation of the vertebral bodies to reduce painful motions at the joint. Spinal fusion has established itself as the current standard of care to treat discogenic back pain. National survey data reports that over 122,000 lumbar fusion surgeries were performed in the United States in 2001, a 113% increase from 1996 (Deyo et al. 2005). Long-term follow-up studies report success rates of over 50% (Guyer et al. 2009). Excluding hospital fees, fusion surgeries cost over $34,000, making them one of the most cost-effective surgical treatment options for discogenic back pain currently on the market (Deyo et al. 2004).

13

Insurance companies have tightened coverage for fusion procedures (Martin et al. 2013), however, amidst suggestions from third-party investigators that surgical innovation has outpaced supporting research on the topic (Deyo et al. 2009). Intensive non-operative treatment options are significantly cheaper and result in similar patient outcomes to fusion (Mirza et al. 2007). Follow-up studies report that post-operative complication rates exceeded 10% (Martin et al. 2008, Zigler et al. 2012) and only 15% of patients were pain-free at 5-year follow-up (Skold et al. 2013). Additionally, lumbar fusion has been associated with an increased incidence of degeneration of neighboring discs (Hoogendoorn et al. 2008), termed adjacent segment degeneration (ASD). Distinctions have been made between radiographic ASD and symptomatic ASD (Lee et al. 2009, Harrop et al. 2008). Diagnosed from radiographs, magnetic resonance images, and computed tomography scans, radiographic ASD is identified by varying parameters including reduction in disc height of more than 3 millimeters, change in angle between adjacent vertebrae of at least 10 degrees, hypertrophic facet joint arthropathy, and osteophyte formation of greater than 3 millimeters of the adjacent segment. Parameters to diagnose symptomatic ASD include symptomatic spinal stenosis, intractable back pain, segmental instability, and parameters from accompanying radiographs (Kaito et al. 2010, Cheh et al. 2007, Park et al. 2004). Prior studies have documented the epidemiology of radiographic and symptomatic ASD over the long-term. Park et al. (2004) report incidence rates of radiographic ASD at 8% to 100% and symptomatic ASD at 5.2% to 18.5%. The United Kingdom's National Institute for Health and Clinical Excellence reviewed almost 2500 lumbar fusion patients and reported that 14% suffered from

symptomatic ASD. Ishihara et al. (2001) examined fusion patients after a minimum of ten years and found prevalence of radiographic ASD in 52% at the superior adjacent segment and 70% at the inferior adjacent segment. Though there is general consensus that ASD emerges at the onset of DDD, the exact pathophysiology of ASD is disputed. Some groups argue that ASD is caused by instability in the initial degenerated disc, not necessarily the fusion performed to correct it. Ruberte et al. (2008) found that mild to moderate degeneration at a single level alters mechanical patterns in neighboring discs including increased annular shear and von Mises stresses, decreased segmental stiffness in flexion/extension, and increased facet contact force. Some investigators find evidence of hypermobility and increased intradiscal pressures at levels adjacent to a fused segment, which supports the theory that fusion of the offending segment is responsible for adjacent degeneration (Weinhoffer et al. 1995). However, several in vivo studies challenge this theory, reporting instead that actual changes in segmental biomechanics adjacent to the fused level do not occur consistently (Frymoyer et al. 1997).

2.3.2 Lumbar Arthroplasty

Lumbar arthroplasty, or total disc replacement (TDR) technology, has been introduced to preserve motion and reduce LBP at the segment. Prior clinical studies have demonstrated the efficacy of TDR procedures and that outcomes after TDR surgery are equivalent and, in some cases, superior to fusion outcomes. In 2005, Blumenthal et al. (2005) was the first group to compare long-term patient outcomes of a total disc replacement, the Charite disc, to ALIF, concluding noninferiority of the TDR device to ALIF instrumentation. The study, which enrolled and randomized 375 patients, reported

15

similar ODI scores, VAS pain scores, health status questionnaire scores, and disc height for both the TDR and ALIF group at five-year follow-up. Further, the study reported more favorable rates for surgical success, patient satisfaction, reoperation, return to employment, long-term disability, and segmental ROM. Subsequent longer-term investigations chronicle largely superior patient outcomes of Charite artificial discs to lumbar fusion at 10 years (Lemaire et al. 2005) and 13.2 years (David et al. 2007) follow up. Subsequent studies compared development of ASD after TDR and fusion surgeries, finding significant lower incidences of ASD in the TDR implanted subjects compared to the fused subjects (Zigler et al. 2012). Rainey et al. (2012) suggests that prevalence of ASD in TDR outcomes could be attributed to pre-existing degenerative conditions at adjacent levels and/or acceleration of degenerative pathologies at the facet joints, proposing that more rigorous pre-operative patient selection can mitigate risks of ASD after TDR surgery.

Two primary TDR designs are currently approved by the FDA for market in the U.S.: the ProDisc-L from DePuy Synthes (Figure 2.3) and the Activ-L from Aesculap (Figure 2.4). DePuy ceased production of the Charite TDR in favor of the ProDisc-L acquired in its merger with Synthes. The ProDisc-L is a ball-and-socket-based design that consists of one superior and one inferior cobalt chrome alloy (CoCrMo) end plates and an ultra-high-molecular-weight polyethylene (UHMWPE) inlay. The end plates are fixed to their respective vertebrae via a central keel, and a plasma-sprayed, porous, titanium coating promotes integration with the bony surfaces. The inlay is constrained within the inferior end plate, and the superior end plate articulates over the inlay, which establishes

a COR located near the inferior edge of the inferior keel. To accommodate an anatomically variable patient population, the modular design offers a variety of sizing combinations including a medium or large footprint, 6° or 11° lordotic angle, and 10, 12, or 14 mm inlay heights. During surgery, patients are positioned in a supine, neutral position where clinicians approach the offending segment from anterior direction. A discectomy is performed to remove degenerated tissue, the end plates are distracted to remobilize the segment, and the implant is inserted into the disc space. Successful clinical outcomes of the ProDisc-L technology depend on proper patient selection, optimal implant sizing and placement, thorough discectomy, and successful remobilization of the joint. Candidates for surgery are diagnosed with mild or moderate DDD, skeletally mature, active, and have no contraindications. Careful pre-operative planning is crucial as optimal implant selection and placement can restore proper disc height, maintain natural spinal lordosis, and successfully remobilize the offending joint. Siepe et al. (2014) reported significant improvement in patient ODI and VAS scores, high patient satisfaction (22.7%), and nominal number of device related complications (7.2%) at 5-to-10-year follow up of ProDisc-L surgery. Zigler et al. compared patient outcomes of the ProDisc-L with circumferential fusion at a five-year follow up. While both groups demonstrated significant improvement in patient-reported outcomes, a higher number of ProDic-L patients indicated they would have the surgery again (82%) compared to the fusion group (68%); reoperation rates were lower in the TDR group (8%) compared to the fusion group (12%). The investigation also reported ASD was three times more incident in the fusion group than the ProDisc group (28.6% vs. 9.2%).

17

Despite significant clinical successes of implants with fixed COR, like the ProDisc-L, some studies suggest that artificial discs with a COR that is free to translate can further increase post-operative ROM and decrease loading at the facet joints (Dreischarf et al. 2015). The Aesculap Activ-L attempts to incorporate controlled anterior-posterior translation of the center inlay to better mimic physiological motion and reduce facet joint degeneration. Like the ProDisc-L, the Activ-L is a ball-and-socket-based design that consists of one superior and one inferior CoCrMo end plates and a UHMWPE inlay. The convex-shaped end plates are fixed to their respective vertebrae via three spikes, and a plasma-sprayed, porous, titanium coating promotes integration with the bony surfaces. The inlay is permitted to translate in the anterior-posterior direction within the inferior end plate, and the superior end plate articulates over the inlay. The configuration allows the center of rotation to translate with the center inlay. Four sizes (small, medium, large, and extra-large) are available to achieve adequate end plate coverage, and a variety of end plate angles are available to maintain natural disc lordosis. Over-distraction of the disc space is avoided by selecting the optimal height of the center inlay (8.5 mm, 10 mm, and 12 mm). Implantation techniques for the Activ-L are similar to the process outlined for the ProDisc-L, with the clinician first removing the diseased disc, distracting the vertebral bodies, and optimally placing the implant within the intervertebral space. A key implantation difference exists in that a ProDisc-L implantation requires two distraction steps to place the inferior and superior end plates, whereas the Activ-L places both end plates simultaneously, thus only requiring one distraction step and avoiding potential over distraction of the FSU. The Activ-L received

18

FDA approval early in the summer of 2015, and there currently is no evidence of the clinical outcomes associated with this device. Yue et al, have proposed conducting a prospective, randomized, multi-center clinical trial consisting of an estimated 414 subjects to compare the clinical outcomes of patients treated with the Activ-L implant to patients treated with the ProDisc-L device at a five-year follow up (Yue et al. In preparation).

2.4 Statistical Shape and Alignment Modeling

There is general consensus that mechanical behavior of the natural and treated human body is dependent upon anatomic structure of bones and soft tissue structures. In an effort to understand the true mechanical behavior of the human body, study developmental processes, identify articular pathology, direct surgical methods, and improve medical device design, biomechanical investigators have utilized a variety of methods to quantify the morphometrics of musculoskeletal structures in the human body including direct measurement, measurement of three-dimensional parametric models, digital scanning, and radiographic measurements. Most modeling techniques, however, use simplified 2D projections, rely on inconsistent landmark identification, or contain noisy data.

2.4.1 Shape Modelling in Literature

The recent development of statistical, or active shape models (SSMs) efficiently quantifies shape differences between members of a population by reducing a high dimensional representation of the structures onto a lower dimensional subspace. Cootes et al. (1995) pioneered this technique by developing an active shape model of a set of

resistors, representing the boundary of each member of the training set as a sequence of points placed at the same key landmarks. Distributions at the boundary were related by a covariance matrix and variation quantified by the eigenvalues, or modes of variation, of the covariance matrix. The group uniquely plotted the first two modes against each other and discovered them to be independent of one another, demonstrating that the model was representative of the training set. Subsequent studies demonstrated that eigenmode analyses can be applied to any shape representation. Point distribution models have quantified variability in object contours represented by Fourier decompositions and parameter vectors containing the contour coordinates (Lorenz et al. 2000). As the utilization of the SSM technique expanded to incorporate more complex shapes, it became clear that one-to-one correspondence between the surface points of each instance is crucial, and more efficient methods to register members of the training set to a common point distribution were explored. Lorenz et al. (2000) applied a novel templating method, where a template point distribution was generated, and point correspondence was established by manually coating the template onto the remaining samples. Myronenko et al. (2010) improved methods of automatic point correspondence for intricate shapes by applying a refined coherent point drift (CPD) algorithm to morph the template mesh to each member of the training set prior to point correspondence.

It comes as no surprise that statistical shape modelling has been extended to applications in the medical domain including radiographic image segmentation, disease diagnosis, fracture risk, object recognition, and capturing variability of biological structures. The technique has been employed to characterize shape and bone quality

variation in the pelvis (Meller et al. 2004), the femur (Bryan et al. 2010, Sarkalkan et al. 2014), and the sacrum (Wagner et al. 2014). Other studies have quantified variation of relative anatomical alignment between structures of the knee (Rao et al. 2013) to investigate the relationship between anatomy and function (Fitzpatrick et al. 2011, Smoger et al. 2015). Applications to the spine are wide-spread. Long et al. (2000) matched contours from a radiograph to an active shape model to assist in DDD and osteoarthritis diagnosis in the cervical spine (Long et al.). Peloquin et al. (2014) utilized SSM to develop population-based finite element analyses to investigate mechanics of the degenerated intervertebral disc. Other studies have statistically quantified variation in healthy, deformed, and pathological lordotic curvatures (Meakin et al. 2013), developed statistical clinical guidelines for spinal needle injections (Khallaghi et al. 2010), and developed methods to quantify vertebral fracture from radiographs (de Bruijne et al. 2007). Huls et al. (2010) explored how variable articular geometry influences lumbar spine mechanics by applying the SSM technique to describe shape variability of a set of lumbar FSUs to assess facet articulation. Bredbenner et al. (2014) built a statistical shape and intensity model to assess injury risk in the cervical spines of warfighters.

2.4.2 Shape Modelling in Practice

The SSM approach utilized in subsequent chapters consists of four primary phases: anatomical data collection, registration to a template, application of statistical methods onto the training set, and shape model evaluation.

Anatomical information was manually extracted from computed tomography (CT) scans to generate three-dimensional, patient-specific geometry. Computed tomography is

a medical imaging modality capable of noninvasively acquiring three-dimensional representations of a patient's internal structure. In conventional CT methods, x-rays are linearly transmitted through the patient's body and are attenuated by the tissues they pass through. Tissue density is proportional to the attenuation experienced by an x-ray along its path, and, thus, a two-dimensional projection of tissue density in a region of interest can be generated. To mitigate limitations of x-ray imaging and to increase image resolution, the gantry, which fixes the x-ray source and detectors into a collinear arrangement, is rotated 180 degrees around the patient, and a filtered back projection algorithm reconstructs the data into a two-dimensional view of the imaged slice. This process is repeated to image subsequent slices until data has been collected for the entire volume of interest. As a result, CT image technology enables segmentation techniques to distinguish different biological structures in each two-dimensional slice and digitally reconstruct three-dimensional instances from the multi-slice volumes. In this study, instances of the lumbar vertebrae were manually masked from their appropriate slices using a segmentation software package, Scan IP (Simpleware Exeter, UK). Pixels size from the scans averaged 0.31 mm with an average slice thickness of 1 mm. Segmentation accuracy is dependent upon CT image resolution and manual masking consistency. To limit segmentation error and noise, filtering techniques such as cavity fill, island removal, Recursive Gaussian smoothing, median filter, and binarisation are applied to the target volume. To capture the surface contours, segmented vertebrae are discretized into triangular elements and point distribution information is digitally stored in stereolithographic (.stl) format.

22

Before statistical analysis can be applied to the population, all subject geometries were registered to a template mesh to ensure adequate point-to-point correspondence. Two-dimensional triangular surface elements comprised the template mesh for the vertebrae, and the L1, L2, L3, L4, L5, and sacral endplate consisted of 3,259, 3,678, 3,671, 3,791, 3,619, and 481 nodes, respectively. An iterative closest point (ICP) algorithm (Besl et al. 1992) was applied to each subject to ensure proper rigid body alignment to the template mesh. The algorithm iteratively revises the rigid body transformation needed to minimize the distance from the subject to the template. For every iteration, a modified K-D tree efficiently identifies the closest template node for every subject node, a mean squared error cost function estimates the best combination of rotations and translations to better align the subject to the template, and the subject geometry is transformed accordingly. After rigid body transformation, proper registration of the posterior elements to the template mesh is challenging as the morphology of the posterior elements are significantly different. Myronenko et al. (2010) developed a CPD algorithm that seeks to alleviate this challenge by probabilistically forcing clouds of points to transform coherently to preserve the surface contour of the cloud. The group applies a simplified mixture model using an optimized weighting value to capture noise and outliers in the data set. After CPD morphing, point-to-point correspondence is established between the subject and the template, and corresponded nodes were added to the register, or training set.

To quantify relative alignment of the structures of the lumbar spine, custom local anatomic coordinate systems were developed for each segment based on systems from

23

Wu et al. (2002) Planes of best fit were generated for the superior and inferior endplates of each vertebral body, and a line connecting the centers of the planes defined the z-axis, with the midpoint as the origin of the local coordinate system. Because the sacrum lacks an inferior end plate, a line connecting the center of the superior plane of best fit to the center of the truncating plane was defined as the z-axis of the sacrum. A perpendicular line from the origin to the centroid of the spinal canal defined the x-axis, and the y-axis was defined as the cross-product of the z and x-axes. Transformations representing the alignment of one local coordinate system to its inferior neighboring coordinate system were extracted by transforming each local coordinate system to the coordinate system at the sacral end plate. Information from the transformation matrices were included in the training set. The final training set contains 3*n+t variables for each subject, and is organized in a matrix of (3*n+t) x m dimensions where n is the number of nodes of each registered geometry, t are the twelve rotation and translation values of the transformation matrices, and m is the number of subjects.

A shape model is created from the training set using principal component analysis (PCA) according to established methods (Tsai et al. 2003). PCA is a statistical procedure that reduces the dimensionality of a data set by converting possibly correlated data variables defined in Euclidean space into a set of linearly uncorrelated variables called principal components (PCs), modes of variation, or eigenvectors. The series of eigenvectors describe the eigenspace by quantifying the direction of the variation of the original variables. Each eigenvector is associated to an eigenvalue that quantifies the magnitude of variance along that eigenvector in the eigenspace. The first eigenvector (PC

1) is associated to the largest eigenvalue, the second eigenvector (PC 2) is associated to the second largest eigenvalue, and so on, until the variance is completely explained in each original variable. PCA also outputs PC scores, which represent the transformation of the original correlated variables defined in Euclidean space into the linearly correlated variables defined in eigenspace. First, mean values of each variable are calculated and subtracted from each subject's shape to generate a set of residuals. Eigenvectors and eigenvalues are computed from the covariance matrix of the residual data. To visualize the variability in Euclidean space, each eigenvector, representing a mode of variation, is multiplied by the original data in eigenspace and transformed to Euclidean space via the associative PC scores.

Simplification of a high dimensionality data set, like the surface coordinates of a lumbar vertebra, to a lower dimensionality is enabled by ignoring the PCs with low eigenvalues, as these PCs do not significantly influence the overall variation, and retaining the PCs with the large eigenvalues. While several criteria including Kaiser's rule (Kaiser 1960), Cattell's Scree test (Cattell 1966), and the minimum average partial method (Velicer 1976) have been proposed to retain the adequate number of components, parallel analysis (PA) (Horn 1965) is widely considered the most accurate of all methods as it effectively minimizes sampling error and reduces noise in the data set (Glorfeld 1995). In PA a number of new data sets of the same sample size and the same number of eigenvalues as the observed data set are populated with random, uncorrelated variables. By performing parallel PCAs on each new data set and isolating the 95th percentile of the results, the data bias or noise is estimated and subtracted from the observed data to yield

a vector of adjusted eigenvalues. The number of components in the observed, correlated data set with adjusted eigenvalues greater than one are retained.

To determine the predictive capability of the statistical model, or the ability of the model to accurately describe a new subject, a leave-one-out (LOO) cross-validation technique can be applied. The technique splits the training set into two sets: the reduced training set and the test set; the reduced training set is the original training set with one subject removed, and the test set is the removed subject. PCA is applied to the reduced training set to obtain a new set of eigenvalues, eigenvectors, and PC scores. The test set is projected into the resulting eigenspace to determine the PC scores of the left-out sample. The predicted residual, or Euclidean distance error between corresponding nodes of the test set and the predicted test set, is computed. This process is repeated as each subject is left out in turn, and root mean squared value of the predicted residual is calculated to indicate the predictive capability of the model. Several advantages of the LOO approach to evaluate a statistical model include correcting for potential overfitting of the data and enabling assessment of sample-specific errors.

2.5 Finite Element Modelling of the Lumbar Spine

To understand the functional biomechanics of the natural spine and to biomechanically evaluate treatment options, a precise, comprehensive understanding of the mechanical behavior, material properties, variable morphology of the spine, and their relationships is necessary. In vitro and in vivo studies have been valuable in this regard but are limited in their ability to accurately measure temporal and spatial variability of stresses, strains, and material properties. Additionally, errors can accumulate in the

26

preparation, performance, and evaluation of an experiment. Finite element methods offer a complementary approach that can improve insights into physiological-mechanical interactions and have grown to cover complex biomechanical systems including irregular anatomical geometries, contacting bodies, crack propagation, and structural failure.

2.5.1 Finite Element Methods of the Spine in Literature

The first FE application in the spine was reported by Belytschko et al. (1974) who investigated material constants, stress distributions, deflections, and stiffnesses within the intervertebral disc under axial loads. In comparing the FE model to in vitro experimental results, the study found that the isotropic material behavior assumed in the experiments do not adequately represent the mechanical behavior of the disc and that in vitro measurements of material properties underestimate the theoretical stiffness of the disc. With steady increases in the affordability and availability of computational power, FE methods of the spine have grown to improve understanding of the natural lumbar and cervical spines (Toosizadeh et al. 2011, Erbulut et al. 2014, Mengoni et al. 2016, Wang et al. 2015, Dreischarf et al. 2013, Dreischarf et al. 2014, Bredbenner et al. 2014, Campbell et al. 2015, Du et al. 2016, Panagiotopoulou et al. 2009, Jaramillo et al. 2015, Tsouknidas et al. 2012), to holistically characterize degenerative diseases such as DDD and ASD (Palepu et al. 2012, Ibarz et al. 2013, Wu et al. 2016, Ryu et al. 2016, Videbaek et al. 2010, Faizan et al. 2012), to provide insight into the biomechanics of spinal deformities (Agarawl et al. 2015, Zheng et al. 2015), and to assist in the evaluation of surgical treatment options (Womack et al. 2011, Rundell et al. 2012, Wang et al. 2013, Kim et al. 2010, Pfeiffer et al. 2015, Gong et al. 2014, Rohlmann et al. 2013).

Model development of the natural spine predicts spatial and temporal distributions of internal stresses, strains, and loads and provides insight into the natural motions of the healthy spine. Mengoni et al. (2016) and Toosizadeh et al. (2011) generated cervical spine models validated to cadaveric animal models to estimate muscle forces and internal loads transmitted across the disc and through the facet joints. A detailed asymmetrical model built by Erbulut et al. (2014) revealed relationships of soft tissue structures to cervical spine stability and motion. Bredbenner et al. (2014) developed a population-based FE model validated with in vitro experiments to evaluate probabilistic loading responses under flexion-extension, lateral bending, and internal rotation. These studies suggest the development of detailed, computational models validated with experiments can reveal the underlying mechanisms of neck injury caused by automobile accidents. Motivated by increased prevalence of low back pain, computational models have made important contributions to our understanding of functional biomechanics of the lumbar spine. Accurate and clinically-relevant modeling of the lumbar spine remains challenging, yet promising, with the potential to enhance the quality of patient care. Dreischarf et al. (2013) and Du et al. (2016) evaluated mechanical parameters through the disc and the facet joint respectively. Tsouknidas et al. (2012) built a computational tool to determine the biomechanical response of a segment when subjected to complex loading conditions. Other studies realize the time expense associated with model development and attempt to automate model development while retaining model accuracy and predictive ability (Campbell et al. 2015, Dreischarf et al. 2014). Jaramillo et al. (2015) validates a multibody FE model including heterogeneous and anisotropic discs and soft

tissue structures to reproduce the biomechanics of the natural lumbar spine with the aim to investigate disc degeneration.

Differences in mobility between degenerative and healthy conditions of the disc were examined with the model developed by Ibarz et al. (2013) ROM simulations in flexion, extension, lateral bending, and internal rotation were compared to radiological measurements. Wu et al. (2016) reported statistically significant relationships between degeneration progression and number of degenerated discs after computationally investigating biomechanics in multiple pathological discs. Other studies have developed FE models examining ASD at the onset of segmental degeneration (Ryu et al. 2016) and after TDR and fusion treatments (Faizan et al. 2012). Results reveal increased loading, stress, and ROM at adjacent levels, which match outcomes of in vitro and in vivo experiments. Finally, Zheng et al. (2015) applied FE methods to expand our understanding of disc degeneration in the scoliotic spines, reporting mobility values in flexion, extension, lateral bending, and internal rotation that were agreeable with outcomes from complementary in vitro experiments.

A comprehensive understanding of the mechanisms behind disc degeneration and spinal injury drive development of improved computational tools to inform device design, guide surgical protocols, and ultimately achieve higher quality patient outcomes. Pfeiffer et al. (2015) investigated parameters that influenced failure of pedicle screw fixation in fusions and found that placement of cement augmentation has substantial influence on the failure load of the simulated geometries. Gong et al. (2014) simulated flexion, extension, lateral bending, and axial rotation in a variety of pedicle screw

fixation techniques to examine displacement and stress distributions throughout the devices. The study concluded that the supplemented unilateral pedicle screw fixation technique achieved superior outcomes to both the bilateral and unilateral pedicle screw fixation options. Probabilistic FE models developed by Rohlmann et al. (2013) report relationships between the misalignment of vertebrae adjacent to a TDR and the facet joint forces and provide insight into the effects of TDR on natural lumbar spine biomechanics. Goel et al. (2005) computationally investigated how cervical TDR device design, orientation, and placement influence sagittal balance, intradiscal stress distributions, and quality and quantity of motion of the cervical spine. Comparisons of the biomechanics of an intact lumbar spine to a spine implanted with one of three popular TDRs, the Charite®, Prodisc® and Maverick®, were computationally evaluated by Kim et al. (2010) The group reported a greater flexion-extension range of motion in the implanted models than in the intact model. The Maverick® device yielded the greatest range of motion and the greatest facet contact load in the L4-L5 FSU.

2.5.2 Finite Element Method in Practice

FE analysis is a method to numerically approximate spatial distributions of field problems described in terms of partial differential equations. Several robust, commercially available FE software packages have been developed to solve complex computational simulations, including ABAQUS^{TM} (Dassault Systemes, Johnston, RI), the solver employed to perform simulations in this study. The basic approach of the FE method is to discretize a body into node-connected finite elements called the mesh. Within each element, a field quantity, such as stress, displacement, and contact area,

30

varies spatially and is described by a polynomial equation, which, across the entire mesh, is represented by a system of differential equations. Approximations of field variables are computed for each element in a piece-wise fashion and are improved by increasing the element density in the mesh. While it is important for computational outcomes to be experimentally validated, the FE method can complement in vivo or in vitro studies because it can be applied to any field problem, is not geometrically restricted, can incorporate any loading or boundary conditions, and can include an extensive library of material property definitions.

Two distinct methods, the implicit and explicit time integration techniques, have emerged. Though both methods solve the same basic set of governing equations, the primary applications for which each method achieves an accurate solution are vastly different. The implicit method applies a forward difference technique, and the general governing equations are evaluated at time t_{n+1}. This approach allows the solution to remain stable with large time steps, but is also computationally intensive as the algorithm requires inversion of the stiffness matrix to solve for the displacement vector. Computational inefficiencies are compounded if nonlinearities are present, as the stiffness matrix itself is a function of the displacement vector. The explicit method is computationally inexpensive when solving nonlinear problems, such as those involving multi-body contact, anisotropic material behavior, or complex dynamic behavior, because it applies the central difference method with the assumption that change in displacements is linear. Inversion of the complex stiffness matrix is avoided as the algorithm solves for the acceleration vector instead of the displacement vector. Accuracy of the solution,

31

however, is dependent upon the size of the time step, with smaller time steps yielding more accurate results and requiring more power from the central processing unit (CPU). An explicit solver was utilized in this study as the dynamic simulations contained multiple nonlinear components including extensive use of contact, multi-body motion, and a combination of non-traditional elements.
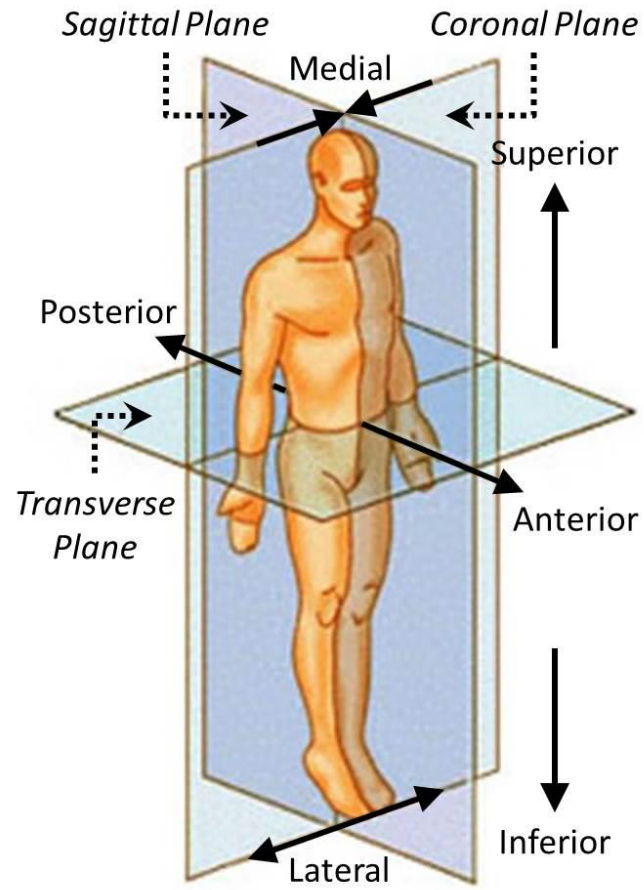
Figure 2.1 Diagram of anatomic planes and clinical directions (SEER's Training Website, 2004).
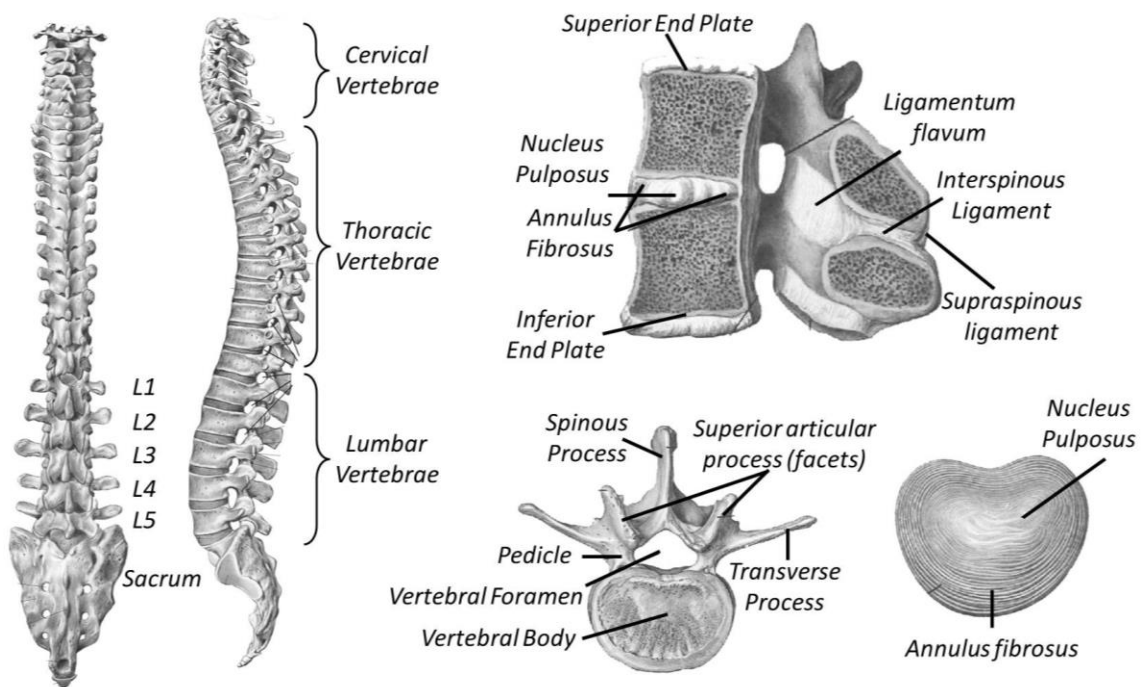
Figure 2.2 Diagrams of spinal column in the coronal plane (far left) and the sagittal plane (second from left), spinal joint or FSU (top right), individual lumbar vertebra (center bottom), and intervertebral disc (bottom right)(www.anatomicprints.com).
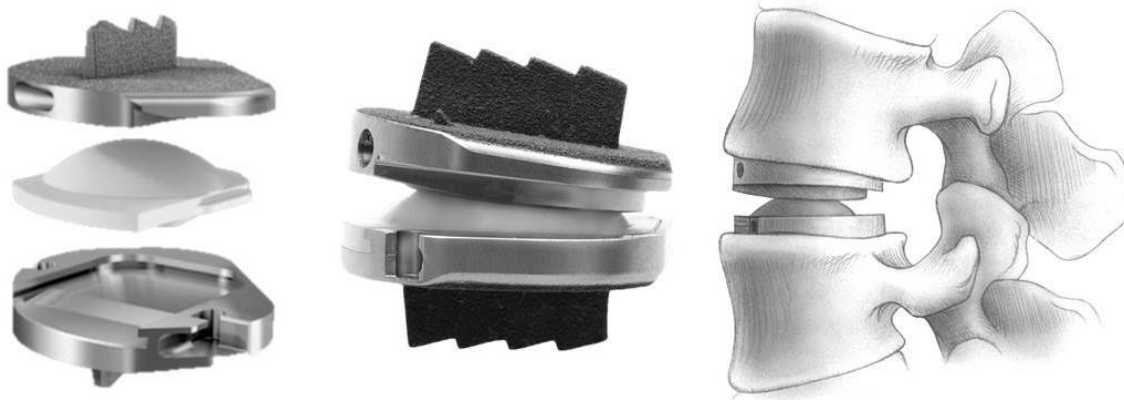
Figure 2.3 The DePuy Synthes ProDisc-L consists of a titanium superior end plate, UHMWPE inlay, and a titanium inferior end plate. The inlay is fixed into the inferior end plate. Exploded view (left) assembly (center) after insertion into FSU (right)(depuysynthes.com and www.bjj.boneandjoint.org.uk).

Figure 2.3 The Aesculap Activ-L consists of a titanium superior end plate, UHMWPE inlay, and a titanium inferior end plate. The inlay is free to translate in the anterior-posterior direction within the inferior end plate. Exploded view (left) assembly (center) after insertion into FSU (right)(www.fda.gov).

CHAPTER 3: STATISTICAL SHAPE AND ALIGNMENT MODELLING OF THE LUMBAR SPINE

3.1 Abstract

Low back pain is experienced by half the adult population in a given year and primarily caused by lower back pathologies including degenerative disc disease, spinal stenosis, and spinal deformities. In order to diagnose lower back pathologies and screen for surgical treatment options clinicians and researchers employ a variety of methods to characterize anatomical lumbar spine variability. Statistical shape modelling has emerged to characterize morphological variation with the capability of characterizing full three-dimensional anatomy. Accordingly, the objective of this study was to develop a comprehensive set of statistical shape-alignment models of each individual vertebrae, the functional spinal unit (FSU) of the L4-L5, the L5-S1 FSU, and the entire lumbar spine to characterize anatomical variability in the lumbar spine. For each shape-alignment model, a training set representing the subjects' geometries were registered to a template and PCA was applied to the set to identify primary modes of variation. Scaling was the most prevalent mode of variation for all models. Subsequent modes of the SSMs of the individual bones characterized shape variation within the posterior elements. Subsequent modes of variation for the FSU SSMs and the SSM of the entire spine yielded alignment changes associated to disc height and lordosis. The successful generation of a shape-

36

alignment model of the lumbar spine identifies anatomical interdependencies between different sub-structures of a body and enables generation of accurate population-based finite element models. Quantification of anatomical variation in the spine can inform implant design, assist clinicians in diagnosing pathologies, screen patients for treatment options, and pre-operatively plan for surgical treatment including TDR.

3.2 Introduction

During any given year, half of the adult population experiences LBP, and two thirds experience LBP at least once in his or her lifetime (Deyo 1986). Some epidemiological studies report that back pain of moderate to severe duration and intensity is annually incident in 15% of the adult population (Andersson 1999) Further, the prevalence of chronic LBP has increased by 64% since 2000 and that the average age of these patients has increased from 48.5 years to 52.2 years (Smith et al. 2013). Expenditure reports reveal that since 1997, the total estimated cost of spinal medical treatment has increased 65% to $86 billion dollars, with medical costs for the average patient eclipsing $6,000 (Martin et al. 2008). While most LBP patients undergo passive treatment options, almost 2% require more expensive surgical interventions (Deyo 1986).

Methods to diagnose lower back pathologies and screen for treatment options typically involve radiographic measurement of key anatomical dimensions. For instance, reduced disc height is a primary indicator of intervertebral degenerative disc disease (DDD) (Kjaer et al. 2005, Yu et al. 2012, Rohlmann et al. 2006) and spinal stenosis (Steurer et al. 2011), and can help screen patients for total disc replacement (TDR) surgery or fusion. Additionally, measures of coronal facet angle can be predictive of facet

arthritis (Jentzsch et al. 2013). Normal spine anatomy includes features that can influence

spinal range of motion (ROM). For example, Masharawi et al. (2004) reported a

sequential decrease in transverse facet angle and sequential increase in sagittal facet angle

from the T1 to the L5 vertebrae, suggesting that variability in facet angle results in

greater flexion-extension ROM in the lumbar region and greater axial rotation ROM in

the thoracic region. In another study, vertebral body dimensions were found to decrease

from T1 to T3 and increase from T4 to L5, which influences the shape of the

intervertebral disc and effectively alters the ROM experienced at those levels (Masharawi

et al. 2011). However, structures of the spine are anatomically complex and exhibit

inherent variability across the patient population. Accordingly, an understanding of

anatomical variation in the spine can provide insight into spinal ROM, assist clinicians in

diagnosing pathologies, and help establish screening protocols for surgical treatment.

Prior studies have attempted to quantify geometric variation in the anatomy of the

spine by direct measurement of key anatomical features (Masharawi et al. 2008,

Masharawi et al. 2011, Di Angelo et al. 2015), measurement of a 3D parametric model

(Kolta et al. 2012), radiographic measurement of key anatomical features (Meakin et al.

2013, Lakshmanan et al. 2012, Wang et al. 2012), or using digital scanning methods

(Wang et al. 2012, Tan et al. 2004). Variability was quantified in endplate morphology to

guide TDR design and reduce implant subsidence (Lakshmanan et al. 2012, Wang et al.

2012), in the dimensions of the vertebral body to assess facture risk (Di Angelo et al.

2015, Masharawi et al. 2008, Kolta et al. 2012, Tan et al. 2004), and dimensions of the

posterior elements to insure proper identification of spinal deformities and to guide the

design of surgical instrumentation (Masharawi et al. 2011, Di Angelo et al. 2015, Tan et al. 2004).

Recently, statistical shape models (SSM) have been developed to describe variation in bone morphology with the capability of characterizing full three-dimensional anatomy. SSM has been employed to characterize shape variation in the cervical spine (Bredbenner et al. 2014), the pelvis (Meller et al. 2004), the femur (Bryan et al. 2010, Sarkalkan et al. 2014), the sacrum (Wagner et al. 2014), and the shape of the lumbar spine as a whole (Boisvert et al. 2008, Meakin et al. 2009). Lately, some studies have incorporated anatomical alignment into a statistical shape model of the knee, in which variation is quantified not only in the multiple structures of the joint, but in their relative alignment as well (Rao et al. 2013). The resulting statistical shape-alignment model (SSAM) can investigate relationships between anatomy and pathology and guide implant design. Other studies have developed SSAMs of the knee that incorporate kinematic variation to investigate the relationship between anatomy and function (Fitzpatrick et al. 2011, Smoger et al. 2015).

The objective of this study was to develop a comprehensive set of statistical shape-alignment models of each individual vertebrae, the functional spinal unit (FSU) of the L4-L5, the L5-S1 FSU, and the entire lumbar spine to characterize anatomical variability in the lumbar spine. The statistical models of individual bones characterize vertebral morphology at each level, the statistical models of the FSUs and the entire lumbar spine characterize normal anatomy for multi-vertebrae geometries, establish

39

levels for diagnosis of pathologies, and assist clinicians in screening patients for treatment options.

3.3 Methods

Computed tomography (CT) scans in the supine position were acquired for a cohort of 52 patients (24 females, 28 males, average age of 35 ±9 with a range from 20 to 58 years old) (Table 3.1) as part of the clinical standard of care. Geometries of the lumbar spine (S1-L1) were segmented from the CT scans (pixel size = 0.31 mm, slice thickness = 1 mm, Figure 3.1) for each patient using Scan IP (Simpleware, Exeter, UK) (Figure 3.1a, 3.1b). To focus on sacral endplate anatomy, the sacrum was truncated at a distance proportional to one eighth of the width of the sacral endplate. The condition of the disc at each FSU was diagnosed as age normal, mild, moderate or severe degeneration by an orthopaedic surgeon (Figure 3.1c).

Local anatomical coordinate systems based on systems defined by Wu et al. (2002) were created for each vertebra (Figure 3.1d). Planes of best fit were generated for the superior and inferior endplates of each vertebral body. Each plane was bounded by the left, right, posterior, and superior margins of the endplate. A line connecting the centers of the planes defined the z-axis, with the midpoint as the origin of the local coordinate system. A perpendicular line from the origin to the centroid of the spinal canal defined the x-axis and the y-axis was defined as the cross-product of the z and x-axes. An ICP algorithm, similar to Rao et al. (2013), was utilized to transform the coordinate frames and geometries of each vertebral body to a reference frame located at the sacral endplate, and the transformation matrices representing the alignment of one

bone relative to its inferior bone was extracted. While the disc itself was not modeled, the transformation matrix relating each vertebral body to its inferior body captured differences in as-scanned alignment and disc condition.

A coarse template mesh of triangular surface elements was developed from the median-sized geometry (average element edge length: 1 mm). The template mesh contained approximately 3,500 nodes per vertebrae and 480 nodes for the sacral endplate. Subject geometries were finely discretized into triangular surface elements (average element edge length: 0.3 mm) and registered to the template mesh. A CPD algorithm was applied to establish accurate nodal correspondence in which nodes were placed at analogous anatomical positions on the surface of the same vertebra (Myronenko et al. 2010) (Figure 3.1e).

In order to describe inter-subject shape and alignment variation, a comprehensive set of statistical shape-alignment models was developed for each individual vertebrae, commonly pathologic levels, L4-L5 FSU, the L5-S1 FSU, and the entire lumbar spine. To generate each statistical model, principal component analysis (PCA) was performed on the training set data, which consisted of three-dimensional Cartesian coordinates describing the nodal locations of each bone in its local coordinate system and, in the multi-vertebral cases, the 4x4 transformation matrix describing the relative alignment between the vertebrae. A parallel analysis was performed on the training set to determine the minimum number of components to retain. Perturbations of ± 2 standard deviations from the mean were applied to the resulting modes of variation to visualize the changes in size, shape, and alignment. Differences in the degeneration state were evaluated with

41

the principal component (PC) scores for each subject. A series of clinical and radiographic measures commonly used in surgical assessment, including disc height, vertebral body dimensions, and facet orientations, were automatically performed to evaluate descriptions of the modes of variation, and distributions of these measures were assessed (Table 3.2, 3.3). To assess how well the cohort in this study represented the population as a whole, measurements of individual vertebrae were compared to values reported in literature (Table 3.4, Figure 3.8). To assess geometrical relationships between anatomical features, measures were plotted against each other and against PC scores, and Pearson correlation coefficients were computed. In addition, composite instances were generated that averaged the 3 smallest and 3 largest geometries to support implant design and sizing (Figure 3.6).

A LOO analysis was performed to assess the ability of the statistical models to accurately describe a new subject. In the analysis, each subject of the training set was iteratively left out to create a new reduced training set. For each iteration, PCA was performed on the reduced training set, and the eigenvectors of the reduced training set were used to transform the shape representation of the left out subject into new PC scores. An increasing number of PC scores were transformed into a new shape representation. Root mean squared errors were calculated between the actual and model-predicted shape.

3.4 Results

The PCA for each statistical model yielded a series of modes of variation which collectively characterized anatomic variability. Parallel analysis identified nine PCs

would be adequate to retain for the L1 model and the entire lumbar model, and eight PCs would be adequate to retain for the other models. The retained PCs accounted for the greatest amount of variability, with the modes of variation of the vertebrae, the L4-L5 FSU, the L5-S1 FSU, and the entire lumbar spine models capturing over 70% of the total variability, respectively (Figure 3.2).

The most prevalent mode of every statistical model described scaling variation, which accounted for over 34% of the total variability in the models of the individual vertebrae, the L4-L5 FSU, the L5-S1 FSU, and the entire lumbar spine (Figure 3.3, 3.4, and 3.5). Strong Pearson correlation coefficients of 0.76, 0.76, 0.74, and 0.76, averaged across all vertebral models, were computed between the PC score of the first mode (PC 1) and the length of the superior endplate, the length of the inferior endplate, the width of the superior endplate, and the width of the inferior endplate, respectively (Table 3.5).

Subsequent modes for each individual vertebra model characterized shape, size, and orientation of the posterior elements. Most notably, the variability in the length of the articular processes was described by the second or third mode capturing 12.8% of the total variability on average (Figure 3.2). Correlations between the second PC score and the average length of the articular processes yielded coefficients of 0.75, 0.71, 0.69, and 0.47 for the L2, L3, L4, and L5 shape models, respectively. For the L1 shape model, an average correlation coefficient of 0.61 was computed between the third PC score and the length of the articular process (Table 3.5).

The statistical models of the FSUs quantified variability in vertebral shape as well as intervertebral alignment. Disc height was characterized as the second mode of

43

variation, capturing 12.1% of the total variability, in the L4-L5 model and the third mode

of variation, capturing 9.3% of the total variability, in the L5-S1 model (Figure 3.3). In

both statistical models, the associated PC scores were highly correlated to disc height

measurements (Figure 3.7), yielding Pearson coefficients of 0.82 and 0.88 for the L4-L5

model and L5-S1 model, respectively (Table 3.6). Further, PC scores of the mild/normal

degenerated subject groups and the moderate/severe degenerated subject groups were

statistically different for both the L4-L5 model (t(45) = 5.14, p=5.81E-6) and the L5-S1

model (t(47) = 5.35, p=3E-6)(Figure 3.7).

The statistical model of the entire lumbar spine quantified variability in shape and

alignment from the sacral endplate to the L1 vertebra. While the most predominant mode,

accounting for 34.1% of total variability, described scaling variation, the mode did not

characterize scaling of the lumbar spine as a whole, but the scaling of each individual

vertebra separately. The first principal component was correlated to the vertebral

anterior-posterior length and medial-lateral width of each vertebra with a correlation

coefficient of 0.73 averaged across every measurement of the vertebrae. The second

mode, which captured 11.1% of the total variability, described changes in disc height at

the more caudal region of the lumbar spine (Figure 3.4). The coefficient correlating the

score of PC 2 and the height of the intervertebral space at the L4-L5 and L5-S1 segments

were 0.74 and 0.32, respectively (Table 3.7). Captured by the third and fourth modes,

variability in lumbar spine height and Cobb angle explained 10.2% of the total

variability, and yielded correlation coefficients of 0.64 and 0.82, respectively (Table 3.7).

Results of the LOO analysis assessed the predictive capability of statistical models by computing a root-mean-squared error of the nodal coordinate differences between the predicted and actual geometry. Averaged across all nodes and specimens, the absolute error for the L1, L2, L3, L4, and L5 bones, L4-L5 and L5-S1 FSU, and the entire spine was 0.96 ± 0.14, 0.97 ± 0.15, 1.04 ± 0.17, 1.09 ± 0.16, 1.23 ± 0.28, 1.40 ± 0.26, 1.32 ± 0.29, and 1.54 ± 0.26 millimeters, respectively (Table 3.8).

Comparisons of key anatomical measures to those found in literature agreed with measures reported in other studies. Mean end plate dimensions, vertebral body heights, and transverse facet angles were under 3%, 13%, and 15% different to mean measures reported for Masharawi et al., respectively. Wolf et al. list mean end plate dimensions and vertebral body height under 7% and 11% different to mean dimensions of geometries in this study, respectively (Table 3.4). Percent difference to the L4 transverse facet angle measure reported by Gulek et al. is 1.2%. Distributions reported in this study closely match normal distributions of end plate dimensions and transverse facet angle published in the study by Masharawi et al. (2007), end plate dimensions published in the study by Wolf et al. (2010), and transverse facet angle dimensions reported by Gulek et al. (2013) (Figure 3.8). Results of an Anderson-Darling test indicate that our measurements are normally distributed (average p-value = 0.53 across models).

3.5 Discussion

The set of statistical models holistically captured complex intersubject shape and alignment variation in the lumbar spine by quantifying variation in the shape and size of individual bones, the shape and relative alignment of the two structures of an FSU, and

the multi-structure anatomy of the entire lumbar spine. Relationships between the first PC of each vertebral model and endplate dimensions can guide TDR design as the mean and statistical deviations of the endplate dimensions can reveal appropriate implant sizing lines for a variable population (Figure 3.6). These techniques have been explored for use in total knee arthroplasty to optimize tibial component design (Fitzpatrick et al. 2007, Dai et al. 2014). Statistical models of the FSUs quantitatively described alignment variability which can establish norms of disc spacing for the age-normal/mild and moderate/severe degeneration cohorts and assist in pre-surgical planning for treatment options, such as TDR or fusion (Figure 3.7). As variation of the anatomy of a whole structure is dependent upon shape-alignment variability of its sub-structures, quantified descriptions of variability of the whole lumbar structure can indicate how shape variation in individual vertebra influences the shape of the lumbar spine as a whole, which can provide insight into the mechanical behavior of scoliotic, kyphotic, and other irregular spine anatomies. Additionally, correlations of disc spacing of the inferior segments with the early PCs of the models of the entire lumbar structure revealed that the L4-L5 and L5-S1 segments are statistically more prone to degeneration than the more superior segments.

A parallel analysis identified nine PCs would be adequate to retain for the set of models. A LOO analysis using all 52 principal components evaluated the predictive capability of the set of statistical models, yielding an average error of 1.19 ± 0.21 millimeters of the models to accurately generate a new subject. A LOO analysis using only nine principal components yielded an average error of 1.60 ± 0.30 millimeters. These error values were similar to errors reported in Smoger et al. (2015) and Rao et al.

(2013). While inclusion of degenerated subjects created statistical models that were representative of a relevant patient population, the inconsistency of subjects' pathologies limit the models' ability to represent a healthy population. The inconsistency in subjects' pathologies as well as a moderate sample size (n=52) are possible reasons for the error reported by the LOO analysis. A larger training set and more consistent pathological conditions might decrease variability captured by the SSM and improve the model's ability to accurately describe a new subject. Strong predictive capabilities of the statistical models can establish confidence that the statistical models are able to generate virtual instances of a population. Further, the study was constrained by limits with the CT imaging as scans were resolved to an average 1 mm slice thickness and 0.31 mm pixel size. Modes of variation correlated to lordosis or disc angle can be attributed to imaging subjects in a supine position. To capture accurate, natural alignment variability, three-dimensional patient models could be aligned to radiographs of the patients in standing, loaded positions before the local anatomic coordinate systems are developed.

Means of geometric measures found in this study are less than 15% different to means of geometric measures reported by Masharawi et al. (2004, 2008, 2011) and Wolf et al. (2001) (Table 3.4) and only 1% different to values reported by Gulek et al. (2013). Results of an Anderson-Darling test indicate that our measurements are normally distributed (average p-value = 0.53 across models); differences in means of the measurement distribution of this study was less than 10% different to means of the other studies. Discrepancies in values reported by Masharawi et al. could be explained by a difference in landmark location, difference in sample size, and inherent error within the

measurement tools. Masharawi et al. measured anatomy with a digitizer; our study automatically measured distances from nodes from manually segmented, meshed geometries. Discrepancies between our results and the results reported by Wolf et al. (2010) and Gulek et al. (2013) most likely derive from differences in difficulty to properly measure three-dimensional anatomic structures with two-dimensional images, as carried out in their studies. All of these studies employed traditional methods including direct measurement, digital scanning (Masharawi et al. 2004, 2007, 2011)), radiographic measurement (Wolf et al. 2010, Gulek et al.), or measurement of a 3D parametric model (Kolta et al. 2012) which limited the utility of their findings.

The statistical shape-alignment approach used in this study is more advantageous in three ways: it captures three-dimensional morphology, differentiates shape variation from alignment variation, and characterizes the dependence between the variability of the full geometry and its relevant sub-structures. Characterization of three-dimensional anatomy, as opposed to traditional linear measurements, identifies anatomical interdependencies between different sub-structures of a body and enables generation of accurate population-based finite element models as demonstrated by Bredbenner et al (2014). Additionally, relative inter-structure alignment is represented by transformation matrices; as such, three-dimensional alignment variability can be differentiated from shape variability, which is defined by nodal locations, allowing variability of complex geometries to be accurately captured and helping to establish relationships between shape and alignment variability. Moreover, the comprehensive shape model, including models of individual bones, relevant FSUs, and the whole spine, reveals how shape variation of a

48

single-structure can influence shape-alignment variation of its parent structure. Variability in vertebra size and articular process shape, for example, induced variability in disc angle at the FSU level and lordosis at the level of the entire lumbar spine. Further studies into these relationships can help identify agents of multi-structure pathologies within single-structure anatomy.

The statistical modeling approach comprehensively described the shape and alignment of the lumbar spine by characterizing variability of shape and size of individual vertebra, relative alignment of relevant FSUs, and overall shape and alignment in the lumbar spine as a whole. Quantifications of shape and size variations of single vertebra can help establish implant sizing lines in TDR treatment to best fit the population; characterizations of relative alignment variation between the bones of an FSU can help clinicians diagnose pathologies, screen patients for treatment options, and pre-operatively plan for surgical treatment including TDR; description of overall shape variation in the entire lumbar spine indicates segments that are susceptible to degeneration and reveals how vertebral shape changes influence the spine as a whole.
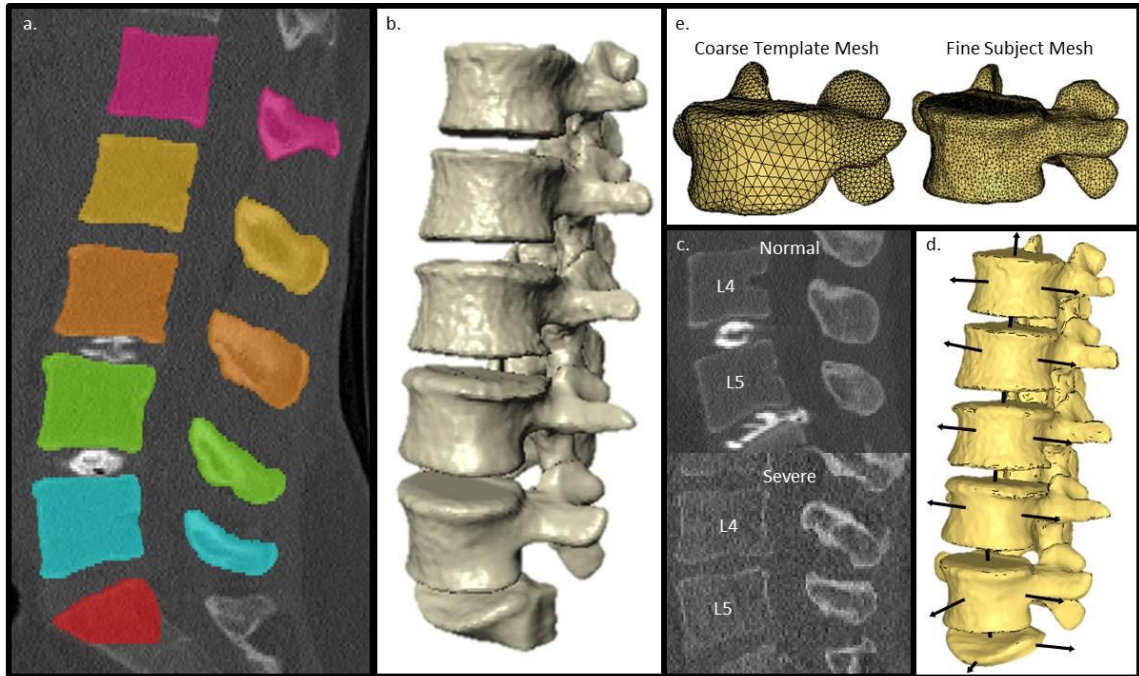
Figure 3.1 a) Geometries segmented from computed tomography images, b) 3D model of patient geometry, c) Healthy normal and severe degeneration cases, d) local anatomic coordinate system developed for each vertebra, e) mesh densities for template and subject meshes.
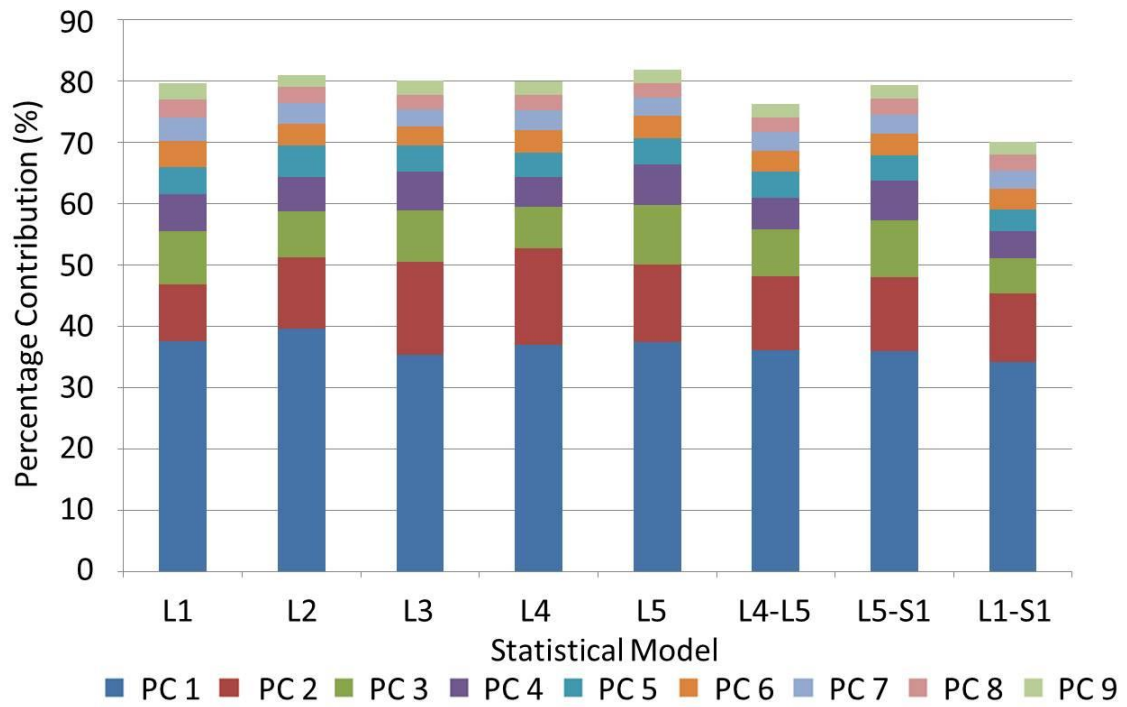
Figure 3.2 Contributions of the first nine principal components (modes of variation) to overall variation, as well as the cumulative variation explained.
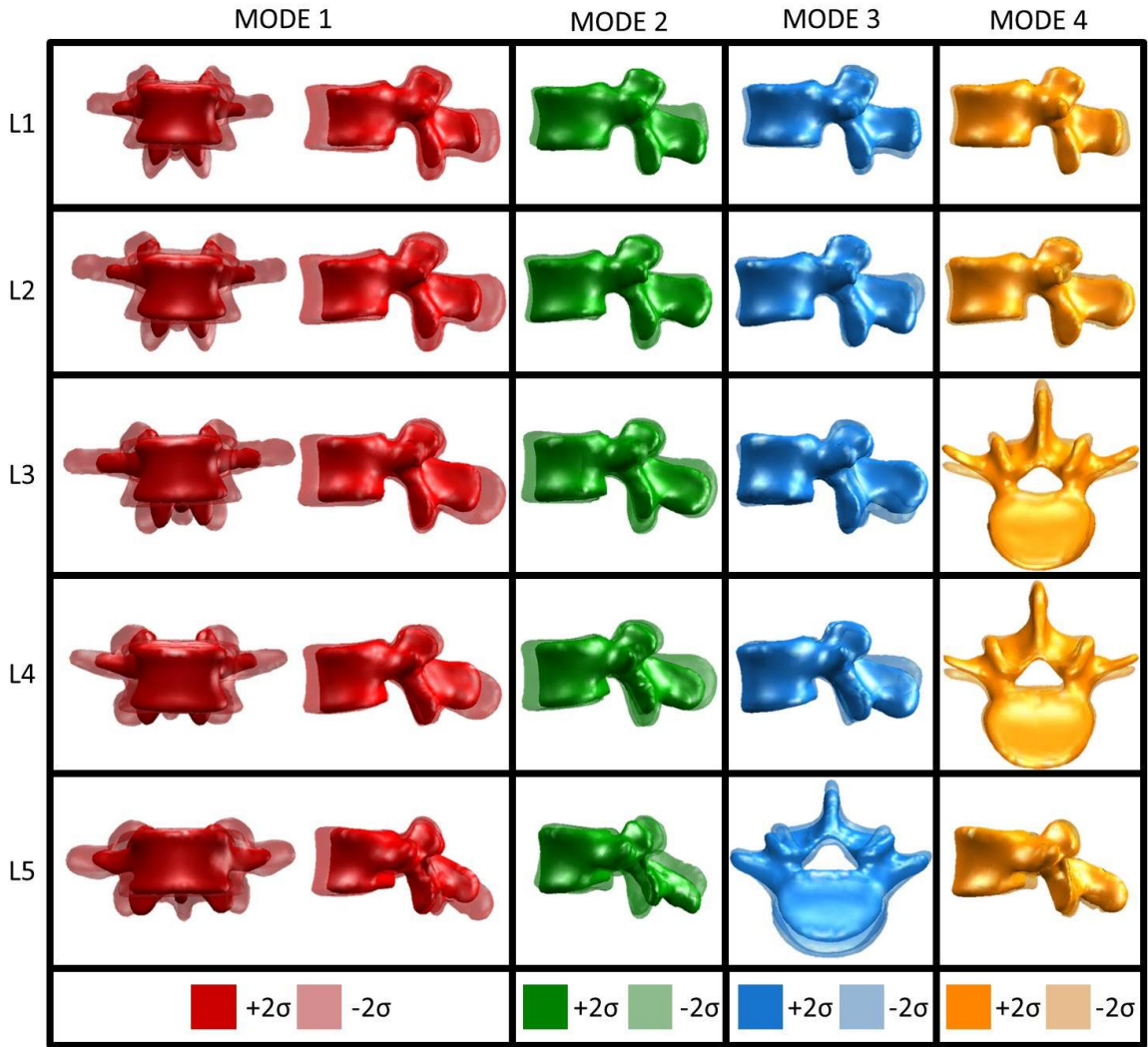
Figure 3.3 First four modes of variation for each individual vertebral model at +/- 2 standard deviations. The first four modes captured 61.5%, 64.3%, 65.2%, 64.3%, 66.3% of the total variability in the L1, L2, L3, L4, and L5 vertebra, respectively.
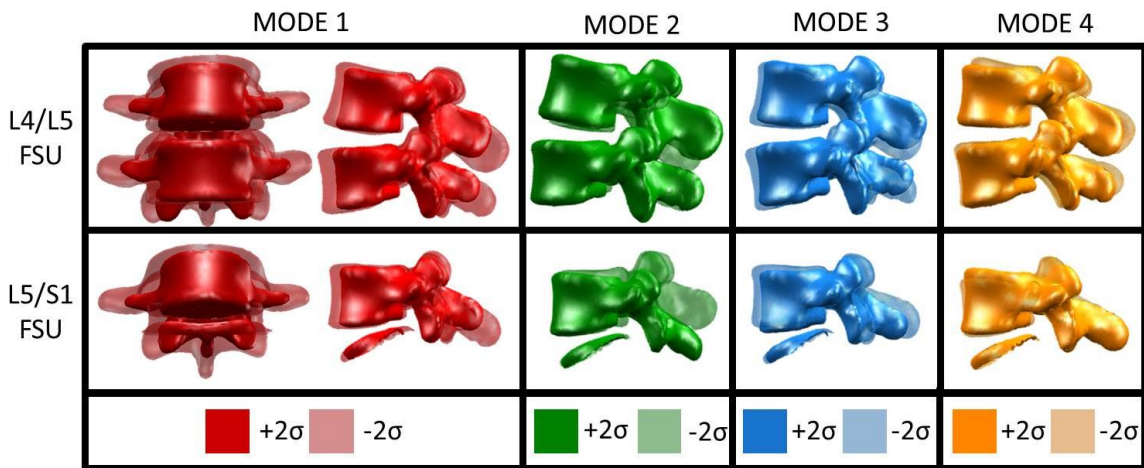
Figure 3.4 First four modes of variation for the L4-L5 FSU and the L5-S1 FSU models at +/- 2 standard deviations. The first four modes captured 60.9% and 63.7% of the total variability in the L4-L5 FSU and the L5-S1 FSU, respectively.
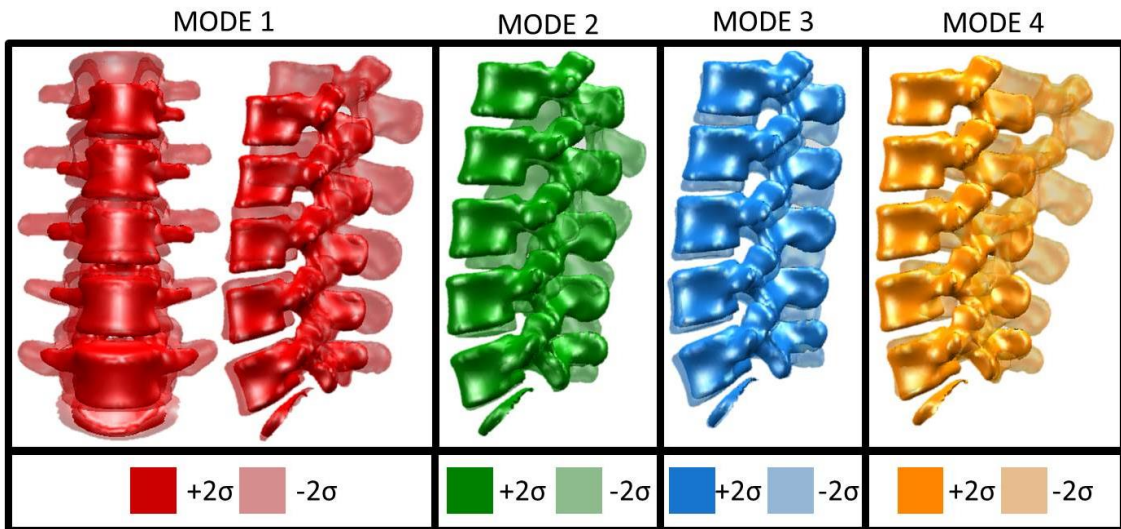
Figure 3.5 First four modes of variation for the entire lumbar spine model at +/- 2 standard deviations. The first four modes captured 55.5 % of the total variability.
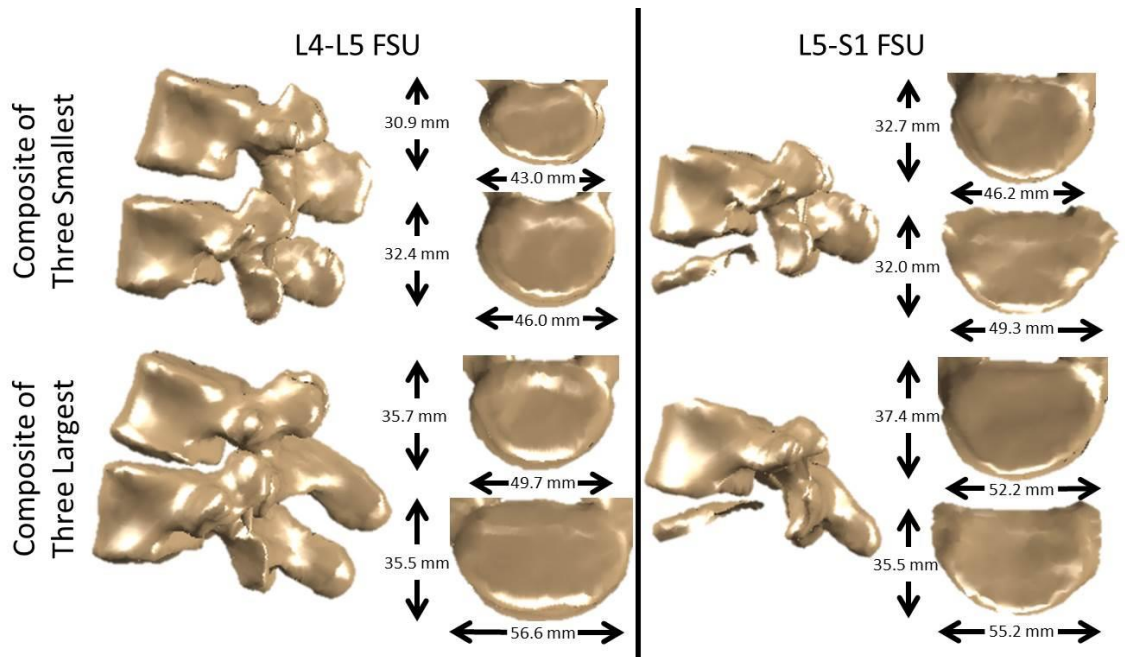
Figure 3.6 Composite instances averaged the 3 smallest and 3 largest geometries to support implant design and sizing for the L4-L5 FSU (left) and the L5-S1 FSU (right).
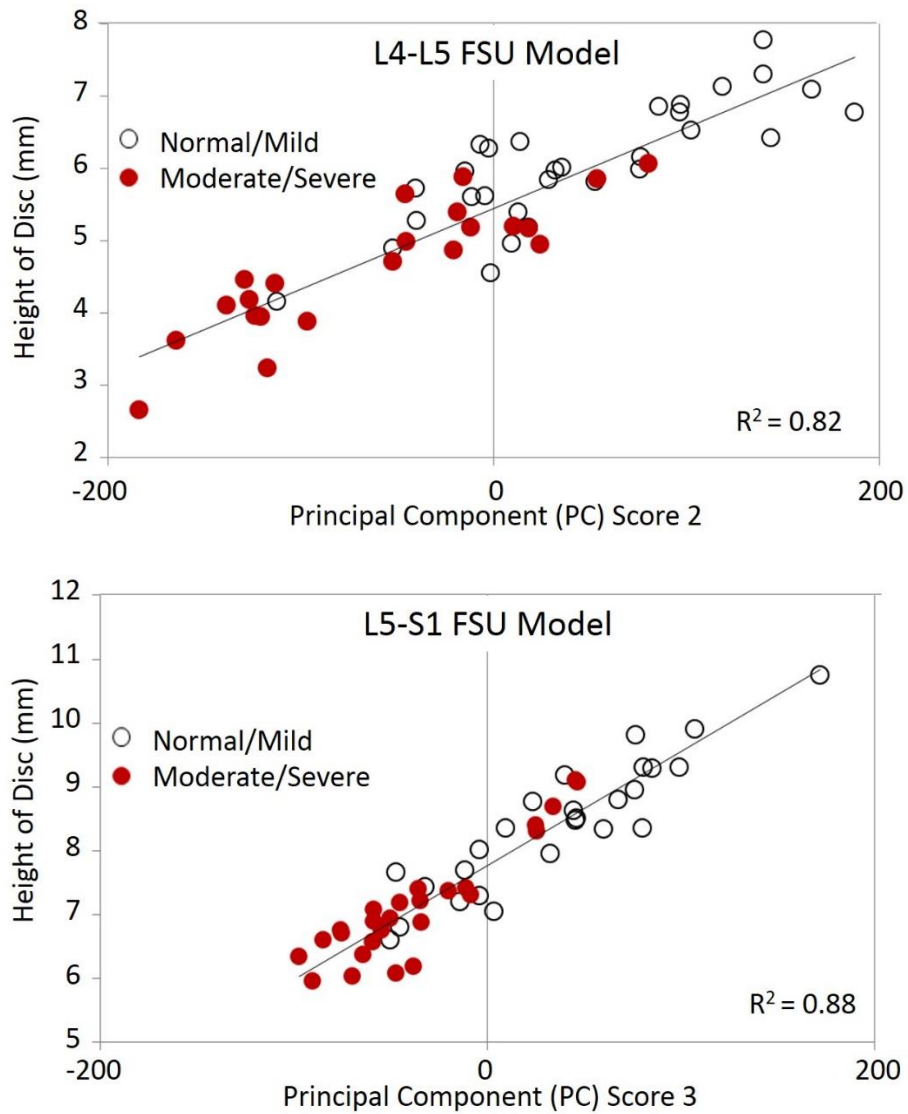
Figure 3.7 Disc height was strongly correlated to PC 2 in L4-L5 FSU model (top) and PC 3 in the L5-S1 FSU model (bottom). Differences in disc height were statistically significant between healthy normal/mild and moderate/severe degenerative groups which can assist in pre-surgical planning for degenerative treatment options.
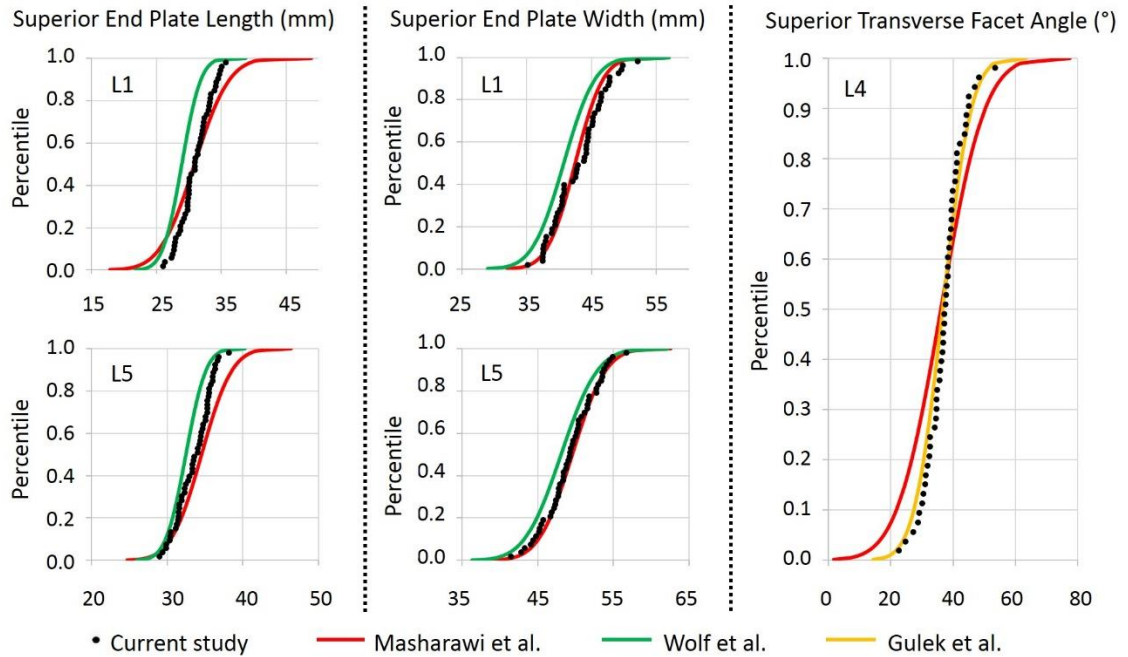
Figure 3.8 Cumulative distribution functions of superior end plate length of the L1 and L5 vertebrae (left), superior end plate width of the L1 and L5 vertebrae (center), and superior transverse facet angle of the L4 vertebra (right), comparisons to cumulative distribution functions of the dimensions reported by Masharawi et al. (2007), Wolf et al. (2001), and Gulek et al. (2013). Results of the Anderson-Darling test indicate that our measurements are normally distributed (average p-value = 0.53 across models); differences in means of the measurement distribution of this study was less than 10% different to means of the other studies.

Table 3.1 Age, weight, height, and BMI statistics differentiated by gender for 52 patients: mean ± standard deviation (range).

	N	Age	Weight (lbs)	Height (in)	BMI
Males	28	35.8 ± 8.8 (23-53)	187.5 ± 26.7 (140-250)	70.6 ± 3.2 (65-79)	26.2 ± 3.1 (20-32)
Females	24	34.4 ± 9.4 (20-58)	167.1 ± 38.0 (112-280)	64.9 ± 2.8 (60-70)	27.8 ± 5.7 (18-41)
Total	52	35.3 ± 9.0 (20-58)	179.6 ± 32.7 (112-280)	68.3 ± 4.2 (60-79)	26.8 ± 4.4 (18-41)

Table 3.2 Mean, standard deviation, minimum, and maximum values of key dimensions of individual vertebrae.

Dimension		Mean	Std. Dev.	Min.	Max.	Dimension		Mean	Std. Dev.	Min.	Max.
Superior End Plate AP Length (mm)	L1	31.0	2.4	26.1	35.7	**Height of Left Articular Process (mm)**	L1	48.1	2.0	42.5	52.5
	L2	31.7	2.3	26.4	36.2		L2	49.5	1.7	46.7	53.4
	L3	33.6	2.4	28.9	37.1		L3	47.9	2.9	41.9	53.0
	L4	32.9	1.9	28.9	36.4		L4	44.6	2.2	39.8	49.1
	L5	33.6	2.2	29.0	38.1		L5	42.9	3.4	35.8	50.0
Inferior End Plate AP Length (mm)	L1	32.1	2.5	27.2	37.9	**Height of Right Articular Process (mm)**	L1	47.8	1.7	41.8	51.4
	L2	32.6	2.3	27.3	36.4		L2	50.1	1.9	46.0	54.6
	L3	33.9	2.3	29.2	37.7		L3	47.7	2.8	42.1	52.7
	L4	32.9	2.1	28.8	37.1		L4	44.3	2.1	40.1	48.8
	L5	32.2	2.5	26.9	37.4		L5	42.3	3.2	34.8	50.4
Superior End Plate ML Width (mm)	L1	42.9	3.9	35.2	52.1	**Length of Spinous Process (mm)**	L1	31.7	1.2	28.8	34.4
	L2	44.2	3.6	36.7	52.2		L2	36.2	3.6	28.4	43.2
	L3	49.4	3.3	43.0	55.1		L3	37.0	3.8	28.8	46.9
	L4	47.7	2.9	42.4	54.0		L4	34.0	3.7	26.0	43.0
	L5	49.3	3.4	41.5	56.7		L5	25.3	3.2	18.1	32.9
Inferior End Plate ML Width (mm)	L1	45.8	3.9	38.6	55.3	**Span of Articular Processes (mm)**	L1	28.2	3.6	21.7	38.1
	L2	46.6	3.5	38.2	53.8		L2	30.1	3.0	22.2	39.2
	L3	46.7	3.4	40.3	53.3		L3	34.5	4.9	21.7	48.7
	L4	47.4	3.0	41.3	54.4		L4	43.8	2.6	37.9	49.2
	L5	50.4	3.3	43.4	56.4		L5	54.4	5.7	41.5	64.9
Anterior Vertebral SI Height (mm)	L1	29.5	1.5	26.1	32.5	**Span of Transverse Processes (mm)**	L1	72.7	6.9	59.3	91.6
	L2	29.5	1.9	25.9	33.7		L2	82.9	8.3	64.7	99.7
	L3	30.0	1.9	26.5	34.9		L3	90.6	8.8	72.5	110.0
	L4	30.5	1.2	28.2	32.8		L4	87.2	5.9	74.6	98.5
	L5	25.9	2.2	20.6	30.1		L5	92.2	7.4	75.2	112.7
Posterior Vertebral SI Height (mm)	L1	28.0	1.6	25.3	31.8	**AP Position of Left Articular Process (mm)**	L1	40.7	2.4	45.7	36.5
	L2	29.3	1.9	25.8	35.6		L2	41.5	2.7	49.7	37.3
	L3	29.3	1.8	26.0	33.3		L3	41.9	2.9	50.7	37.7
	L4	27.9	1.7	24.6	32.5		L4	41.2	2.8	49.0	36.4
	L5	29.7	2.1	25.0	34.6		L5	47.7	4.2	41.6	61.6
Angle of Spinous Process (°)	L1	-12.6	7.6	-30.5	0.7	**AP Position of Right Articular Process (mm)**	L1	40.1	2.2	44.4	35.5
	L2	4.1	3.4	-3.9	13.8		L2	39.9	2.5	45.4	34.3
	L3	13.9	3.1	8.5	20.6		L3	42.1	3.0	50.6	37.3
	L4	15.6	4.8	4.4	29.9		L4	47.6	4.5	40.1	62.5
	L5	30.8	6.3	10.7	41.8		L5	48.1	4.5	40.6	63.0
Angle of Left Transverse Process (°)	L1	-20.8	4.0	-27.9	-10.4	**Transverse Angle of Left Superior Facet (°)**	L1	30.3	3.7	21.7	39.1
	L2	-3.1	1.6	-6.9	1.2		L2	27.7	4.0	13.9	35.3
	L3	19.6	4.9	8.4	30.3		L3	29.2	6.6	10.9	42.6
	L4	25.5	6.4	14.6	41.2		L4	29.0	6.1	14.0	43.0
	L5	36.8	2.9	30.4	41.9		L5	43.4	5.4	31.8	56.7
Angle of Right Transverse Process (°)	L1	18.5	5.1	5.6	33.0	**Transverse Angle of Right Superior Facet (°)**	L1	35.0	4.9	21.2	46.6
	L2	-9.3	2.2	-17.1	-6.2		L2	33.1	4.7	22.1	45.7
	L3	14.1	5.5	-1.1	25.1		L3	25.7	3.7	18.7	36.0
	L4	3.9	6.5	-10.3	21.9		L4	37.2	5.9	22.7	53.5
	L5	1.0	1.7	-2.8	5.7		L5	39.5	6.6	25.2	58.9

Table 3.3 Mean, standard deviation, minimum, and maximum values of key dimensions of the L4-L5 FSU, L5-S1 FSU, and the entire spine.

Dimension		Mean	Standard Deviation	Minimum	Maximum
Disc Height (mm)	L4-L5 FSU	5.5	1.1	2.6	7.8
	L5-S1 FSU	7.8	1.1	6	10.7
Disc Angle (°)	L4-L5 FSU	12.4	1.7	10	18.7
	L5-S1 FSU	13.6	1.8	9.8	17.4
Cobb Angle (°)	Entire Spine	44.4	6.3	30.1	57.4
Total Spine Height (mm)	Entire Spine	162.7	2.8	154.5	168.6

Table 3.4 Comparisons of key anatomical measures of Caucasian Americans including superior end plate length, inferior end plate length, superior end plate width, inferior end plate width, anterior vertebral height, posterior vertebral height, length of spinous process, transverse angle of left superior facet, and transverse angle of right superior facet to values reported by Masharawi et al. (2004, 2007, 2011) and Wolf et al. (2010). Number of subjects is denoted as "n".

Dimension		Current Study n=52	Masharawi et al. n=120	Wolf et al. n=55
Superior End Plate AP Length (mm)	L1	31.0 ± 2.4	31.0 ± 4.2	28.9 ± 2.3
	L2	31.7 ± 2.3	31.9 ± 4.1	29.8 ± 2.3
	L3	33.6 ± 2.4	33.3 ± 3.8	32.3 ± 1.3
	L4	32.9 ± 1.9	33.7 ± 3.7	31.7 ± 2.1
	L5	33.6 ± 2.2	34.5 ± 3.2	32.5 ± 2.1
Inferior End Plate AP Length (mm)	L1	32.1 ± 2.5	30.4 ± 3.3	-
	L2	32.6 ± 2.3	31.5 ± 3.1	-
	L3	33.9 ± 2.3	32.4 ± 3.5	-
	L4	32.9 ± 2.1	33.9 ± 3.4	-
	L5	32.2 ± 2.5	33.1 ± 2.9	-
Superior End Plate ML Width (mm)	L1	42.9 ± 3.9	42.5 ± 3.4	40.7 ± 3.8
	L2	44.2 ± 3.6	44.3 ± 3.4	39.8 ± 4.6
	L3	49.4 ± 3.3	45.3 ± 4.5	43.1 ± 3.8
	L4	47.7 ± 2.9	47.2 ± 3.7	44.1 ± 4.6
	L5	49.3 ± 3.4	49.6 ± 3.5	48.1 ± 3.8
Inferior End Plate ML Width (mm)	L1	45.8 ± 3.9	45.3 ± 2.9	-
	L2	46.6 ± 3.5	48.2 ± 3.5	-
	L3	46.7 ± 3.4	50.0 ± 3.0	-
	L4	47.4 ± 3.0	50.4 ± 4.1	-
	L5	50.4 ± 3.3	49.9 ± 3.1	-
Anterior Vertebral SI Height (mm)	L1	29.5 ± 1.5	24.9 ± 2.5	-
	L2	29.5 ± 1.9	25.8 ± 2.5	-
	L3	30.0 ± 1.9	26.1 ± 2.2	-
	L4	30.5 ± 1.2	25.8 ± 2.5	-
	L5	25.9 ± 2.2	26.8 ± 2.7	-
Posterior Vertebral SI Height (mm)	L1	28.0 ± 1.6	27.5 ± 2.3	24.9 ± 2.4
	L2	29.3 ± 1.9	27.5 ± 3.3	25.4 ± 1.1
	L3	29.3 ± 1.8	27.0 ± 2.8	25.6 ± 1.6
	L4	27.9 ± 1.7	25.4 ± 2.8	26.5 ± 0.6
	L5	29.7 ± 2.1	23.2 ± 2.9	28.6 ± 1.3
Transverse Angle of Left Superior Facet (°)	L1	30.3 ± 3.7	29.0 ± 12.5	-
	L2	27.7 ± 4.0	23.7 ± 10.9	-
	L3	29.2 ± 6.6	27.5 ± 8.7	-
	L4	29.0 ± 6.1	36.1 ± 11.1	-
	L5	43.4 ± 5.4	47.1 ± 13.0	-
Transverse Angle of Right Superior Facet (°)	L1	35.0 ± 4.9	27.1 ± 10.8	-
	L2	33.0 ± 4.7	22.9 ± 10.3	-
	L3	25.7 ± 3.7	28.9 ± 10.5	-
	L4	37.2 ± 5.9	36.9 ± 12.0	-
	L5	39.5 ± 6.6	41.9 ± 12.4	-

Table 3.5 Pearson's correlation coefficients relating anatomical measures of individual vertebrae to principal component scores. All measurements were calculated from anatomical landmarks and correlated to PC scores using an automated process. Correlations are presented as absolute values and rounded to the nearest tenth.

Dimensions	L1				L2				L3				L4				L5			
	PC 1	PC 2	PC 3	PC 4	PC 1	PC 2	PC 3	PC 4	PC 1	PC 2	PC 3	PC 4	PC 1	PC 2	PC 3	PC 4	PC 1	PC 2	PC 3	PC 4
Superior End Plate Length	0.7	0	0	0	0.7	0	0	0	0.8	0	0	0	0.8	0	0	0	0.7	0	0	0
Inferior End Plate Length	0.7	0	0	0	0.8	0	0	0	0.9	0	0	0	0.7	0	0	0	0.7	0	0.1	0
Superior End Plate Width	0.7	0	0	0.1	0.8	0	0	0	0.8	0	0	0	0.7	0	0	0	0.7	0	0	0
Inferior End Plate Width	0.7	0.1	0	0	0.8	0	0	0.1	0.7	0	0	0	0.7	0	0	0	0.8	0	0	0
Anterior Vert. Height	0.2	0	0.1	0	0.4	0.1	0	0	0.1	0.1	0	0	0	0.3	0	0.1	0.1	0	0	0.1
Posterior Vert. Height	0.2	0	0	0.1	0.5	0.1	0	0	0.1	0.4	0	0	0	0.4	0	0	0	0.4	0	0
Angle of Spin. Process	0.1	0.7	0	0	0	0	0.8	0	0	0	0.7	0	0	0	0.8	0	0	0.1	0.1	0.2
Angle of Left Trans. Process	0	0.3	0	0.1	0	0	0	0	0	0	0	0.5	0.2	0.1	0	0.3	0.2	0	0	0
Angle of Right Trans. Process	0	0	0	0.1	0	0	0	0.1	0	0.1	0	0.5	0.1	0.1	0	0.4	0.1	0	0.2	0.1
Height of Left Art. Process	0.3	0	0.3	0	0.1	0.7	0	0	0.1	0.7	0	0	0	0.6	0	0	0.2	0.4	0	0
Height of Right Art. Process	0.1	0	0.6	0	0	0.8	0	0	0.1	0.7	0	0	0	0.7	0	0	0	0.5	0.1	0
Length of Spin. Process	0	0	0	0.7	0.6	0	0	0	0.4	0.2	0.1	0	0.1	0.5	0	0	0	0	0.3	0.2
Span of Art. Processes	0.2	0	0.2	0	0	0.8	0	0	0.4	0.3	0	0	0	0.7	0	0	0.5	0	0.1	0.1
Span of Transverse Process	0.8	0.1	0	0.1	0.8	0	0	0	0.8	0	0	0	0.2	0.5	0	0	0.6	0.2	0	0
AP Position of Left Art. Process	0.5	0	0	0	0.5	0.1	0	0.2	0.3	0.1	0.1	0.1	0.3	0.4	0.1	0	0.5	0.1	0.1	0
AP Position of Right Art. Process	0.5	0	0	0.1	0.5	0.1	0	0.1	0.3	0.2	0.1	0	0.5	0.1	0	0.1	0.5	0.1	0.2	0
Transverse Angle of Left Superior Facet	0	0.2	0.2	0.1	0	0.1	0.1	0	0.1	0.3	0.1	0	0.2	0.3	0.1	0	0	0	0.4	0
Transverse Angle of Right Superior Facet	0	0	0.2	0.2	0	0.1	0.2	0.1	0.1	0.2	0.1	0.1	0.2	0.2	0.1	0	0.1	0.1	0.4	0

☐ 0.0 to 0.3   ▦ 0.3 to 0.6   ■ 0.6 to 0.8

61

Table 3.6 Pearson's correlation coefficients relating anatomical measures of the L4-L5 FSU and the L5-S1 FSU to principal component scores. All measurements were calculated from anatomical landmarks and correlated to PC scores using an automated process. Correlations are presented as absolute values and rounded to the nearest tenth.

Dimensions	L4/L5 FSU				L5/S1 FSU			
	PC 1	PC 2	PC 3	PC 4	PC 1	PC 2	PC 3	PC 4
Superior End Plate Length of Inferior Bone	0.7	0.1	0	0	0.8	0	0	0
Inferior End Plate Length of Inferior Bone	0.7	0	0	0	0.8	0	0	0
Superior End Plate Width of Inferior Bone	0.7	0.1	0	0	0.8	0	0	0
Inferior End Plate Width of Inferior Bone	0.7	0	0	0	0.8	0	0	0
Disc Height	0	0.8	0	0	0	0	0.9	0
Disc Angle	0	0	0.7	0	0	0	0	0.7
Height of Right Superior Articular Process	0	0	0	0	0	0.7	0	0
Height of Left Superior Articular Process	0	0.7	0	0	0	0.7	0	0

☐ 0.0 to 0.3   ▨ 0.3 to 0.6   ■ 0.6 to 0.8

Table 3.7 Pearson's correlation coefficients relating anatomical measures of the entire lumbar spine to principal component scores. All measurements were calculated from anatomical landmarks and correlated to PC scores using an automated process. Correlations are presented as absolute values and rounded to the nearest tenth.

Dimensions		PC 1	PC 2	PC 3	PC 4
Superior Endplate Length	L1	0.6	0.1	0	0
	L2	0.7	0.1	0	0
	L3	0.8	0	0	0
	L4	0.8	0	0	0
	L5	0.7	0	0	0
Inferior Endplate Length	L1	0.6	0.1	0	0
	L2	0.7	0.1	0	0
	L3	0.9	0	0	0
	L4	0.7	0	0	0
	L5	0.7	0	0	0
Superior Endplate Width	L1	0.8	0	0	0
	L2	0.8	0	0	0
	L3	0.7	0	0	0
	L4	0.7	0	0	0
	L5	0.7	0	0	0
Inferior Endplate Width	L1	0.7	0	0	0
	L2	0.7	0	0	0
	L3	0.7	0	0	0
	L4	0.7	0	0	0
	L5	0.7	0	0	0
Disc Height of L4/L5 FSU		0	0.7	0.1	0
Disc Height of L5/S1 FSU		0	0.3	0.0	0.2
Total Disc Height		0.2	0.2	0.6	0.0
Cobb Angle		0	0	0	0.8

☐ 0.0 to 0.3   ▨ 0.3 to 0.6   ■ 0.6 to 0.8

Table 3.8 A leave-one-out analysis was performed to evaluate the predictive capabilities of the statistical models. Average root mean squared errors for all models just exceeded 1.0 millimeter using 52 principal components and under 2 millimeters using 9 principal components. These results established confidence in the models to generate virtual instances that are representative of a variable population.

Model	Root Mean Squared Error (mm)	
	52 Principal Components	9 Principal Components
L1	0.96 ± 0.14	1.33 ± 0.21
L2	0.97 ± 0.15	1.36 ± 0.24
L3	1.04 ± 0.17	1.48 ± 0.26
L4	1.09 ± 0.16	1.60 ± 0.24
L5	1.23 ± 0.28	1.70 ± 0.39
L4-L5 FSU	1.40 ± 0.26	1.83 ± 0.35
L5-S1 FSU	1.32 ± 0.29	1.79 ± 0.40
Whole Spine	1.54 ± 0.26	1.83 ± 0.31

CHAPTER 4: TEMPLATING PRODISC-L TOTAL DISC REPLACEMENT SURGERY

4.1 Abstract

Studies reveal that after TDR surgery, 34% of patients with less than 5° of post-operative ROM developed ASD. As patient anatomy and implant parameters affect post-operative ROM, pre-operative patient selection and surgical planning could maximize ROM and improve clinical outcomes. The aims of the current study were to validate a proposed pre-operative templating process and to determine if templating would have altered surgical decisions. Twenty two ProDisc-L TDRs were implanted in seventeen patients. To measure post-operative ROM, 3D models of bone and implant components were manually overlayed onto flexion, extension, and neutral follow-up radiographs. Flexion and extension rotations were also computationally simulated for each operatively aligned level, and the predicted ROM was compared with measured ROM from the radiographs. Computational templating was then performed to determine optimal implant size and position to maximize ROM. ROM was limited by facet impingement in flexion and implant impingement in extension. The difference between the actual and predicted total ROM averaged 11.8%. Results from the templating procedure indicated that ROM in 19 cases could have been improved had implant placement and/or selection been different. In one case, the patient would have been counseled against proceeding with

TDR as the predicted ROM was less than 5°. Finite element analyses accurately predicted ROM in the cohort and suggested changes to TDR implant size selection and alignment to improve ROM. Pre-operative templating can be an important tool to achieve maximum ROM and optimal clinical outcomes.

4.2 Introduction

Motion-preserving technologies, such as TDR, have been introduced as alternative surgical treatments to lumbar fusion to relieve LBP caused by DDD (Blumenthal et al. 2005, Guyer et al. 2009, Delamarter et al. 2011, Gornet et al. 2011, Ha et al. 2008, Kumar et al. 2001, Harrop et al. 2008). Prior studies have reported that patients implanted with a TDR achieved significantly greater post-operative ROM, maintained natural disc height more consistently, experienced lesser device translation, lower pain scores, and greater success rate than patients who underwent fusion surgeries (Blumenthal et al. 2005, Guyer et al. 2009, Delamarter et al. 2011, Gornet et al. 2011). In addition, Harrop et al. (2008) reported a lower prevalence of ASD in TDR patients compared to fusion patients. Huang et al. (2006) found clear relationships between TDR motion and the presence of ASD at 8.7 year follow-up, revealing that patients with post-operative motion greater than or equal to 5° had 0% prevalence of ASD, while patients with motion less than 5° had a 34% prevalence of ASD. Recently, the clinical efficacy of TDR treatment were elucidated by a variety of clinical, long-term class I and class II studies. David (2007) and Lemaire et al. (2005) reported positive post-operative outcomes in over 82% and negative post-operative outcomes in less than 10% of Charite

TDR patients, and the outcomes of a ProDisc-L study conducted by Tropiano et al.

(2005) reported positive post-operative results for 70% of their patient cohort.

According to the Nationwide Inpatient Sample (NIS), 2,917 lumbar TDR

surgeries were performed annually in approximately 1,000 hospitals, which accounts for

20% of all U.S. inpatient hospitalizations. Average expenditures for each TDR surgery

exceeded $60,000 and $80,000 for primary and revision surgeries, respectively. Private

insurance carriers paid for 52.8% and 47.6% of primary and revision surgeries,

respectively (Kurtz et al. 2010); yet many healthcare carriers are reluctant to cover

lumbar TDR because it is regarded as unproven technology that yields unclear outcomes.

UnitedHealthcare® (2012) justified its refusal to cover TDR surgeries by assessing

several studies that had investigated its clinical efficacy. While the assessment

acknowledged investigations by Skold et al. (2013), Blumenthal et al. (2005), McAfee et

al. (2005), Lemaire et al. (2005), David (2007), Delamarter et al. (2011), and Tropiano et

al. (2007) who reported that TDR outcomes were at least noninferior to outcomes after

fusion, it also highlighted limitations of these investigations including their small sample

sizes, lack of control groups, short-term follow-ups, and lack of randomization

(UnitedHealthcare 2012).

Other research groups suggest that more diligent and accurate screening methods

could boost overall outcomes and persuade healthcare insurers to provide coverage for

lumbar TDR (Siepe et al. 2012, Strube et al. 2013). Siepe et al. (2012) expands upon

prevailing exclusion criteria (Geisler et al. 2008, Quirno et al. 2011) to suggest that

patients with pre-existing degenerative facet joint arthropathies (FJA) should be advised

against a TDR procedure. Strube et al. (2013) cautions that over-distraction of the facet joint or excessive translation of the superior vertebra can accelerate FJA and lead to negative patient outcomes. Proper implant design and sizing decisions can reproduce patient-specific ROM, reduce facet joint loads, and maintain natural lordosis, leading to positive patient outcomes. Dreischarf et al. (2015) reports that a more posterior placement of a fixed-axis implant (ProDisc-L, etc.) increases ROM at the operated level. Findings by Rohlmann et al. (2009) indicate that the most posterior implant placement is not guaranteed to achieve maximum ROM, and optimal implant placement is patient-specific. Patient-specific pre-operative templating can assist in identifying optimal implant size and placement to maximize ROM and improve clinical outcomes.

The objectives of this study were 1) to validate a proposed templating process by comparing predicted ROM with that measured from lateral radiographs, and 2) to retrospectively determine if pre-operative templating would have altered surgical decisions regarding patient suitability, implant size, and implant placement.

4.3 Methods

The second generation ProDisc-L TDR is a modular arthroplasty device composed of two cobalt chromium alloy end plates and a high-modulus, semi-constrained, polyethylene inlay (Figure 4.1). The device end plates are fixed to the superior and inferior vertebral end plates through a central keel and two lateral spikes, and are coated with porous titanium to achieve long-term fixation through bony ingrowth. The polyethylene inlay snap-locks into the inferior end plate and the semi-spherical, bearing surface creates a single articulation with the superior end plate. This arrangement

establishes a fixed center of rotation located within the inferior vertebral bone which approximates the natural motion of the joint and prevents independent component translation. The end plates are manufactured in two sizes (medium, large) and the superior end plate is manufactured in two angles (6 degree, and 11 degree) to accommodate variation in bony morphology and lordotic angle across the patient set.

During surgery, the patient lies in a neutral, supine position on a radiolucent operating table. Under lateral radiographic control, anterior access to the operative disc level is achieved through a standard mini-level retroperitoneal approach. Using anterior-posterior (AP) fluoroscopy, the vertebral midline is identified and marked on the superior and inferior bones. A partial discectomy is performed by resection of the anterior annulus, posterior annulus, and nucleus pulposus. The vertebrae are gradually distracted and the posterior longitudinal ligament is disengaged from the posterior vertebral bodies to remobilize the motion segment. A set of geometrically variable trials are intraoperatively placed into the intervertebral space to determine the optimal disc height, lordotic angle, and implant footprint for the operative level. Under the guidance of lateral imaging, trials are oriented to the vertebral midline, aligned with the sagittal plane, and advanced to the posterior margin of the vertebral bodies. Traditional methods encourage clinicians to choose an implant that maximizes footprint coverage, conforms to the natural lordosis of the lumbar spine, and increases the disc height of the operative level to match normal disc space based on adjacent levels. A chisel is advanced into the superior and inferior vertebral bodies along the shaft of the trial until an appropriate cut depth is achieved. The implant keels are aligned with the chisel cuts and, and the endplates are

69

inserted in a collapsed condition to the posterior edge of the vertebral bodies. The polyethylene inlay is gradually inserted and snap-locked between the end plates so that the appropriate disc height of the operative level is realized. The final implant position is verified using lateral and AP radiographs.

The patient undergoes post-operational occupational and physical therapy until he or she is medically stable and not dependent on intravenous medication. Follow-up appointments are scheduled for six weeks, three months, six months, and one year after date of surgery. Prior to the first follow-up, the patient is discouraged to avoid lifting objects heavier than ten pounds, avoid twisting, and avoid prolonged sitting. Flexion, extension, and neutral radiographs are typically obtained in a loaded, standing position at the six-week follow-up (Figure 4.2).

In the current study, twenty-two ProDisc-L total disc replacements were implanted in seventeen patients. The patient set consisted of eleven males and six females with an average age of 36 ranging from 21 to 50. Single-level surgery was performed on twelve patients, and multi-level surgery was performed on five patients (Table 4.1). Flexion, extension, and neutral radiographs of all patients were obtained at the six-week follow-up.

Three-dimensional models of the operative vertebrae of each patient were extracted from computed tomography (CT) scans using Scan IP (Simpleware, Exeter, UK). The average CT image pixel size was 0.31 millimeters, and the average slice thickness was 1 millimeter. Computer-aided design (CAD) models of four ProDisc-L TDR implant sizes were obtained (6° Medium, 6° Large, 11° Medium, 11° Large) from

70

DePuy Synthes (West Chester, PA). Vertebral models and actually implanted device geometries of each operative level were manually overlaid onto their lateral flexion-extension radiographs using a custom MATLAB script (MathWorks, Natick, MA). Using Hypermesh (Altair, Troy, MI), the superior end plate of the implant was rotationally adjusted to match the intercomponent alignment observed in the radiograph. The actual range of motion (ROM) of the operative level was calculated as the difference between the angular position of the superior end plate in flexion and its angular position in extension (Figure 4.3).

The overlay method was verified with ROM measurements using the technique outlined in Lim et al. (2006) In an effort to reduce error of Cobb angle measurements, the group measured implanted lumbar spine ROM as the change in angle of radiographic landmarks on the metallic end plates and keels of the TDR implant. This method yielded greater precision in ROM measurement than the using the standard Cobb angle measurement. As radiographic measurement of the change in Cobb angle from flexion to extension is a common method to determine spinal ROM, the method by Lim et al. was considered the most accurate method to measure ROM in an implanted segment.

A dynamic, explicit finite element model was developed for each operative level (Figure 4.4). The initial positions of the vertebrae were manually aligned to loaded, neutral positions observed in the lateral radiographs. The vertebrae were discretized into rigid, first-order, tetrahedral elements. A ProDisc-L TDR anterior approach was simulated by removal of the anterior and posterior annulus, the entire nucleus pulposus, and the posterior longitudinal ligament. The lateral regions of the annulus remained intact

71

and were represented by deformable, first-order, hexahedral elements. A hyperelastic, anisotropic material with circumferential fiber orientation was assigned to the lateral annulus. Five major ligaments were included in the model and were represented as two-noded, nonlinear connector elements. These include the superspinous ligament, intraspinous ligaments, intratransverse ligaments, facet capsular ligaments, and ligamentum flavem representations. The implant, which was discretized into rigid, first-order, tetrahedral elements, was initially positioned at the anterior margin of the inferior vertebral body, and the superior end plate was aligned to the loaded, neutral position observed in the lateral radiographs. Rigid body reference nodes, which were created for the end plates and the inlay, were located within the appropriate components. An inferior vertebral rigid body reference node was created and placed within the inferior vertebrae, and a superior vertebral rigid body reference node was placed at the center of rotation of the superior end plate of the implant. The superior and inferior nodes of the lateral annulus were tied to their respective reference node with beam elements. The rigid body reference node of the superior end plate was tied to the superior vertebral rigid body reference node, and the rigid body reference nodes of the inferior end plate and the inlay were tied to the inferior vertebral rigid body reference node. A pressure-overclosure relationship, which was based on prior computational efficiency studies, defined the contact behavior. Contact pairs with linear pressure-overclosure relationships of 10.0 were established between the vertebrae, the superior end plate, and the inferior end plate.

The inferior vertebral body was fixed in all degrees of freedom at its rigid body reference node. Pure moments were applied to the superior rigid body reference node to

72

simulate flexion and extension in the motion segment. Range of motion was limited by bony impingement and implant impingement at the facets and between the end plates respectively (Figure 4.5). Maximum range of motion was defined as the range of motion limited by bony impingement in flexion in addition to the range of motion limited by implant impingement in extension. The implant was advanced in 0.5-millimeter intervals from the initial position to the posterior margin of the inferior vertebra, and the templating procedure was repeated at every interval. This process was performed for each of the four implant sizing configurations outlined previously.

Range of motion data was compiled for all levels implanted with devices of every size at all positions along the AP length of the vertebral body. Using patient-specific lateral radiography images, the actual device position and implant size were identified, and the associate template, or predicted, ROM data was reported. Maximum ROM values were identified for each level, and the corresponding AP position, implant size, and implant angle were reported. An independent-samples t-test was conducted between the actual and predicted motion data to determine the predictability of the templating method in flexion, extension, and total (extension plus flexion) ROM. Predicted ROM data was compared to optimal ROM in flexion, extension, and in total.

4.4 Results

Actual segmental motion data was measured for extension, flexion, and total from lateral radiographs. Extension ranged from 1.5° to 5.0° with an average of 3.1° and a standard deviation of 0.8° (Figure 4.6). Flexion ranged from 1.0° to 11.5° with an average of 5.7° and a standard deviation of 2.8° (Figure 4.7). Total motion ranged from 3.3° to

15.0° with an average of 8.5° and a standard deviation of 3.0° (Figure 4.8). Total

segmental motion was also measured using techniques introduced by Lim et al. (2006),

which yielded total segmental motion data ranging from 4.3° to 14.5° with an average of

8.8° and a standard deviation of 2.9° (Figure 4.3). These ROM values were not

statistically different from ROM values using the radiograph overlay method; t (42)=-

0.25, p=0.804.

Predicted segmental motion data at the actual implant position was acquired for

extension, flexion, and total from the previously described templating procedure.

Extension ranged from 0.9° to 6.7° with an average of 3.2° and a standard deviation of

1.4° (Figure 4.6). Flexion ranged from 1.5° to 10.8° with an average of 5.7° and a

standard deviation of 2.6° (Figure 4.7). Total motion ranged from 2.8° to 14.2° with an

average of 8.9° and a standard deviation of 3.1° (Figure 4.8). At a 95% confidence

interval predicted ROM was not statistically different to the actual ROM. In flexion, there

was no significant difference in the predicted ROM data (M=5.5°, SD=2.6°) and the

actual ROM data (M=5.5°, SD=2.8°); t (42)=0.018, p=0.986. In extension, there was no

significant difference in the predicted ROM data (M=3.2°, SD=1.4°) and the actual ROM

data (M=3.1°, SD=0.8°); t (35)=-0.413, p=0.682. For total motion, there was no

significant difference in the predicted ROM data (M=8.7°, SD=3.1°) and the actual ROM

data (M=8.5°, SD=3.0°); t (42)=-0.137, p=0.892. The percent differences between the

predicted and the actual motion data in extension, flexion, and total was calculated.

Percent differences in extension ranged from 0% to 110% with an average of 25.2% and

standard deviation of 23.2%. Percent differences in flexion ranged from 0% to 94.3%

with an average of 22.6% and standard deviation of 21.3%. Percent differences in total

motion ranged from 2.9% to 27.1% with an average of 11.7% and standard deviation of

5.8% (Table 4.2).

Optimal segmental motion data and implant position were acquired for extension,

flexion, and total from the templating procedure. Extension motion ranged from 1.6° to

6.7° with an average of 3.8° and a standard deviation of 1.6° (Figure 4.6). Flexion ranged

from 1.5° to 10.8 ° with an average of 6.0° and a standard deviation of 2.6° (Figure 4.7).

Total motion ranged from 4.3° to 16.3° with an average of 9.7° and a standard deviation

of 3.2° (Figure 4.8). ROM improvement, or the difference between predicted and optimal

ROM, was achieved in at least half of the segments in flexion, extension, and total

motion. In flexion, improvements ranged from 0° to 3.2° with an average of 0.5° and a

standard deviation of 0.8°. In extension, improvements ranged from 0° to 3.4° with an

average of 0.6° and a standard deviation of 1.0°. In total motion, improvements ranged

from 0° to 4.4° with an average of 1.1° and a standard deviation of 1.3°. Greater

segmental motion could have been achieved in 86% of the cohort, and greater motion of

over 1.0° could have been achieved in 36% of the cohort had implant selection and

placement been ideal. Optimal position relative to the implanted position ranged from 4.5

mm posterior to 0.75 mm anterior with an average of 0.8 mm posterior and a standard

deviation of 1.4 mm. Optimal ROM of one segment was found to be less than 5°.

4.5 Discussion

Actual ROM values were effectively evaluated by calculating the change in angle

of 3D models overlaid onto lateral flexion-extension radiographs. The method was

validated by comparison to ROM values calculated from techniques outlined by Lim et al. (2006). Application of the overlay method enables 3D FE models of the structures of the spine to be accurately aligned to in vivo, loaded positions as observed in lateral radiographs and enables models of orthopedic devices, including TDR implants, to be properly aligned to their in vivo alignment and configuration. Proper initial alignment of components of the natural or implanted spine within computational models can yield more realistic and more accurate outcomes.

Templated, model-based predictions of ROM were validated by comparison to measured ROM for 22 TDR surgeries. Actual and predicted values were not significantly different and yielded an average percent difference in total ROM of 11.7%. Results of this study were not sensitive to the loading conditions of the models, including compressive follower loads and moments, as flexion-extension ROM was predicted accurately based on facet and implant impingement alone. In reality, soft tissue structures such as the facet capsules can also play a role in load sharing and, thus, ROM in the spinal segment during motion. This is evident in the lateral radiographs as facet and implant impingement was not observed in the flexion and extension x-rays for every segment. While currently impossible to measure in clinic, load sharing contributions can be determined in vitro by modeling the torque-rotation behavior of the joint. For the purposes of this study however, the effect of soft tissue structures on load sharing and ROM were not studied, and only contact between the facets and components of the implant were considered as limiting factors of ROM in flexion and extension. Factors that might limit ROM such ligament laxity in the facet capsule or the presence of scar tissue

were not considered. On the other hand, soft tissue structures, not implant impingement, likely combine with facet anatomy to limit ROM in axial rotation and lateral bending. For this reason, only flexion and extension motions were modeled in this study. Post-operative computational evaluations of TDR surgeries can inform clinicians of expected ROM at patient follow-up and guide preparation for post-operative therapies, ultimately improving patient outcomes.

The three-dimensional templating procedure effectively optimized implant selection and placement to maximize ROM for a patient undergoing TDR surgery. Average optimal ROM values for flexion, extension, and total motion were greater than average ROM values of the as-implanted cases. 0.5 mm was chosen as the interval for implant position during the optimization procedure because ROM was not significantly different when using 0.1 mm and was over 10% different when using 1.0 mm intervals. Additionally, clinicians are able to align implants within 0.5 mm of the template via perioperative radiographs. Retrospectively ROM could have been improved by at least one degree in over 63% of the cohort had a pre-operative templating procedure been performed. Inappropriate implant selection in 9 cases and imperfect implant placement in 16 cases prevented 86% of the cohort from realizing their maximum ROM. In one case, the templating procedure would have predicted inadequate post-operative ROM and would have prompted alternative treatment.

The procedure can provide insight into relationships between patient anatomy and post-operative ROM at the implanted level. With deeper understanding of these relationships, TDR manufacturers can design devices that serve larger, more variable

populations, and clinicians can more accurately judge post-operative ROM based on patient anatomy. Templating results in the current study elucidated how key anatomical differences influenced ROM. The anatomy of one level, who had achieved less than 5° ROM, featured a smaller transverse facet joint angle of 140°. Observations of the facets in flexion revealed that the smaller angle closed the facet motion pathway, inducing earlier facet impingement, and reducing ROM. In contrast, the anatomy of the segment that achieved the greatest total ROM featured a larger transverse facet joint angle of 164°. Observations of the facets in flexion revealed that the larger angle opened the facet motion pathway, resulting in later facet impingement, and increasing ROM (Figure 4.9).

This investigation is limited in several ways. First, the sample size is limited to 22 segments, which yields large variation in the results and may not reflect the anatomical variability of the population. To increase sample size of the study, double-level TDR surgeries were included and might have had an effect on the ROM results as ROM of the inferior implanted level after a double-level TDR surgery is known to be typically less than ROM of the superior level. Additionally, actual ROM as measured by both the overlay method and the method by Lim et al. (2006) was performed by a single observer, which generates additional uncertainty in the results of actual ROM. It is important to note that data acquisition is inherently limited by the accuracy of the data itself. Accuracy of the segmentation methods and techniques to measure actual ROM are dependent upon the resolution of the radiographs, which in this case are resolved to 0.31 mm pixel sizes and 1 mm slice thicknesses.

While previous groups have clinically investigated patient ROM after TDR surgery for a cohort of over one hundred subjects (Lemaire et al. 2005, David 2007, Siepe et al. 2014), this study looks to evaluate post-operative TDR surgery, screening patients for TDR surgery, and pre-operatively identifying optimal implant size and placement using finite element techniques. Development of accurate, robust computational models is time intensive as each operative level must be segmented slice by slice, the bones and implant must be properly meshed, and the implant must be manually aligned to its initial orientation. To determine optimal implant size and position, flexion and extension must be simulated with four different implant sizes placed in approximately twelve positions along the anterior-posterior length of the vertebral end plate. This amounts to approximately fifty explicit finite element evaluations for each operative level. As a result, a cohort size of 22 segments is sufficient to achieve the objectives of this study including to validate the proposed preoperative templating process and to retrospectively determine if pre-operative templating would have altered surgical decisions regarding patient suitability, implant size, and implant placement.

The successes of the templating method are built on the premise that increased ROM leads to more favorable patient outcomes, but it is important to note that results yielded by the procedure can lead to some negative outcomes. First, capsular tensile forces and facet joint forces are dependent upon implant placement with more posterior positioned implants yielding larger facet joint loads. Misalignment or imbalance in the anterior-posterior implant position can transfer increased loads through the facet joints and accelerate facet joint disease (FJD). Consideration of facet joint loads in the

79

templating method can improve patient outcomes and reduce revision surgeries due to FJD. Secondly, while post-operative ROM is linked to positive patient outcomes, excessive ROM can over-articulate the facet joints, causing facet capsule ligament injuries. Facet over-articulation should be considered when reviewing implant placement and sizing values reported by the templating method. Finally, the templating method typically identifies smaller implant sizes as ideal because the location of the center of rotation in smaller implants closely matches the natural center of rotation, leading to greater projected ROM. However, the smaller footprint size may insufficiently cover the end plate, which can lead to increased risks of device migration and subsidence.

Future work will focus to improve templating method by increasing the size of the cohort, differentiating the cohort by gender, age, and implanted level, and isolate double-level from single-level surgeries. Verification the overlay method with multiple observers can reduce the uncertainty in actual ROM measurements and increase confidence in the overlay method. Improvements to the templating procedure will include multi-segment, validated FE models to assess load transfer through facet joints, risk of facet capsule strain and injury, likelihood of device subsidence and migration, and effects on soft tissues at the adjacent levels. In the long term, the group would like to develop templating software to assist clinicians in patient screening for TDR, pre-surgical planning, and post-operative patient evaluation.

Model-based predictions of segmental ROM were validated to measured ROM for 22 levels with TDRs, indicating that ROM can successfully be predicted based on facet and implant impingement. Relationships between anatomy, implant sizing and alignment

were effectively evaluated through a three-dimensional templating procedure.

Retrospectively, the templating process demonstrated that ROM could be achieved in

86% of the cohort had the implant been selected and/or positioned differently, and

identified one case where anatomy was not suitable for TDR and would have prompted

an alternative treatment. By maximizing post-operative ROM for implanted patients and

pre-operatively disqualifying patients unsuitable for TDR treatment, the proposed pre-

operative templating procedure can improve patient outcomes and encourage advances to

TDR technologies in the long term.
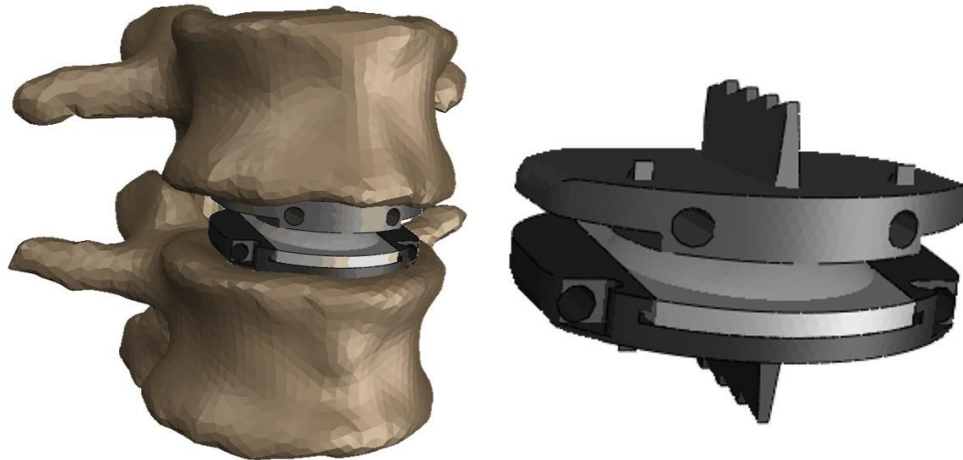
Figure 4.1 Second generation ProDisc-L total disc replacement device is based on a ball-and-socket concept. The design consists of a superior end plate with central keel, a high-modulus polyethylene inlay, and an inferior end plate with central keel.

Extension　Neutral　Flexion
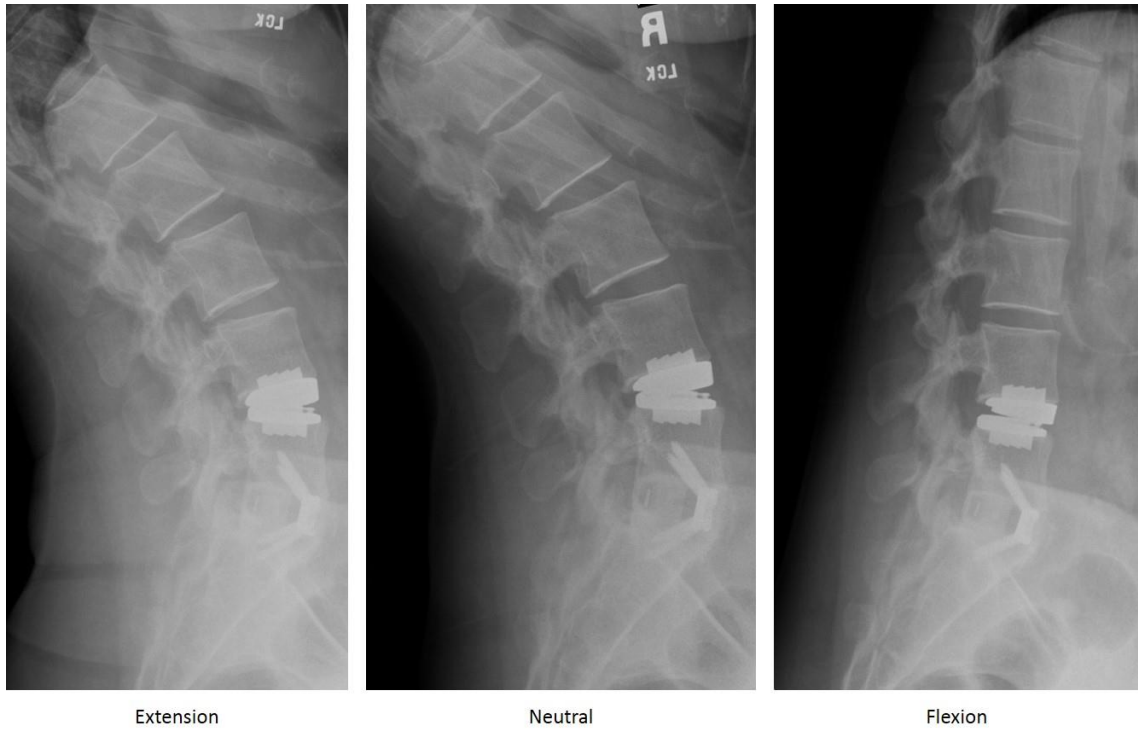
Figure 4.2 Post-operative follow-up examination at six weeks. Standing, loaded fluoroscopic images taken of flexion, neutral, and extension.
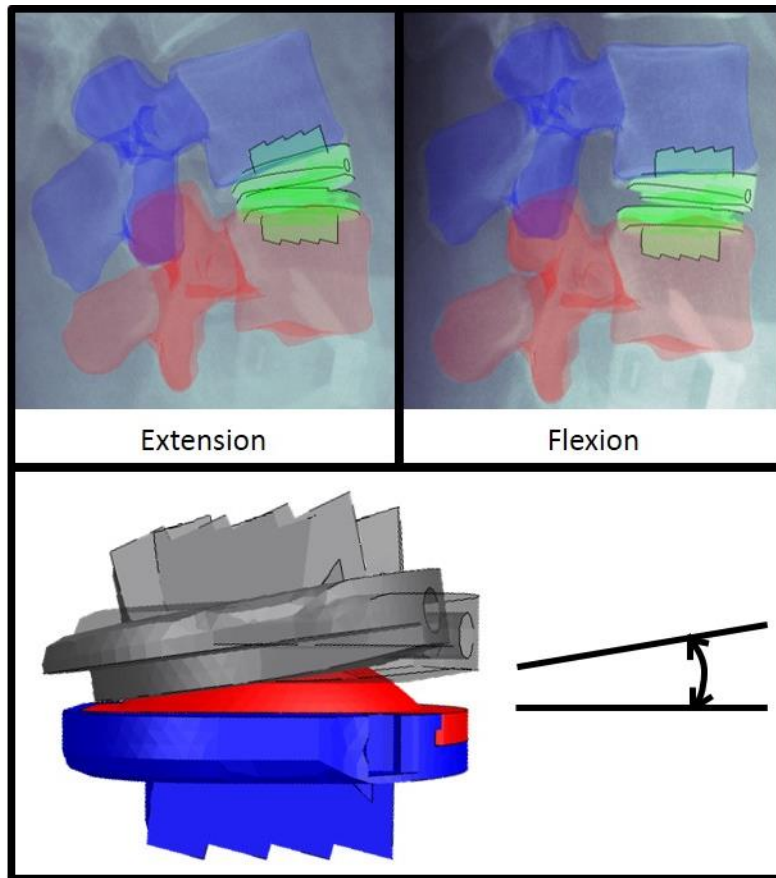
Figure 4.3 Three-dimensional model overlay with flexion-extension x-ray images. Change in angle measured from resulting 3D model.
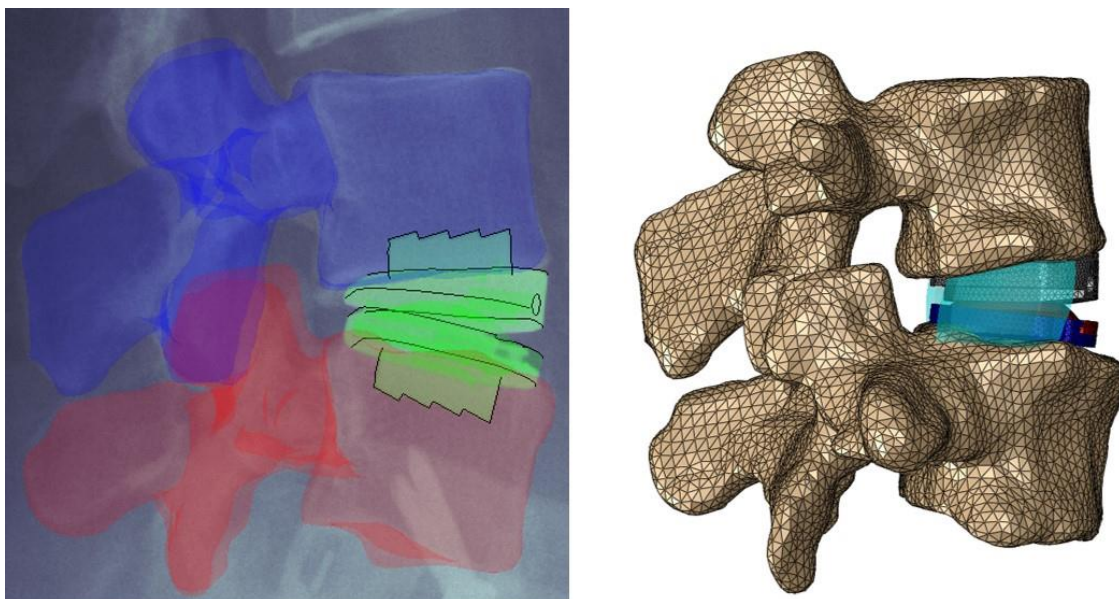
Figure 4.4 Three-dimensional model overlay with loaded, neutral-position x-ray images for finite element model. Finite element model includes vertebral bodies, implant in neutral position, lateral annulus, and major ligaments.
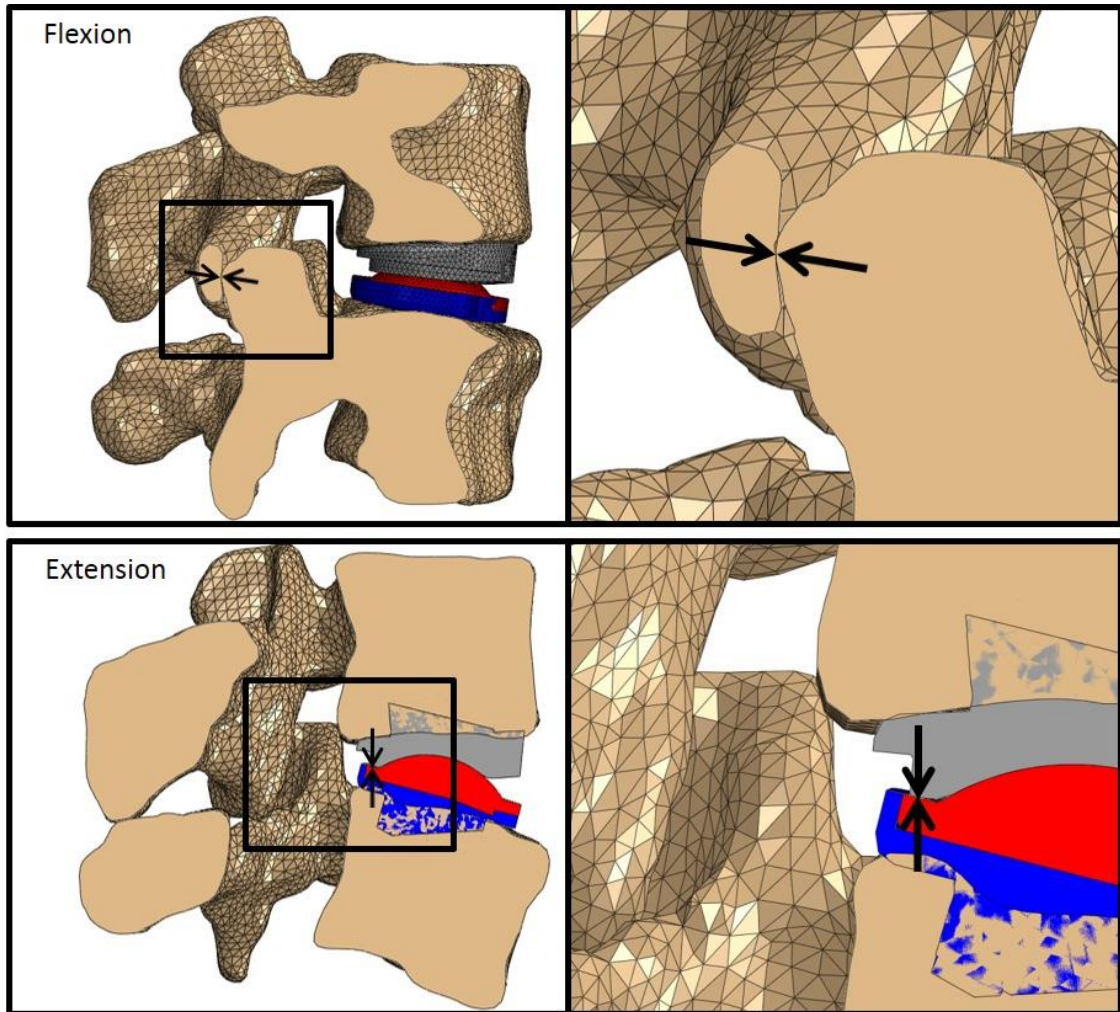
Figure 4.5 ROM evaluation from templating procedure is typically limited by facet impingement in flexion (above) and implant impingement in extension (below).

Comparison of Range of Motion in Extension
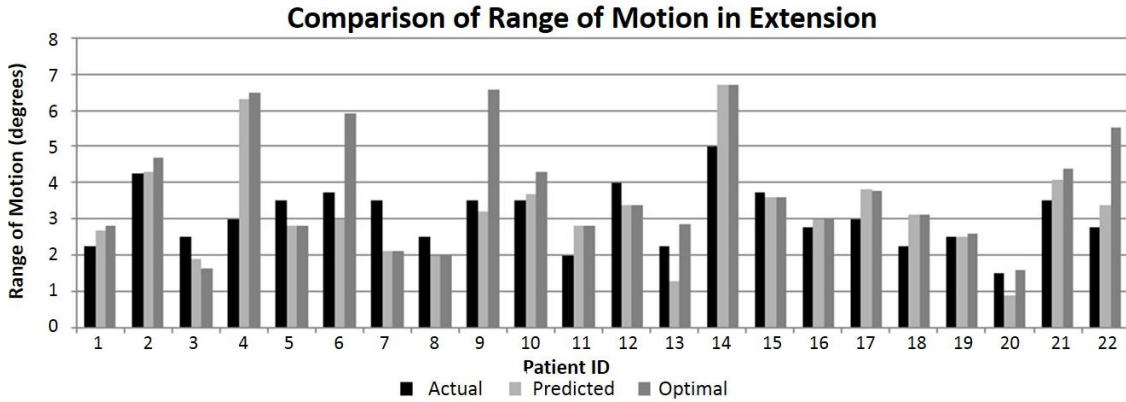
Figure 4.6 Comparison of actual, predicted, and optimal range of motion in extension for patient cohort. The difference between the actual and predicted ROM averaged 25.2%. ROM in extension of eleven of the twenty two cases could have been improved by change in implant size and/or position, and could have improved by over one degree in four cases.

Comparison of Range of Motion in Flexion
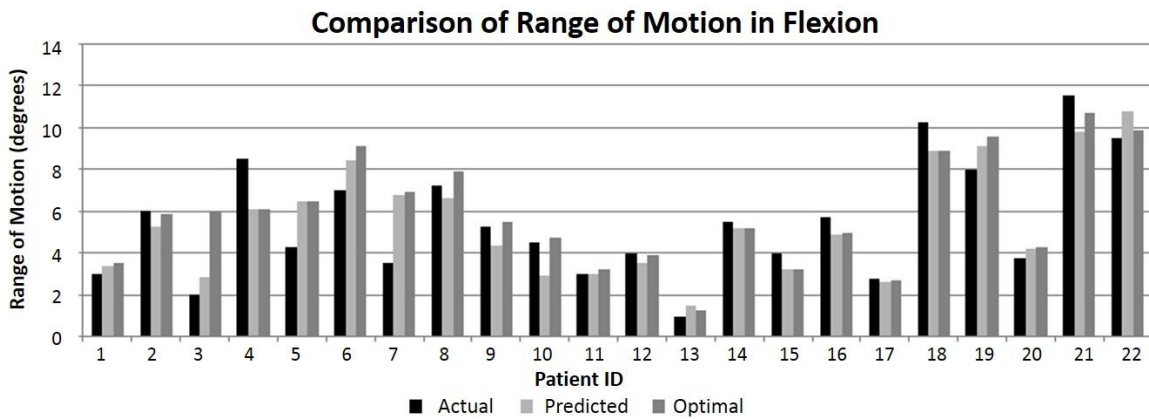
Figure 4.7 Comparison of actual, predicted, and optimal range of motion in flexion for patient cohort. The difference between the actual and predicted ROM averaged 22.6%. ROM in flexion of fifteen of the twenty two cases could have been improved by change in implant size and/or position, and could have improved by over one degree in four cases.

Comparison of Total Range of Motion
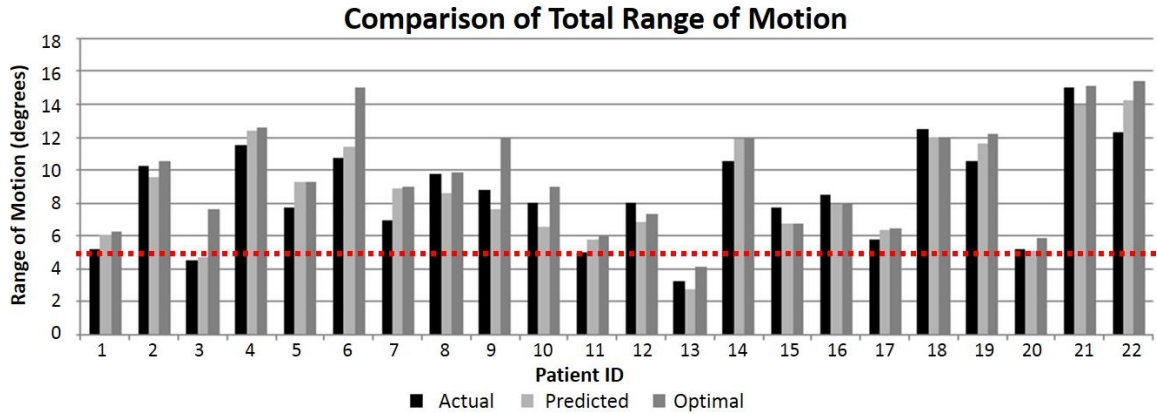
Figure 4.8 Comparison of actual, predicted, and optimal range of motion for patient cohort. The difference between the actual and predicted total ROM averaged 11.8%. ROM of nineteen of the twenty two cases could have been improved by change in implant size and/or position, and could have improved by over one degree in eight cases. Increased risk of ASD can occur if post-operative ROM does not exceed 5 degrees, shown here with the dotted line. Had a templating procedure been utilized pre-operatively, Patient 13 would not have qualified for TDR as he would be at risk of ASD.
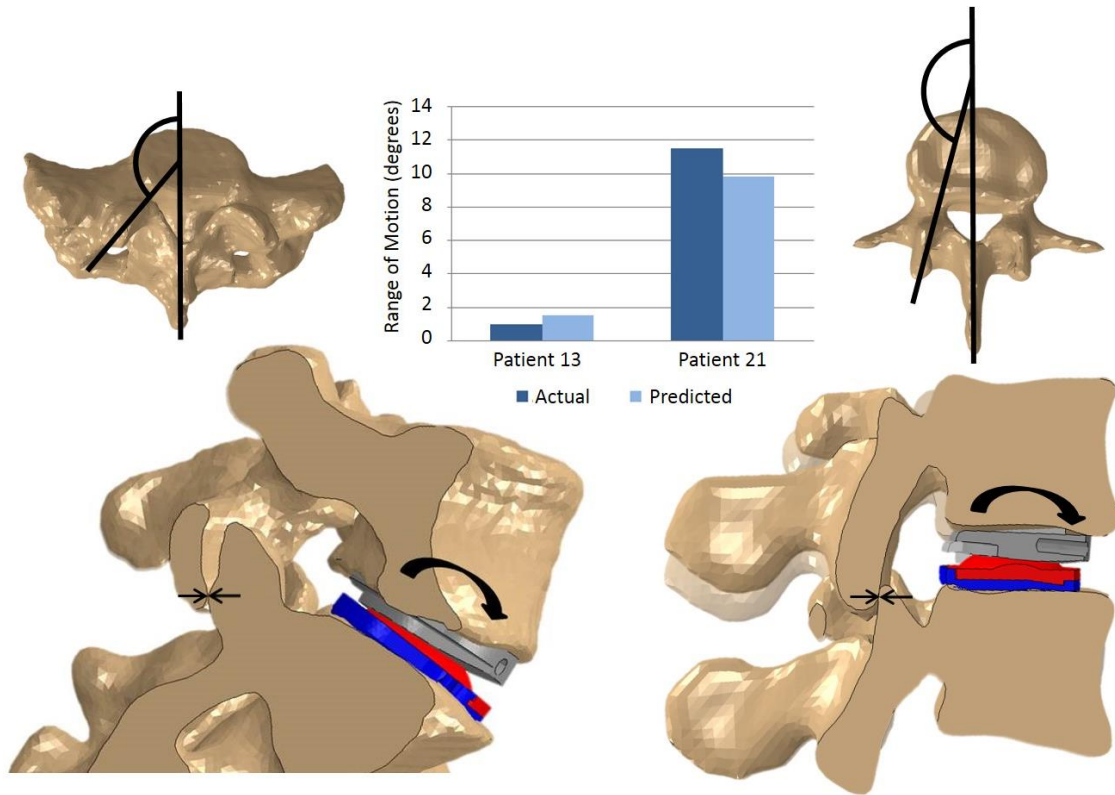
Figure 4.9 Patient geometry influences range of motion in flexion. The smaller transverse facet angle of the sacrum of Patient 13 yields earlier facet impingement, which results in poor ROM (left). On the contrary, larger transverse facet angles of the L5 of Patient 21 yields advanced facet impingement, which results in greater ROM (right).

Table 4.1 Age, weight, height, and BMI statistics differentiated by gender for 22 patients: mean ± standard deviation (range).

	N	Age	Weight (lbs)	Height (in)	BMI
Males	16	36.3 ± 6.7 (24-50)	190.6 ± 37.5 (147-257)	69.4 ± 3.1 (65-74)	27.6 ± 3.4 (23-33)
Females	6	34.5 ± 6.9 (21-40)	173.0 ± 62.0 (125-280)	65.6 ± 3.1 (63-69)	27.7 ± 7.6 (22-41)
Total	22	35.8 ± 6.6 (21-50)	185.9 ± 44.0 (125-280)	68.3 ± 3.5 (63-74)	27.6 ± 4.6 (22-41)

Table 4.2 Comparison of actual versus predicted percent difference data for flexion, extension, and total ROM.

PATIENT	EXTENSION			FLEXION			TOTAL		
			%			*%*			*%*
ID	*ACTUAL*	*PREDICTED*	*DIFF.*	*ACTUAL*	*PREDICTED*	*DIFF.*	*ACTUAL*	*PREDICTED*	*DIFF.*
1	2.3	2.6	15.6	3.0	3.4	13.3	5.3	6.0	14.3
2	2.8	3.0	9.1	5.8	4.9	14.8	8.5	7.9	7.1
3	5.0	6.7	34.0	5.5	5.2	5.5	10.5	11.9	13.3
4	3.5	3.7	5.7	4.5	2.9	35.6	8.0	6.6	17.5
5	2.5	2.0	20.0	7.3	6.6	9.0	9.8	8.6	11.8
6	3.5	3.2	8.6	5.3	4.4	16.2	8.8	7.6	13.1
7	2.3	1.3	42.2	1.0	1.5	50.0	3.3	2.8	13.8
8	3.0	3.8	26.7	2.8	2.6	5.5	5.8	6.4	11.3
9	4.3	4.3	1.2	6.0	5.3	11.7	10.3	9.6	6.3
10	2.0	2.8	40.0	3.0	3.0	0.0	5.0	5.8	16.0
11	4.0	3.4	15.0	4.0	3.5	12.5	8.0	6.9	13.8
12	2.5	1.9	24.0	2.0	2.8	41.5	4.5	4.7	5.1
13	3.0	6.3	110.0	8.5	6.1	28.2	11.5	12.4	7.8
14	3.8	3.6	4.0	4.0	3.2	20.0	7.8	6.8	12.3
15	3.5	2.1	40.0	3.5	6.8	94.3	7.0	8.9	27.1
16	3.5	2.8	20.0	4.3	6.5	52.9	7.8	9.3	20.0
17	3.8	3.0	20.0	7.0	8.4	20.0	10.8	11.4	6.0
18	2.3	3.1	37.8	10.3	8.9	13.2	12.5	12.0	4.0
19	2.5	2.5	0.0	8.0	9.1	13.8	10.5	11.6	10.5
20	1.5	0.9	40.0	3.8	4.2	12.0	5.3	5.1	2.9
21	3.5	4.1	17.1	11.5	9.8	14.8	15.0	13.9	7.3
22	2.8	3.4	23.6	9.5	10.8	13.7	12.3	14.2	15.9
AVERAGES	3.1	3.2	25.2	5.5	5.5	22.6	8.5	8.7	11.7
STD DEV	0.8	1.4	23.2	2.8	2.6	21.3	3.0	3.1	5.8
MAX	5.0	6.7	110.0	11.5	10.8	94.3	15.0	14.2	27.1
MIN	1.5	0.9	0.0	1.0	1.5	0.0	3.3	2.8	2.9

CHAPTER 5: TEMPLATING ACTIV-L TOTAL DISC REPLACEMENT SURGERY

5.1 Abstract

Post-operative outcomes of lumbar TDR have been shown to be noninferior to

outcomes of fusion, the current clinical standard of care to treat chronic low back pain

(LBP). Aesculap's Activ-L is an FDA-approved implant with a variable center of rotation

(COR) which looks to eliminate LBP, restore disc height, and achieve greater range of

motion (ROM) than total disc replacement (TDR) devices with a fixed COR including

the Depuy Synthes' ProDisc-L. The Activ-L consists of one superior end plate that

articulates over a plastic, spherical center inlay that is permitted to translate in the

anterior-posterior direction within the inferior end plate. The configuration allows the

center of rotation to translate with the center inlay. There are currently no reported

clinical outcomes associated with this device, so the objectives of the current study were

to perform a pilot study to characterize unconstrained mechanical behavior of the Activ-L

implant, assess optimal ROM and inlay translation of the Activ-L implant in its post-

operative configuration, and compare post-operative ROM between patients implanted

with the Activ-L and the ProDisc-L devices. Five subjects were implanted with the Activ-

L TDR and post-operative ROM was evaluated via radiographs at six-week follow up.

Subject anatomy was segmented and virtually implanted with Activ-L implant geometry.

FE analyses that allowed the center inlay to translate freely were performed. Model

results revealed that subjects with greater inlay translation achieved greater ROM. Next, implants were virtually positioned in their inserted flexion and extension locations separately, and ROM was accurately predicted via FEA at those locations. For all subjects, optimal ROM values were consistently greater than actual ROM at the post-insertion location. It is important to note that while two subjects achieved over 20 degrees of optimal ROM, this magnitude of ROM is not physiologic and would be likely constrained by soft tissue structures. Finally, patients implanted with the Activ-L achieved greater ideal ROM than patients implanted with the ProDisc-L device. Results of the study are limited by a small sample size, modeling assumptions, and resolution of the radiographs. Computational assessments of implant behavior validated to results from in vivo studies could prompt device manufactures to optimize key design features and encourage clinicians to improve implantation methods. Comparisons between post-operative ranges of motions of different devices can reveal design considerations that significantly influence ROM and patient outcomes.

5.2 Introduction

TDR has been shown to be viable alternative to fusion in treating chronic LBP (Blumenthal et al., Lemaire et al., David et al., Rainey et al.). At long-term follow-up, ODI scores, VAS pain scores, health status questionnaire scores, and disc height were reported non-inferior to fusion groups. Moreover, higher rates of surgical success, patient satisfaction, return to employment, and segmental ROM and lower rates of revision surgeries, long-term disability, and incidence of ASD were reported after TDR surgery than fusions. Incidence of device failures, ASD, and FJD leading to revision surgeries

93

remain significant, and the development of treatment substitutes like dynamic

stabilization and nucleus replacements cast doubts upon the future of lumbar TDR

surgery. Improvement TDR outcomes in the long term can prove clinical efficacy and

establish disc arthroplasty as a viable treatment option for LBP.

Success of TDR surgery is dependent upon many factors including appropriate

patient selection, proper surgical alignment, and optimal implant design. In an effort to

optimize design, spine biomechanics companies have improved material selection and

device geometry. Biocompatible materials of the articular surfaces are selected to exhibit

reduced wear characteristics and low friction behavior, and biocompatible materials at the

bony interfaces are chosen to maximize fixation, efficiently transfer loads across the

joint, and resist corrosion (Hallab et al.). Ideal device geometry simplifies the surgical

procedure to reduce chances of implant failure due to technical error, to remain stable

once inserted, to restore neural foramina and disc height, and to most accurately

reproduce natural physiological movement at the instrumented level without overloading

the facet joints. In an attempt to design a TDR that mimics normal motion, DePuy

Synthes developed the ProDisc-L which allows rotation about a fixed point. However,

Gertzbein et al. have shown that natural segmental center of rotation tends to move along

a curved pathway. As such, devices with a fixed rotation center can inadequately mimic

natural spinal motion, which could lead to increased facet joint loads, insufficient post-

operative ROM, and poor patient outcomes. The Activ-L TDR designed by Aesculap is

designed to more accurately match physiological motion whilst maintaining adequate

stabilization by incorporating anterior-posterior translation capabilities of its UHMWPE

inlay. The device has only recently been approved by the FDA for use in the United States, and few studies have quantified the biomechanical behavior of the Activ-L to date (Ha et al. 2009, Austen et al. 2012); even fewer have compared mechanical behavior of the Activ-L with the ProDisc-L (Zander et al. 2009). A computational templating technique similar to the one described in Chapter 4 is employed to predict ROM of the Activ-L implant in its post-operative flexion-extension configurations.

The objectives were to perform a pilot study to 1) evaluate mechanical behavior of the Activ-L implant in ideal conditions, allowing free, frictionless translation of the inlay within the end plate, 2) evaluate flexion and extension ROM at the radiographically-measured inlay positions and compare these values to ideal ROM and ROM measured from radiographs, 3) to analyze actual post-operative inlay translation to optimal inlay translation, and 4) compare ideal ROM of the Activ-L implant to optimal range of motion of the DePuy Synthes ProDisc-L.

5.3 Methods

In the current study, Activ-L TDRs were implanted in five patients. The patient set consisted of two males and three females with an average age of 36 ranging from 20 to 53. Weight, height, and body mass index averaged 168.4 ± 15 pounds, 68 ± 5 inches, and 26 ± 3, respectively. Single-level surgery was performed on all five patients (Table 5.1). Flexion, extension, and neutral radiographs of all patients were obtained at the six-week follow-up.

Three-dimensional models of the operative vertebrae of each patient were extracted from computed tomography (CT) scans using Scan IP (Simpleware, Exeter,

95

UK). The average CT image pixel size was 0.31 millimeters, and the average slice

thickness was 1 millimeter. Activ-L implant geometry was generated from laser scan of

an acquired device and publically-available documentation (Figure 5.1c, 5.1d). Vertebral

models and actually implanted device geometries of each operative level were manually

overlaid onto their lateral neutral configurations using the overlay method described and

verified Chapter 4. With the implant aligned to its neutral position, a dynamic, explicit

FE model was developed for each case including representations of lateral annulus

fibrosus and ligamentous structures (Figure 5.1e). A 500 N-m pure moment was applied

to the superior bone about the rotational center of the inlay to simulate flexion and

extension motions, and a nominal compressive force normal to superior endplate of the

bone was applied to the superior end plate of the device. The inferior bone and inferior

end plate of the device were fixed in all degrees of freedom. Frictionless, rigid body

contact definitions with linear pressure-overclosure relationships of 10.0 were established

between the superior end plate, center inlay, and the inferior end plate (Figure 5.1f),

which were defined as rigid bodies. To simulate ideal device conditions, the inlay was

free to translate a maximum of 2 millimeters in the anterior-posterior direction. Resulting

ROM was measured as the angular difference in final position of the superior vertebra

from extension to flexion, and inlay translation was measured as changed in anterior-

posterior position from extension to flexion.

Actual ROM was measured using the overlay method. Vertebral models and

actually implanted device geometries of each operative level were manually overlaid onto

their lateral flexion and extension radiographs (Figure 5.2). The actual ROM of the

operative level was calculated as the difference between the angular position of the superior end plate in flexion and its angular position in extension. The actual translation of the center inlay was calculated as the difference in its anterior-posterior position in flexion and extension. To evaluate flexion ROM in the actual inlay position, the implant was aligned and fixed to its actual configuration in flexion, and flexion was simulated in that alignment. To evaluate extension ROM in the actual inlay position, the implant was aligned and fixed to its actual configuration in extension, and extension was simulated in that alignment. The sum of the flexion and extension ROM was compared to actual ROM and ROM determined from the ideal case.

Using data reported in Chapter 4, Subject 22, the subject who had achieved the most post-operative ROM with a ProDisc-L device, was virtually implanted with the Activ-L implant. Implant position was optimized to achieve maximum ROM. With translation of the center inlay unconstrained, flexion and extension motions were simulated, and the resulting ROM was reported and compared to optimal ROM values from the ProDisc-L simulations (Figure 5.3). FSUs of subjects who had received the Activ-L devices were also virtually implanted with ProDisc-L devices of equivalent size. ROM was compared between the group implanted with the ProDisc-L and the group implanted with the Activ-L.

5.4 Results

FE simulations of ideal flexion and extension motions were completed, allowing free, frictionless translation of the inlay within the end plate. Translations of the center inlay averaged 1 mm in flexion and 0.25 mm in extension across all subjects. Inlays in

97

three subjects translated over 1 millimeter, and in 2 subjects, the inlay translated

approximately 0.5 millimeters. Four subjects achieved over 10 degrees ROM, and

Subject 1 achieved under 7 degrees ROM (Figure 5.4). Observations of the motions

provided insight into the mechanical behavior of the implanted joint. In a typical flexion

motion, facets make initial contact, forcing the center inlay to translate to its posterior

margin and allowing the facets to slide over one another until implant or hard facet

impingement occur. In typical extension motions, implant or facet impingement limits

ROM. The ROM of Subject 1 was limited by facet impingement in both flexion and

extension, and the ROM of Subject 2 was limited by implant impingement in both flexion

and extension.

FE simulations of flexion and extension of the Activ-L device in its actual

configurations revealed expected ROM for each subject, which were compared to actual

and ideal kinematic values. Percent difference between the sum of flexion and extension

motions in the actual configurations and actual ROM averaged 10%. Four subjects

achieved ROM in their actual inlay positions of less than 7 degrees (Figure 5.5). ROM of

Subject 1 was limited by facet impingement in flexion and extension, and ROM was

limited by a combination of facet and implant impingement in the other subjects. Subject

2 achieved range of motion in its actual implant configuration of over 15 degrees, which

was limited by implant impingement in flexion and extension. Actual translation of the

center inlay did not occur in extension for any subject. Percent difference between ideal

and actual inlay translations for Subject 1 was 5% and for other subjects was over 100%.

The difference in resulting ROM between the ideal and actual cases averaged 9.7 degrees

(Figure 5.5).

Ideal ROM of subjects implanted with the Activ-L was compared to optimal

ROM of subjects implanted with the ProDisc-L. When virtually implanted into the

ProDisc-L patient, the Activ-L achieved over 5 degrees more ROM than the ProDisc-L

(Figure 5.6). ROM was limited by both facet and implant impingement in the ProDisc-L

case and limited by only implant impingement in the Activ-L case. When virtually

implanted into the Activ-L subjects, the ProDisc-L achieved lesser ROM than actual

Activ-L range of motion in three cases. The ProDisc-L achieved lesser ROM than

optimal Activ-L range of motion in all cases. Motion in Subject 2 was over ten degrees

more in the Activ-L case than the ProDisc-L case. For the other subjects, difference in

ROM averaged 1.8 degrees between Activ-L and ProDisc-L cases.

5.5 Discussion

This study successfully developed a tool for evaluating the idealized mechanical

behavior of the Aesculap Activ-L implant and assessing the allowable motion of an

implanted segment by allowing free, frictionless translation of the inlay within the end

plate. ROM was defined as the difference in implant angle from the motion extent in

flexion to the motion extent in extension. Thus, initial placement of the implant in its

neutral configuration was inconsequential to total ROM and center inlay translation; total

ROM and inlay translation was the same when the implant was initially placed in the

extension configuration and rotated to its flexion configuration. All implant and bony

components were defined as rigid body, and all contact interactions were defined as rigid

body contact. Additionally, friction was zero between the implant components. In reality, outcomes may be influenced by soft tissue balancing of ligaments, the lateral annulus, and scar tissue, contact pressures between implant components, and friction at articular surfaces. This may explain why the realized center inlay translation and ROM are significantly lower than in the ideal cases reported in this study.

Patient geometry proved to play a significant role in ROM in the unconstrained cases as subject-specific differences in range of motion and inlay translation was observed. For subjects where the center inlay translated over 1 mm from extension to flexion ROM of over ten degrees was achieved (Figure 5.4). Subject 2 achieved the greatest ROM of 27 degrees and was limited by implant impingement in both flexion and extension. Adequate space was evident between the facets of the zygopophysial joint, resulting in no facet impingement and a larger ROM. Subject 1, one of two cases where the center inlay translated approximately 0.5 mm, achieved the least ROM of 7.4 degrees (Figure 5.4). In this particular case facet impingement restricted motion in flexion and extension as the space between facets was limited. It is important to note that for the ideal simulations,

The study accurately predicted ROM at the actual position of the center inlay for all five subjects. Predicted ROM values averaged 10% different to actual ROM (Figure 5.5), indicating that motion calculated from facet and implant impingement can be predictive of actual post-operative ROM. Actual translation of the center inlay may have only occurred in flexion because posterior translation of the center inlay in flexion opens the facets, allowing increased motion at the joint. While in extension, compressive loads

seen through the joint may force the inlay more anterior and close the facet joints. A more anterior post-operative neutral position of the center inlay may yield larger translation of the inlay and increased ROM. Optimal ROM was calculated to be significantly larger than the actual ROM values in all five cases, and anterior translation of the center inlay during extension was evident in four cases. Actual ROM may have failed to achieve optimal values because the center inlay did not actually translate in a majority of the subjects in flexion and failed to translate for all subjects in extension, resulting in earlier impingement and lesser ROM. Failure of the inlay to translate as the segment is in motion might be indicative that other nonlinearities, such as scar tissue or stiff ligament behaviors, are actually present within the implanted joint. Evaluations of post-operative magnetic resonance images might elucidate the strength of this hypothesis.

The study effectively compared the motion behaviors of subjects implanted with the Activ-L to subjects implanted with the ProDisc-L. A subject, actually implanted with the ProDisc-L, achieved virtually greater ideal ROM when implanted with the Activ-L implant than in the actual case (Figure 5.6). In both flexion and extension, ROM was limited by only facet impingement using the ProDisc-L and limited by only implant impingement using the Activ-L. This suggests that the fixed COR of the ProDisc-L yields earlier facet impingement, while the variable COR of the Activ-L avoids facet impingement and maximizes ROM. While Subject 2 achieved 11.6 degrees more actual ROM with the Activ-L than with the ProDisc, actual ROM was comparable between the two devices for the other four cases (Figure 5.6), indicating that ROM of a total disc replacement device is variable with patient anatomy. ROM of Subject 1 and Subject 5 did

101

not exceed 5 degrees ROM, and these patients may have been prompted for alternative treatment had this information been known preoperatively. Subject 2 achieved over 20.5 degrees more ideal ROM with the Activ-L than with the ProDisc-L, and its inlay actually translated over 0.8 mm in flexion. It is clear that the ability of the inlay to post-operatively translate during flexion and extension plays a significant role in the ideal ROM outcomes of the patient. ROM outcomes of patients implanted with a device whose inlay is incapable of independent translation, like the ProDisc-L, are dependent upon optimal implant selection and placement to maximize ROM. It is important to note that post-operative ROM is not always indicative of patient outcome. Reduced bone mineral density, presence of scar tissue, post-operative ligament laxity, adjacent segment degeneration, and evidence of osteoarthritis at the facet joints are a few of the many external factors that can influence post-operative outcomes. Excessive ROM at the implanted level has the potential to over-distract the facet joints leading to ligament strain, facet joint pain, and facet joint arthritis.

As a pilot study, this study is limited to five subjects and a short follow up duration. Continuing work looks to increase the size of the cohort and monitor subjects at longer follow-up dates. Additionally, actual ROM as measured by the overlay method was performed by a single observer. Accuracy of the segmentation methods and techniques to measure actual ROM are dependent upon the resolution of the radiographs, which in this case are resolved to an average pixel size of 0.31 mm and average slice thickness of 1 mm. While simplifications of the computational models significantly reduced computational time, accuracy of the results may have been compromised. The

simulations assumed frictionless, rigid body contact at the interfaces between implant

components. In reality, establishing master/slave contact definitions between the implant

components permits deformable contact which may improve the accuracy of the

simulations. Inclusion of nonzero friction factors and optimized pressure-overclosure

relationships may allow the simulations to better mimic the contact environment with the

Activ-L device. In addition, improvements to computational models will be made to

incorporate additional nonlinear elements, such as ligament laxity and scar tissue, to input

patient-specific loading parameters, and to output additional measures of interest, such as

facet contact area, facet contact pressure, and facet ligament elongation. Further insight

into the mechanical behavior of TDR implants with variable centers of rotation and

comparisons to implants with fixed rotational centers can provide insight into optimal

design features, maximize post-operative ROM, and improve long term patient outcomes.
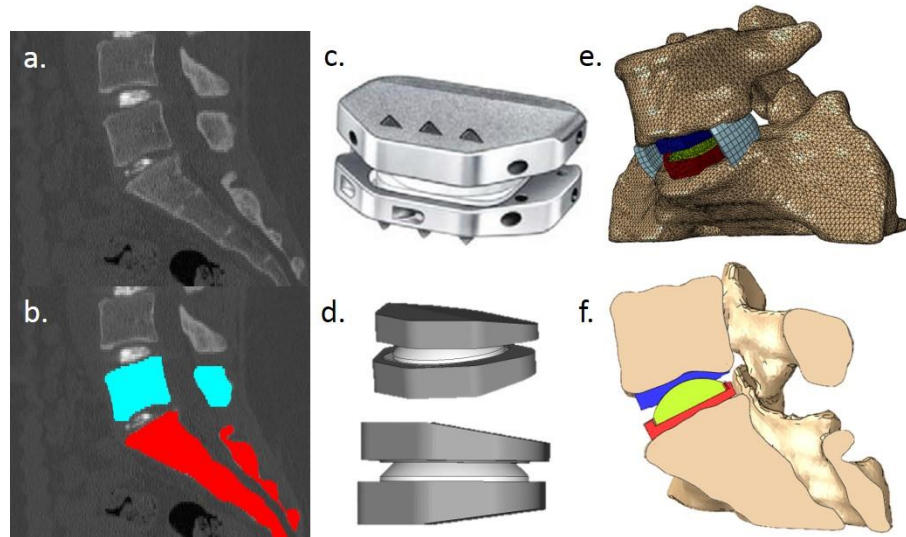
Figure 5.1 a) Acquired subject CT scans, b) segmentation of vertebral geometry, c) acquired Aesculap Activ-L, d) implant geometry developed from laser scan and public documentation, e) subject-specific finite element model, f) center inlay (yellow) free to translate in the anterior-posterior directions within the inferior end plate. (www.fda.gov)
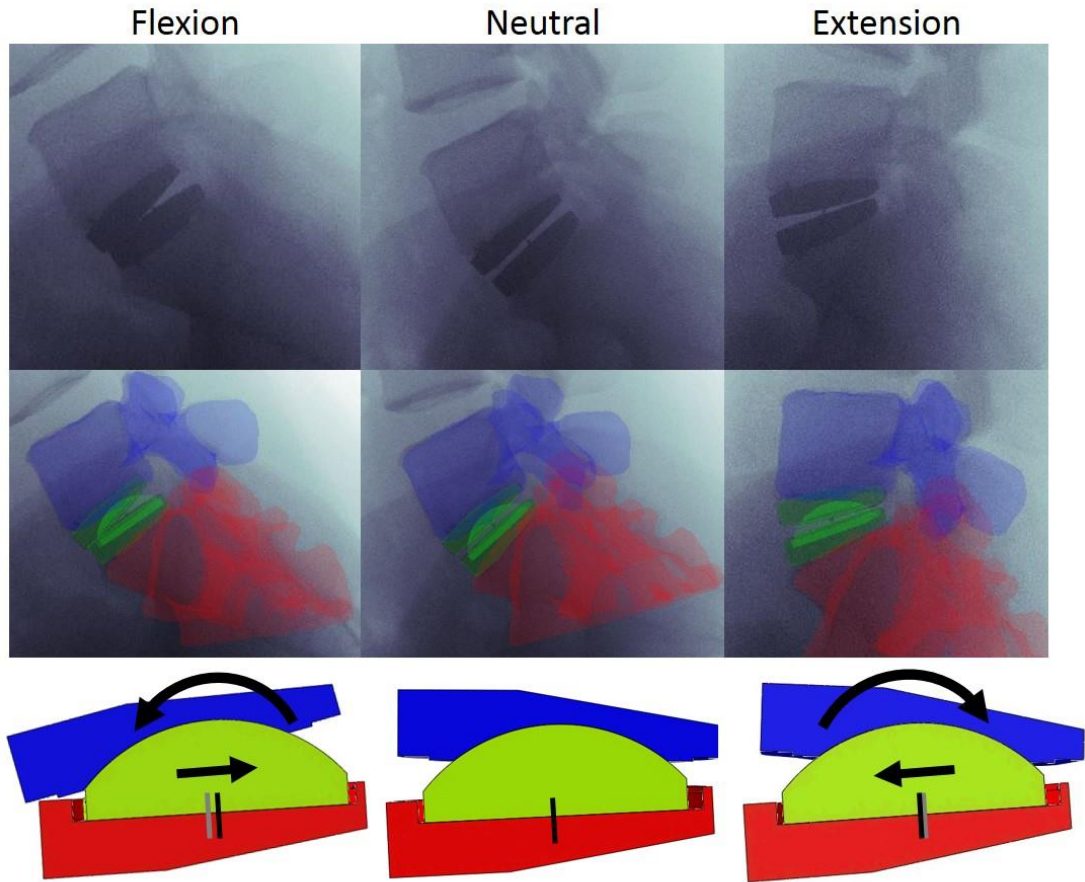
Figure 5.2 Three-dimensional model overlay with flexion-extension radiographs of Subject 2. Actual inlay translation measured from initial neutral position (gray) to final position (black). Extension and flexion ROM evaluated at actual inlay position during flexion and extension. Change in angle measured from resulting 3D model.
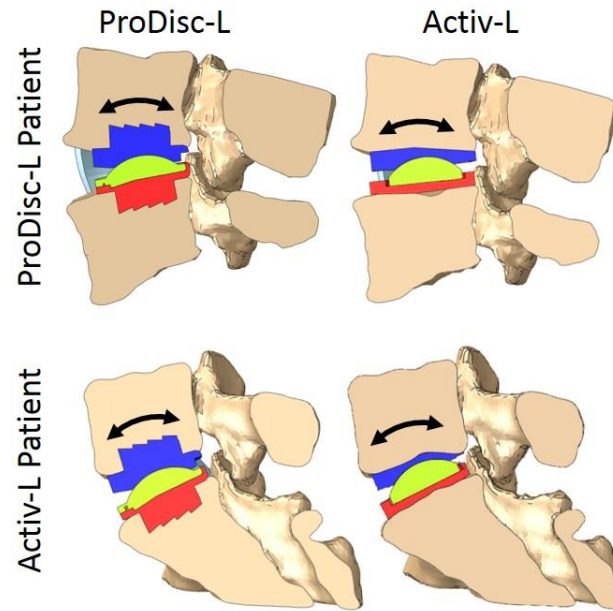
Figure 5.3 Post-operative ROM compared between implant with fixed COR and implant with variable COR. Patient actually implanted with ProDisc-L, was also virtually implanted with Activ-L implant (top). Five patients actually implanted with Activ-L, were also virtually implanted with ProDisc-L implant (bottom).
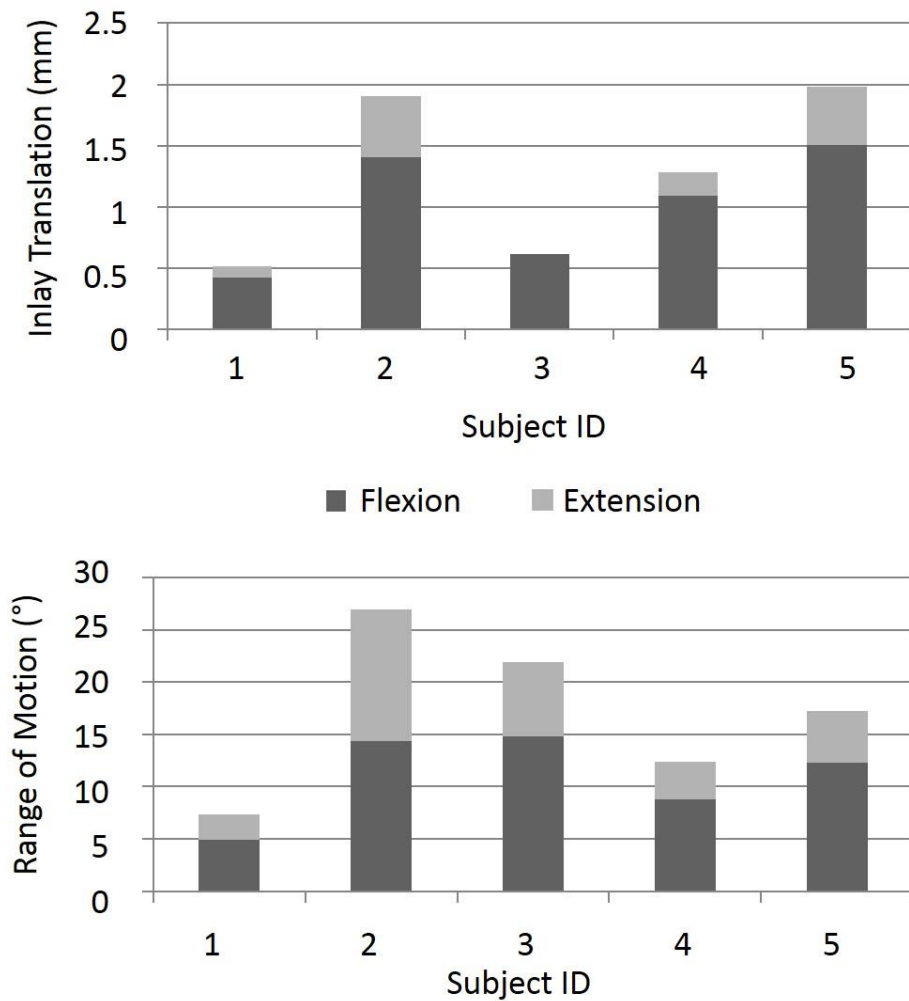
Figure 5.4 Implant behavior of the Activ-L cohort with an inlay that is free to translate in the anterior-posterior direction within the inferior end plate. Inlay translation (top) and resulting range of motion (bottom) was measured in flexion and extension for each subject. Implant impingement alone limited ROM in Subject 1, and bony impingement alone limited ROM in Subject 2. For all other subjects, a combination of implant and bony impingement limited ROM.
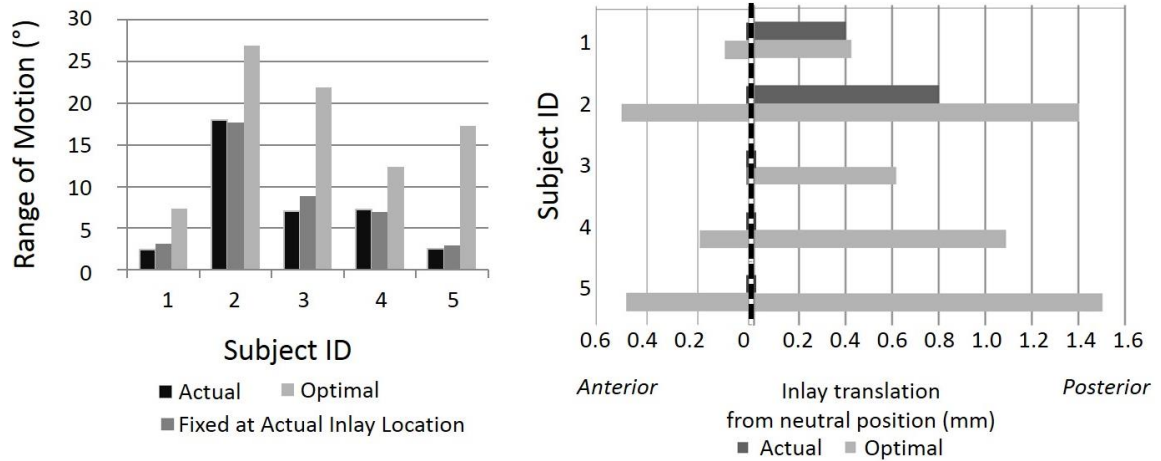
Figure 5.5 Comparisons of actual, total ROM at actual inlay locations, and ideal ROM values for patients implanted with the Activ-L total disc replacement (left). ROM predicted at actual inlay locations were less than 10% different to the actual ROM at that location. Ideal ROM averaged almost 10 degrees more than the actual ROM achieved (left). Comparisons were made of actual and optimal translations of the center inlay during flexion and extension motions. The inlays of two subjects translated to the posterior direction during flexion, and actual anterior translation during extension was not evident in any cases (right).
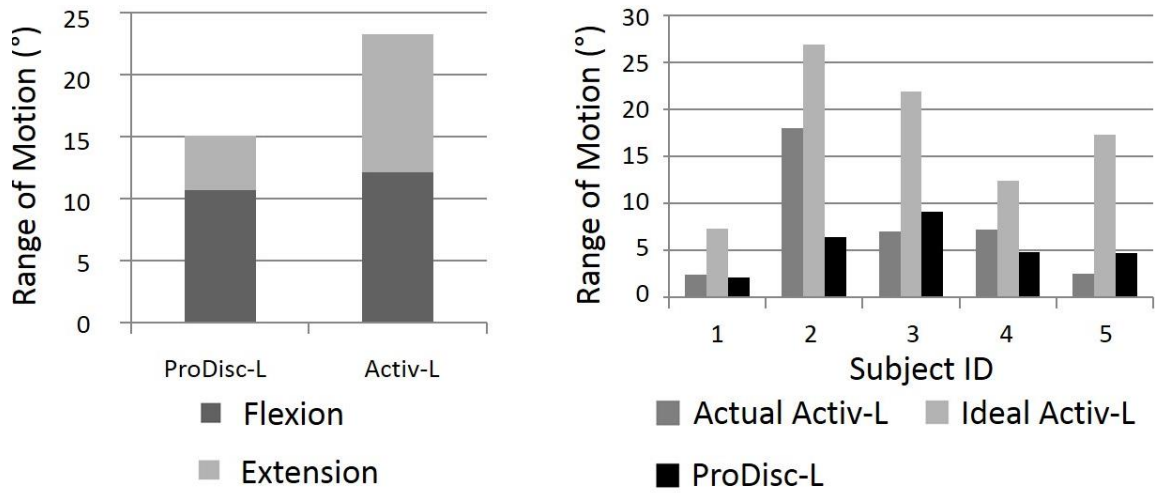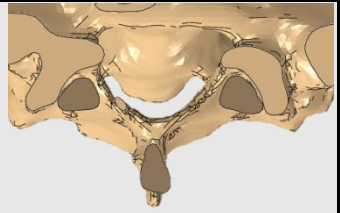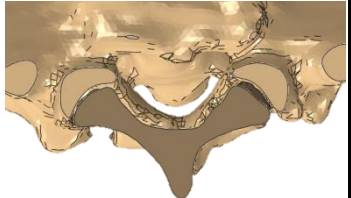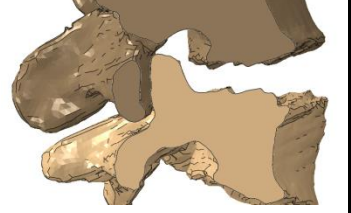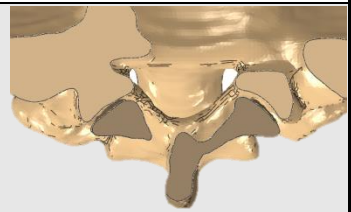
Figure 5.6 Comparisons of total ROM for the ProDisc-L and Activ-L when implanted in Subject 22 of study outlined in Chapter 4, a patient who had actually received the ProDisc-L device (left). Comparisons of total ROM for the ProDisc-L and Activ-L when implanted in five patients who had actually received the Activ-L device (right). ROM outcomes of the Activ-L was consistently greater than outcomes of the ProDisc-L.

Table 5.1 Patient data including operative level, actual implant size parameters, and key anatomical features of the facet joint.

Subject ID	Operative Level	Implant Size	Facet Joint Geometry	
1	L5-S1	Extra Large footprint Sup. Endplate: 6° Inf. Endplate: 5° Inlay Height: 8.5 mm	- Coronal Plane - Limited space around facets	
2	L5-S1	Small footprint Sup. Endplate: 6° Inf. Endplate: 5° Inlay Height: 8.5 mm	- Coronal Plane - Adequate space around facets	
3	L4-L5	Small footprint Sup. Endplate: 6° Inf. Endplate: 0° Inlay Height: 8.5 mm	- Sagittal Plane - Steep angle of articular processes	
4	L4-L5	Medium footprint Sup. Endplate: 6° Inf. Endplate: 0° Inlay Height: 8.5 mm	- Sagittal Plane - Steeper angle of articular processes	
5	L5-S1	Medium footprint Sup. Endplate: 11° Inf. Endplate: 0° Inlay Height: 8.5 mm	- Coronal Plane - Limited space around facets	

CHAPTER 6: CONCLUSION AND RECOMMENDATIONS

The aims of this thesis were to describe anatomic variability of the lumbar spine and to develop computational templating tools used to identify optimal device selection and placement in contemporary implants to maximize ROM and optimize patient outcome. A comprehensive set of statistical shape-alignment models were developed for the vertebrae of the entire lumbar spine, the bones of relevant functional spinal units, and each individual vertebra to quantify anatomical variation of the vertebrae of the lumbar spine. Explicit finite element methods were employed to predict flexion and extensions motions at the operative levels of patients implanted with the ProDisc-L TDR and identify optimal device placement to maximize patient ROM. Computational methods simulated mechanical behavior of a TDR with an inlay that is free to translate within the end plate, accurately predicted ROM at the actual location of the center inlays, and demonstrated superior ROM outcomes of the Activ-L to the ProDisc-L.

The collection of statistical models presented in Chapter 3 comprehensively characterized the shape and alignment of the lumbar spine by quantifying shape and size variation of single vertebra, relative alignment of relevant FSUs, and overall shape and alignment in the lumbar spine as a whole. Characterizations of shape and size variability of individual vertebra may guide TDR implant sizing lines to fit the population. Descriptions of variability relative vertebral alignment in an FSU can help screen patients for treatment options, assist in clinical diagnosis of pathologies, and improve pre-

111

operative planning for surgical treatment options including TDR. Quantification of overall shape variation in the entire lumbar spine can identify segments that are susceptible to degeneration and reveals how vertebral shape changes influence the spine as a whole. The study was limited by the size of the subject cohort, limitations in raw radiographic data, and the inclusion of males and females into the same population. Future work looks to increase the size of the training set to better represent the population, differentiate training set to study anatomic variability within gender, ethnicity, and pathological groups, improve models to investigate variation in bone mineral density and kinematics, and expand the capabilities of the SSMs to be used in computational evaluations

This investigation is limited in several ways. First, the sample size is limited to 22 subjects, which yields large variation in the results and may not reflect the anatomical variability of the population. To increase sample size of the study, double-level TDR surgeries were included and might have had an effect on the ROM results as ROM of the inferior implanted level after a double-level TDR surgery is known to be typically less than ROM of the superior level. Additionally, actual ROM as measured by both the overlay method and the method by Lim et al. (2006) was performed by a single observer, which generates additional uncertainty in the results of actual ROM. It is important to note that data acquisition is inherently limited by the accuracy of the data itself. Accuracy of the segmentation methods and techniques to measure actual ROM are dependent upon the resolution of the radiographs, which in this case are resolved to 0.31 mm pixel sizes and 1 mm slice thicknesses.

The efficacy of the proposed templating procedure presented in Chapter 4 was successfully demonstrated. Templated, model-based predictions of patient ROM were validated by comparison to actual ROM for 22 TDR surgeries implanted with the fixed-COR ProDisc-L implant. The overlay method used in this study to calculate actual ROM values was validated to a measurement system outlined by Lim et al. (2006). Post-operative computational evaluations of TDR surgeries can inform clinicians of expected ROM at patient follow-up and guide preparation for post-operative therapies. The three-dimensional templating procedure effectively optimized implant selection and placement to maximize ROM for a patient undergoing TDR surgery. If computational templating were included in pre-operative surgical planning used pre-operatively, this procedure may ensure maximum post-operative ROM and improve patient outcome. Additionally, results reported in the current study elucidated how key anatomical differences influenced ROM at the implanted level. With a deeper understanding of these relationships, TDR manufacturers can design devices that serve larger, more variable populations, and clinicians can more deliberately judge post-operative ROM based on patient anatomy. Limitations to the study include the size of the subject cohort, the inclusion of multi-level implantations, resolution of raw radiographic data, and single observer data acquisition. Recommendations for future work include expansion of the patient cohort and inclusion of multiple observers to improve confidence in preoperative templating, inclusion of post-operative evaluation of patients who have been pre-operatively templated to determine efficacy of the method, and improvements to the computational model.

Chapter 5 presented a characterization of the mechanical behavior of a TDR implant with a variable COR, or an inlay that is free to translate within the implant end plate. Patient geometry influenced unconstrained motion as facet impingement limited translation of the center inlay and the resulting ROM. Methods to predict ROM at the actual inlay locations were largely accurate and compared to ideal outcomes. Chapter 5 also revealed significant comparisons in post-operative ROM between two contemporary TDR designs: one with a fixed-COR and one with a variable COR. Post-operative computational evaluations of implant behavior can provide clinicians and implant manufactures valuable insight into ideal design features and surgical practices. Results of the analyses performed in this study, for instance, revealed actual translation of the inlay was not optimal, and that actual translation of the inlay during extension did not occur. Computational assessments of implant behavior validated to results from in vivo studies could prompt device manufactures to alter key design features and encourage clinicians to improve implantation methods. Comparisons between post-operative ranges of motions of different devices can reveal design considerations that significantly influence ROM and patient outcomes. For example, results reported in Chapter 5 revealed greater ROM outcomes are achieved for patients virtually implanted with a device with a variable COR than a device with a fixed COR. The study was limited by the size of the subject cohort, the resolution of raw radiographic data, and single observer data acquisition. While simplifications to the computational models may have reduced computational time, may have also limited accuracy of the results. Expansion of the patient cohort and inclusion of multiple observers can improve accuracy of the results.

114

Inclusion of nonzero friction factors, pressure-overclosure relationships, and nonlinear elements, such as ligament laxity and scar tissue, may allow the simulations to better mimic the motions of the Activ-L device.

By developing a suite of statistical and computational tools, population-based anatomical variation was characterized and improvements to the design and implantation methods of the TDR technology were identified. Quantification of anatomic variability can improve implant sizing lines and pre-operative planning, pre-operative templating can maximize post-operative ROM for a ProDisc-L TDR procedure, and computational models of TDR implants with a variable COR can identify design features that maximize ROM. Employing all three tools can improve long term patient outcomes after TDR surgery to serve a larger, variable population.

LIST OF REFERENCES

Agarwal, A., Zakeri, A., Agarwal, A.K., Jayaswal, A. and Goel, V.K., 2015. Distraction magnitude and frequency affects the outcome in juvenile idiopathic patients with growth rods: finite element study using a representative scoliotic spine model. *The Spine Journal*, 15(8), pp.1848-1855.

Albietz, J.S., RosasArellano, P., Fleming, J.C., Gurr, K.R., Bailey, S.I. and Bailey, C.S., 2012. An anatomic study of the interspinous space of the lumbosacral spine. *European Spine Journal*, 21(1), pp.145-148.

Andersson, G.B., 1999. Epidemiological features of chronic low-back pain. *The lancet*, 354(9178), pp.581-585.

Andersson, G.B.J., Örtengren, R. and Schultz, A., 1980. Analysis and measurement of the loads on the lumbar spine during work at a table.*Journal of Biomechanics*, *13*(6), pp.513-520.

Austen, S., Punt, I.M., Cleutjens, J.P., Willems, P.C., Kurtz, S.M., MacDonald, D.W., van Rhijn, L.W. and van Ooij, A., 2012. Clinical, radiological, histological and retrieval findings of Activ-L and Mobidisc total disc replacements: a study of two patients. European Spine Journal, 21(4), pp.513-520.

Battié, M.C., Videman, T., Gill, K., Moneta, G.B., Nyman, R., Kaprio, J. And Koskenvuo, M., 1991. 1991 Volvo Award in Clinical Sciences: Smoking and Lumbar Intervertebral Disc Degeneration: An MRI Study of Identical Twins. *Spine*, *16*(9), pp.1015-1021.

Battié, M.C., Videman, T., Levälahti, E., Gill, K. and Kaprio, J., 2008. Genetic and environmental effects on disc degeneration by phenotype and spinal level: a multivariate twin study. *Spine*, *33*(25), pp.2801-2808.

Belytschko, T., Kulak, R.F., Schultz, A.B. and Galante, J.O., 1974. Finite element stress analysis of an intervertebral disc. *Journal of Biomechanics*,*7*(3), pp.277-285.

Bendix, T., Kjaer, P. and Korsholm, L., 2008. Burned-out discs stop hurting: fact or fiction?. *Spine*, *33*(25), pp.E962-E967.

Besl, P.J. and McKay, N.D., 1992, April. Method for registration of 3-D shapes. In *Robotics-DL tentative* (pp. 586-606). International Society for Optics and Photonics.

Blumenthal, S., McAfee, P.C., Guyer, R.D., Hochschuler, S.H., Geisler, F.H., Holt, R.T., Garcia Jr, R., Regan, J.J. and Ohnmeiss, D.D., 2005. A prospective, randomized, multicenter food and drug administration investigational device exemptions study of lumbar total disc replacement with the CHARITE™ artificial disc versus lumbar fusion: part i: evaluation of clinical outcomes. *Spine*, *30*(14), pp.1565-1575.

Boisvert, J., Cheriet, F., Pennec, X., Labelle, H. and Ayache, N., 2008. Geometric variability of the scoliotic spine using statistics on articulated shape models. *Medical Imaging, IEEE Transactions on*, *27*(4), pp.557-568.

Boos, N., Rieder, R., Schade, V., Spratt, K.F., Semmer, N. and Aebi, M., 1995. 1995 Volvo Award in clinical sciences. The diagnostic accuracy of magnetic resonance imaging, work perception, and psychosocial factors in identifying symptomatic disc herniations. *Spine*, *20*(24), pp.2613-2625.

Bredbenner, T.L., Eliason, T.D., Francis, W.L., McFarland, J.M., Merkle, A.C. and Nicolella, D.P., 2014. Development and validation of a statistical shape modeling-based finite element model of the cervical spine under low-level multiple direction loading conditions. *Frontiers in bioengineering and biotechnology*, *2*.

Bressler, H.B., Keyes, W.J., Rochon, P.A. and Badley, E., 1999. The prevalence of low back pain in the elderly: a systematic review of the literature. *Spine*, *24*(17), p.1813.

Bryan, R., Mohan, P.S., Hopkins, A., Galloway, F., Taylor, M. and Nair, P.B., 2010. Statistical modelling of the whole human femur incorporating geometric and material properties. *Medical engineering & physics*, *32*(1), pp.57-65.

Campbell, J.Q. and Petrella, A.J., 2015. An Automated Method for Landmark Identification and Finite-Element Modeling of the Lumbar Spine. *Biomedical Engineering, IEEE Transactions on*, *62*(11), pp.2709-2716.

Carter, D. And Haynes, S.G., 1987. Prevalence rates for scoliosis in US adults: results from the first National Health and Nutrition Examination Survey. *International journal of epidemiology*, *16*(4), pp.537-544. Int. J. Epidemiol 1987; 16: 537–44.

Cattell, R.B., 1966. The scree test for the number of factors. *Multivariate behavioral research*, *1*(2), pp.245-276.

Cheh, G., Bridwell, K.H., Lenke, L.G., Buchowski, J.M., Daubs, M.D., Kim, Y. and Baldus, C., 2007. Adjacent segment disease followinglumbar/thoracolumbar fusion with pedicle screw instrumentation: a minimum 5-year follow-up. *Spine*, *32*(20), pp.2253-2257.

Cheung, K.M., Karppinen, J., Chan, D., Ho, D.W., Song, Y.Q., Sham, P., Cheah, K.S., Leong, J.C. and Luk, K.D., 2009. Prevalence and pattern of lumbar magnetic resonance imaging changes in a population study of one thousand forty-three individuals. *Spine*, *34*(9), pp.934-940.

Cho, K.J., Kim, Y.T., Shin, S.H. and Suk, S.I., 2014. Surgical treatment of adult degenerative scoliosis. *Asian spine journal*, *8*(3), pp.371-381.

Cootes, T.F., Taylor, C.J., Cooper, D.H. and Graham, J., 1995. Active shape models-their training and application. *Computer vision and image understanding*, *61*(1), pp.38-59.

Crostelli, M. and Mazza, O., 2013. AIS and spondylolisthesis. *European Spine Journal*, *22*(2), pp.172-184.

Daffner, S.D. and Vaccaro, A.R., 2003. Adult degenerative lumbar scoliosis.*American journal of orthopedics (Belle Mead, NJ)*, *32*(2), pp.77-82.

Dagenais, S., Caro, J. and Haldeman, S., 2008. A systematic review of low back pain cost of illness studies in the United States and internationally. *The spine journal*, *8*(1), pp.8-20.

Dai, Y., Scuderi, G.R., Bischoff, J.E., Bertin, K., Tarabichi, S. and Rajgopal, A., 2014. Anatomic tibial component design can increase tibial coverage and rotational alignment accuracy: a comparison of six contemporary designs.*Knee Surgery, Sports Traumatology, Arthroscopy*, *22*(12), pp.2911-2923.

David, T., 2007. Long-term results of one-level lumbar arthroplasty: minimum 10-year follow-up of the CHARITE artificial disc in 106 patients. *Spine*, *32*(6), pp.661-666.

de Bruijne, M., Lund, M.T., Tankó, L.B., Pettersen, P.C. and Nielsen, M., 2007. Quantitative vertebral morphometry using neighbor-conditional shape models. *Medical Image Analysis*, *11*(5), pp.503-512.

de Schepper, E.I., Damen, J., van Meurs, J.B., Ginai, A.Z., Popham, M., Hofman, A., Koes, B.W. and Bierma-Zeinstra, S.M., 2010. The association between lumbar disc degeneration and low back pain: the influence of age, gender, and individual radiographic features. *Spine*, *35*(5), pp.531-536.

118

Delamarter, R., Zigler, J.E., Balderston, R.A., Cammisa, F.P., Goldstein, J.A. and Spivak, J.M., 2011. Prospective, randomized, multicenter Food and Drug Administration investigational device exemption study of the ProDisc-L total disc replacement compared with circumferential arthrodesis for the treatment of two-level lumbar degenerative disc disease. *J Bone Joint Surg Am*, *93*(8), pp.705-715.

Denard, P.J., Holton, K.F., Miller, J., Fink, H.A., Kado, D.M., Marshall, L.M., Yoo, J.U. and Osteoporotic Fractures in Men (MrOS) Study Group, 2010. Back pain, neurogenic symptoms, and physical function in relation to spondylolisthesis among elderly men. *The Spine Journal*, *10*(10), pp.865-873.

Deyo, R.A., Mirza, S.K. and Martin, B.I., 2006. Back pain prevalence and visit rates: estimates from US national surveys, 2002. *Spine*, *31*(23), pp.2724-2727.

Deyo, R.A., 1986. Early diagnostic evaluation of low back pain. *Journal of General Internal Medicine*, *1*(5), pp.328-338.

Deyo, R.A., Gray, D.T., Kreuter, W., Mirza, S. and Martin, B.I., 2005. United States trends in lumbar fusion surgery for degenerative conditions. *Spine*,*30*(12), pp.1441-1445.

Deyo, R.A., Mirza, S.K., Turner, J.A. and Martin, B.I., 2009. Overtreating chronic back pain: time to back off?. *The Journal of the American Board of Family Medicine*, *22*(1), pp.62-68.

Deyo, R.A., Nachemson, A. and Mirza, S.K., 2004. Spinal-fusion surgery—the case for restraint. *The Spine Journal*, *4*(5), pp.S138-S142.

Di Angelo, L. and Di Stefano, P., 2015. A new method for the automatic identification of the dimensional features of vertebrae. *Computer methods and programs in biomedicine*, *121*(1), pp.36-48.

Dreischarf, M., Rohlmann, A., Zhu, R., Schmidt, H. and Zander, T., 2013. Is it possible to estimate the compressive force in the lumbar spine from intradiscal pressure measurements? A finite element evaluation. *Medical engineering & physics*, *35*(9), pp.1385-1390.

Dreischarf, M., Zander, T., Shirazi-Adl, A., Puttlitz, C.M., Adam, C.J., Chen, C.S., Goel, V.K., Kiapour, A., Kim, Y.H., Labus, K.M. and Little, J.P., 2014. Comparison of eight published static finite element models of the intact lumbar spine: Predictive power of models improves when combined together.*Journal of biomechanics*, *47*(8), pp.1757-1766.

119

Dreischarf, M., Schmidt, H., Putzier, M. and Zander, T., 2015. Biomechanics of the L5–S1 motion segment after total disc replacement–Influence of iatrogenic distraction, implant positioning and preoperative disc height on the range of motion and loading of facet joints. *Journal of biomechanics*, *48*(12), pp.3283-3291.

Dreischarf, T. Zander, A. Shirazi-Adl, C.M. Puttlitz, C.J. Adam, C.S. Chen, V.K. Goel, A. Kiapour, Y.H. Kim, K.M. Labus, J.P. Little, W.M. Park, Y.H. Wang, H.J. Wilke, A., Du, C.F., Yang, N., Guo, J.C., Huang, Y.P. and Zhang, C., 2016. Biomechanical response of lumbar facet joints under follower preload: a finite element study. *BMC Musculoskeletal Disorders*, *17*(1), p.1.

Erbulut, D.U., Zafarparandeh, I., Lazoglu, I. and Ozer, A.F., 2014. Application of an asymmetric finite element model of the C2-T1 cervical spine for evaluating the role of soft tissues in stability. *Medical engineering & physics*, *36*(7), pp.915-921.

Faizan, A., Goel, V.K., Biyani, A., Garfin, S.R. and Bono, C.M., 2012. Adjacent level effects of bi level disc replacement, bi level fusion and disc replacement plus fusion in cervical spine-a finite element based study.*Clinical biomechanics*, *27*(3), pp.226-233.

Fitzpatrick, C.K., Baldwin, M.A., Rullkoetter, P.J. and Laz, P.J., 2011. Combined probabilistic and principal component analysis approach for multivariate sensitivity evaluation and application to implanted patellofemoral mechanics. *Journal of biomechanics*, *44*(1), pp.13-21.

Fitzpatrick, C., FitzPatrick, D., Lee, J. and Auger, D., 2007. Statistical design of unicompartmental tibial implants and comparison with current devices. *The Knee*, *14*(2), pp.138-144.

Frymoyer, J.W., Hanley Jr, E.N., Howe, J., Kuhlmann, D. and Matteri, R.E., 1979. A comparison of radiographic findings in fusion and nonfusion patients ten or more years following lumbar disc surgery. *Spine*,*4*(5), pp.435-440.

Geisler, F.H., Guyer, R.D., Blumenthal, S.L., McAfee, P.C., Cappuccino, A., Bitan, F. and Regan, J.J., 2008. Patient selection for lumbar arthroplasty and arthrodesis: the effect of revision surgery in a controlled, multicenter, randomized study. *J Neurosurg Spine, 8,* pp. 13-16.

Glorfeld, L.W., 1995. An improvement on Horn's parallel analysis methodology for selecting the correct number of factors to retain.*Educational and psychological measurement*, *55*(3), pp.377-393.

Goel, V.K., Ebraheim, N.A., Biyani, A., Rengachary, S. and Faizan, A., 2005. Role of mechanical factors in the evaluation of pedicle screw type spinal fixation devices. *Neurology India*, *53*(4), p.399.

Gong, Z., Chen, Z., Feng, Z., Cao, Y., Jiang, C. and Jiang, X., 2014. Finite element analysis of 3 posterior fixation techniques in the lumbar spine.*Orthopedics*, *37*(5), pp.e441-e448.

Gornet, M.F., Burkus, J.K., Dryer, R.F. and Peloza, J.H., 2011. Lumbar disc arthroplasty with MAVERICK disc versus stand-alone interbody fusion: a prospective, randomized, controlled, multicenter investigational device exemption trial. *Spine*, *36*(25), pp.E1600-E1611.

Gray, H., 1918. *Anatomy of the human body*. Lea & Febiger.

Grip, H. and Häger, C., 2013. A new approach to measure functional stability of the knee based on changes in knee axis orientation. *Journal of biomechanics*, *46*(5), pp.855-862.

Gulek, B., Durgun, B., Alparslan, N., Erken, E., Ozer, H. and Sarpel, T., 2013. The linear and angular dimensions of the L4-L5 facet in healthy adults: Measurements on the axial and parasagittal-oblique mri planes. Global Advanced Research Journal of Medicine and Medical Sciences, 2(3), pp.067-074.

Guyer, R.D., McAfee, P.C., Banco, R.J., Bitan, F.D., Cappuccino, A., Geisler, F.H., Hochschuler, S.H., Holt, R.T., Jenis, L.G., Majd, M.E. and Regan, J.J., 2009. Prospective, randomized, multicenter Food and Drug Administration investigational device exemption study of lumbar total disc replacement with the CHARITE artificial disc versus lumbar fusion: five-year follow-up. *The Spine Journal*, *9*(5), pp.374-386.

Ha, K.Y., Lee, J.S. and Kim, K.W., 2008. Degeneration of sacroiliac joint after instrumented lumbar or lumbosacral fusion: a prospective cohort study over five-year follow-up. *Spine*, *33*(11), pp.1192-1198.

Ha, S.K., Kim, S.H., Kim, D.H., Park, J.Y., Lim, D.J. and Lee, S.K., 2009. Biomechanical study of lumbar spinal arthroplasty with a semi-constrained artificial disc (Activ L) in the human cadaveric spine. Journal of Korean Neurosurgical Society, 45(3), pp.169-175.

Harrop, J.S., Youssef, J.A., Maltenfort, M., Vorwald, P., Jabbour, P., Bono, C.M., Goldfarb, N., Vaccaro, A.R. and Hilibrand, A.S., 2008. Lumbar adjacent segment

degeneration and disease after arthrodesis and total disc arthroplasty. *Spine*, *33*(15), pp.1701-1707.

Hoogendoorn, R.J., Helder, M.N., Wuisman, P.I., Bank, R.A., Everts, V.E. and Smit, T.H., 2008. Adjacent segment degeneration: observations in a goat spinal fusion study. *Spine*, *33*(12), pp.1337-1343.

Horn, J.L., 1965. A rationale and test for the number of factors in factor analysis. *Psychometrika*, *30*(2), pp.179-185.

Huang, R.C., Tropiano, P., Marnay, T., Girardi, F.P., Lim, M.R. and Cammisa, F.P., 2006. Range of motion and adjacent level degeneration after lumbar total disc replacement. *The Spine Journal*, *6*(3), pp.242-247.

Huls K., Agarwala A., Rullkoetter P., Laz P., Petrella A., 2010 A Statistical Shape Model for Use in Probabilistic Modeling of the Lumbar Spine. *Trans. ORS*.

Ibarz, E., Herrera, A., Más, Y., Rodríguez-Vela, J., Cegoñino, J., Puértolas, S. and Gracia, L., 2012. Development and kinematic verification of a finite element model for the lumbar spine: application to disc degeneration.*BioMed research international*, *2013*.

Ishihara, H., Osada, R., Kanamori, M., Kawaguchi, Y., Ohmori, K., Kimura, T., Matsui, H. and Tsuji, H., 2001. Minimum 10-year follow-up study of anterior lumbar interbody fusion for isthmic spondylolisthesis. *Journal of Spinal Disorders & Techniques*, *14*(2), pp.91-99.

Jaramillo, H., Gomez, L.E.S.S.B.Y. and Garcia, J.J., 2015. A finite element model of the L4-L5-S1 human spine segment including the heterogeneity and anisotropy of the discs. *Acta of Bioengineering and Biomechanics*, *17*(2).

Jensen, M.C., Brant-Zawadzki, M.N., Obuchowski, N., Modic, M.T., Malkasian, D. and Ross, J.S., 1994. Magnetic resonance imaging of the lumbar spine in people without back pain. *New England Journal of Medicine*,*331*(2), pp.69-73.

Jentzsch, T., Geiger, J., Zimmermann, S.M., Slankamenac, K., Nguyen-Kim, T.D.L. and Werner, C.M., 2013. Lumbar facet joint arthritis is associated with more coronal orientation of the facet joints at the upper lumbar spine. *Radiology research and practice*, *2013*.

Kaiser, H. F., 1960. The application of electronic computers to factor analysis. *Educational and Psychological Measurement, 20*, pp. 141–151.

Kaito, T., Hosono, N., Mukai, Y., Makino, T., Fuji, T. and Yonenobu, K., 2010. Induction of early degeneration of the adjacent segment after posterior lumbar interbody fusion by excessive distraction of lumbar disc space: Clinical article. *Journal of Neurosurgery: Spine*, *12*(6), pp.671-679.

Kalichman, L., Kim, D.H., Li, L., Guermazi, A., Berkin, V. and Hunter, D.J., 2009. Spondylolysis and spondylolisthesis: prevalence and association with low back pain in the adult community-based population. *Spine*, *34*(2), p.199.

Kauppila, L.I., Eustace, S., Kiel, D.P., Felson, D.T. and Wright, A.M., 1998. Degenerative Displacement of Lumbar Vertebrae: A 25-year Follow-up Study in Framingham. *Spine*, *23*(17), pp.1868-1873.

Kettler, A., Marin, F., Sattelmayer, G., Mohr, M., Mannel, H., Dürselen, L., Claes, L. and Wilke, H.J., 2004. Finite helical axes of motion are a useful tool to describe the three-dimensional in vitro kinematics of the intact, injured and stabilised spine. *European Spine Journal*, *13*(6), pp.553-559.

Khallaghi, S., Mousavi, P., Gong, R.H., Gill, S., Boisvert, J., Fichtinger, G., Pichora, D., Borschneck, D. and Abolmaesumi, P., 2010. Registration of a statistical shape model of the lumbar spine to 3D ultrasound images. In*Medical Image Computing and Computer-Assisted Intervention–MICCAI 2010* (pp. 68-75). Springer Berlin Heidelberg.

Kim, K.T., Lee, S.H., Suk, K.S., Lee, J.H. and Jeong, B.O., 2010. Biomechanical changes of the lumbar segment after total disc replacement: Charite®, Prodisc® and Maverick® using finite element model study.*Journal of Korean Neurosurgical Society*, *47*(6), pp.446-453.

Kjaer, P., Leboeuf-Yde, C., Korsholm, L., Sorensen, J.S. and Bendix, T., 2005. Magnetic resonance imaging and low back pain in adults: a diagnostic imaging study of 40-year-old men and women. *Spine*, *30*(10), pp.1173-1180.

Kolta, S., Kerkeni, S., Travert, C., Skalli, W., Eastell, R., Glüer, C.C. and Roux, C., 2012. Variations in vertebral body dimensions in women measured by 3D-XA: a longitudinal in vivo study. *Bone*, *50*(3), pp.777-783.

Kumar, M.N., Jacquot, F. and Hall, H., 2001. Long-term follow-up of functional outcomes and radiographic changes at adjacent levels following lumbar spine fusion for degenerative disc disease. *European Spine Journal*,*10*(4), pp.309-313.

Kurtz, S.M., Lau, E., Ianuzzi, A., Schmier, J., Todd, L., Isaza, J. and Albert, T.J., 2010. National revision burden for lumbar total disc replacement in the United States: epidemiologic and economic perspectives. *Spine*, *35*(6), pp.690-696.

Lakshmanan, P., Purushothaman, B., Dvorak, V., Schratt, W., Thambiraj, S. and Boszczyk, B.M., 2012. Sagittal endplate morphology of the lower lumbar spine. *European Spine Journal*, *21*(2), pp.160-164.

Lee, C.S., Hwang, C.J., Lee, S.W., Ahn, Y.J., Kim, Y.T., Lee, D.H. and Lee, M.Y., 2009. Risk factors for adjacent segment disease after lumbar fusion.*European spine journal*, *18*(11), pp.1637-1643.

Lemaire, J.P., Carrier, H., Ali, E.H.S., Skalli, W. and Lavaste, F., 2005. Clinical and radiological outcomes with the CHARITÉ™ Artificial Disc: a 10-year minimum follow-up. *Journal of spinal disorders & techniques*, *18*(4), pp.353-359.

Lim, M.R., Loder, R.T., Huang, R.C., Lyman, S., Zhang, K., Sama, A., Papadopoulos, E.C., Warner, K., Girardi, F.P. and Cammisa Jr, F.P., 2006. Measurement error of lumbar total disc replacement range of motion. *Spine*,*31*(10), pp.E291-E297.

Liu, Z., Tsai, T.Y., Wang, S., Wu, M., Zhong, W., Li, J.S., Cha, T., Wood, K. and Li, G., 2015. Sagittal Plane Rotation Center of Lower Lumbar Spine during a Dynamic Weight-lifting Activity. *Journal of Biomechanics*.

Long, L.R. and Thoma, G.R., 2000, June. Segmentation and image navigation in digitized spine x rays. In *Medical Imaging 2000* (pp. 169-179). International Society for Optics and Photonics.

Lorenz, C. and Krahnstöver, N., 2000. Generation of point-based 3D statistical shape models for anatomical objects. *Computer vision and image understanding*, *77*(2), pp.175-191.

Martin, B.I., Deyo, R.A., Mirza, S.K., Turner, J.A., Comstock, B.A., Hollingworth, W. and Sullivan, S.D., 2008. Expenditures and health status among adults with back and neck problems. *Jama*, *299*(6), pp.656-664.

Martin, B.I., Mirza, S.K., Franklin, G.M., Lurie, J.D., MacKenzie, T.A. and Deyo, R.A., 2013. Hospital and surgeon variation in complications and repeat surgery following incident lumbar fusion for common degenerative diagnoses.*Health services research*, *48*(1), pp.1-25.

Martin, B.I., Turner, J.A., Mirza, S.K., Lee, M.J., Comstock, B.A. and Deyo, R.A., 2009. Trends in health care expenditures, utilization, and health status among US adults with spine problems, 1997–2006. *Spine*, *34*(19), pp.2077-2084.

Masharawi, Y., Rothschild, B., Dar, G., Peleg, S., Robinson, D., Been, E. and

Hershkovitz, I., 2004. Facet orientation in the thoracolumbar spine: three-dimensional anatomic and biomechanical analysis. *Spine*, *29*(16), pp.1755-1763.

Masharawi, Y.M., Alperovitch-Najenson, D., Steinberg, N., Dar, G., Peleg, S., Rothschild, B., Salame, K. and Hershkovitz, I., 2007. Lumbar facet orientation in spondylolysis: a skeletal study. Spine, 32(6), pp.E176-E180.

Masharawi, Y., Salame, K., Mirovsky, Y., Peleg, S., Dar, G., Steinberg, N. and Hershkovitz, I., 2008. Vertebral body shape variation in the thoracic and lumbar spine: characterization of its asymmetry and wedging. *Clinical Anatomy*, *21*(1), pp.46-54.

Masharawi, Y. and Salame, K., 2011. Shape variation of the neural arch in the thoracic and lumbar spine: characterization and relationship with the vertebral body shape. *Clinical Anatomy*, *24*(7), pp.858-867.

Masharawi, Y., 2012. Lumbar shape characterization of the neural arch and vertebral body in spondylolysis: a comparative skeletal study. Clinical Anatomy, 25(2), pp.224-230.

McAfee, P.C., Cunningham, B., Holsapple, G., Adams, K., Blumenthal, S., Guyer, R.D., Dmietriev, A., Maxwell, J.H., Regan, J.J. and Isaza, J., 2005. A prospective, Randomized, Multicenter Food and Drug Administration Investigational Device Exemption Study of Lumbar Total Disc Replacement With the CHARITÉ™ Artificial Disc Versus Lumbar Fusion: Part II: Evaluation of Radiographic Outcomes and Correlation of Surgical Technique Accuracy With Clinical Outcomes. *Spine*, *30*(14), pp.1576-1583.

McClintic, J.R., 1978. *Physiology of the human body*. John Wiley & Sons.

Meakin, J.R., Fulford, J., Seymour, R., Welsman, J.R. and Knapp, K.M., 2013. The relationship between sagittal curvature and extensor muscle volume in the lumbar spine. *Journal of anatomy*, *222*(6), pp.608-614.

Meakin, J.R., Gregory, J.S., Aspden, R.M., Smith, F.W. and Gilbert, F.J., 2009. The intrinsic shape of the human lumbar spine in the supine, standing and sitting postures: characterization using an active shape model. *Journal of anatomy*, *215*(2), pp.206-211.

Meller, S. and Kalender, W.A., 2004, June. Building a statistical shape model of the pelvis. In *International Congress Series* (Vol. 1268, pp. 561-566). Elsevier.

Mengoni, M., Vasiljeva, K., Jones, A.C., Tarsuslugil, S.M. and Wilcox, R.K., 2015. Subject-specific multi-validation of a finite element model of ovine cervical functional spinal units. *Journal of biomechanics*, *49*, 259-266

Miller, J.A.A., Schmatz, C. and Schultz, A.B., 1988. Lumbar disc degeneration: correlation with age, sex, and spine level in 600 autopsy specimens. *Spine*, *13*(2), pp.173-178.

Mirza, S.K. and Deyo, R.A., 2007. Systematic review of randomized trials comparing lumbar fusion surgery to nonoperative care for treatment of chronic back pain. *Spine*, *32*(7), pp.816-823.

Myronenko, A. and Song, X., 2010. Point set registration: Coherent point drift. *Pattern Analysis and Machine Intelligence, IEEE Transactions on*,*32*(12), pp.2262-2275.

National Health Service (NHS): Prosthetic Intervertebral Disc Replacement in the Lumbar Spine: Interventional Procedure Guidance (vol 306). London, UK, National Institute for Health and Clinical Excellence (NICE), July 2009

Palepu, V., Kodigudla, M. and Goel, V.K., 2012. Biomechanics of disc degeneration. *Advances in orthopedics*, *2012*.

Panagiotopoulou, O., 2009. Finite element analysis (FEA): applying an engineering method to functional morphology in anthropology and human biology. *Annals of human biology*, *36*(5), pp.609-623.

Park, P., Garton, H.J., Gala, V.C., Hoff, J.T. and McGillicuddy, J.E., 2004. Adjacent segment disease after lumbar or lumbosacral fusion: review of the literature. *Spine*, *29*(17), pp.1938-1944.

Peloquin, J.M., Yoder, J.H., Jacobs, N.T., Moon, S.M., Wright, A.C., Vresilovic, E.J. and Elliott, D.M., 2014. Human L3L4 intervertebral disc mean 3D shape, modes of variation, and their relationship to degeneration.*Journal of biomechanics*, *47*(10), pp.2452-2459.

Pfeiffer, F.M., Choma, T.J. and Kueny, R., 2015. Finite element analysis of Stryker Xia pedicle screw in artificial bone samples with and without supplemental cement augmentation. *Computer methods in biomechanics and biomedical engineering*, *18*(13), pp.1459-1467.

Quirno, M., Goldstein, J.A., Bendo, J.A., Kim, Y. and Spivak, J.M., 2011. The incidence of potential candidates for total disc replacement among lumbar and cervical fusion patient populations. *Asian spine journal*, *5*(4), pp.213-219.

Rainey, S., Blumenthal, S.L., Guyer, R.D., Zigler, J.E. and Ohnmeiss, D.D., 2010. Analysis of Adjacent Segment Re-Operation Following Lumbar Total Disc Replacement. *The Spine Journal*, *10*(9), p.S66.

Rao, C., Fitzpatrick, C.K., Rullkoetter, P.J., Maletsky, L.P., Kim, R.H. and Laz, P.J., 2013. A statistical finite element model of the knee accounting for shape and alignment variability. *Medical engineering & physics*, *35*(10), pp.1450-1456.

Rohlmann, A., Lauterborn, S., Dreischarf, M., Schmidt, H., Putzier, M., Strube, P. and Zander, T., 2013. Parameters influencing the outcome after total disc replacement at the lumbosacral junction. Part 1: misalignment of the vertebrae adjacent to a total disc replacement affects the facet joint and facet capsule forces in a probabilistic finite element analysis. *European Spine Journal*, *22*(10), pp.2271-2278.

Rohlmann, A., Mann, A., Zander, T. and Bergmann, G., 2009. Effect of an artificial disc on lumbar spine biomechanics: a probabilistic finite element study. *European Spine Journal*, *18*(1), pp.89-97.

Rohlmann, A., Zander, T., Schmidt, H., Wilke, H.J. and Bergmann, G., 2006. Analysis of the influence of disc degeneration on the mechanical behaviour of a lumbar motion segment using the finite element method. *Journal of biomechanics*, *39*(13), pp.2484-2490.

Ruberté, L.M., Natarajan, R.N. and Andersson, G.B., 2009. Influence of single-level lumbar degenerative disc disease on the behavior of the adjacent segments—a finite element model study. *Journal of biomechanics*, *42*(3), pp.341-348.

Rundell, S.A., Day, J.S., Isaza, J., Guillory, S. and Kurtz, S.M., 2012. Lumbar total disc replacement impingement sensitivity to disc height distraction, spinal sagittal orientation, implant position, and implant lordosis.*Spine*, *37*(10), pp.E590-E598.

Ryu, R., Techy, F., Varadarajan, R. and Amirouche, F., 2016. Effect of Interbody Fusion on the Remaining Discs of the Lumbar Spine in Subjects with Disc Degeneration. *Orthopaedic Surgery*, *8*(1), pp.27-33.

Sarkalkan, N., Weinans, H. and Zadpoor, A.A., 2014. Statistical shape and appearance models of bones. *Bone*, *60*, pp.129-140.

Schmidt, H., Heuer, F. and Wilke, H.J., 2008. Interaction between finite helical axes and facet joint forces under combined loading. *Spine*, *33*(25), pp.2741-2748.

Andersson, G.B. and Schultz, A.B., 1979. Effects of fluid injection on mechanical properties of intervertebral discs. *Journal of biomechanics*, *12*(6), pp.453-458.

Siepe, C.J., Heider, F., Haas, E., Hitzl, W., Szeimies, U., Stäbler, A., Weiler, C., Nerlich, A.G. and Mayer, M.H., 2012. Influence of lumbar intervertebral disc degeneration on the outcome of total lumbar disc replacement: a prospective clinical, histological, X-ray and MRI investigation. *European Spine Journal*, *21*(11), pp.2287-2299.

Siepe, C.J., Heider, F., Wiechert, K., Hitzl, W., Ishak, B. and Mayer, M.H., 2014. Mid-to long-term results of total lumbar disc replacement: a prospective analysis with 5-to 10-year follow-up. *The Spine Journal*, *14*(8), pp.1417-1431.

Siepe, C.J., Hitzl, W., Meschede, P., Sharma, A.K., Khattab, M.F. and Mayer, M.H., 2009. Interdependence between disc space height, range of motion and clinical outcome in total lumbar disc replacement. *Spine*, *34*(9), pp.904-916.

Sköld, C., Tropp, H. and Berg, S., 2013. Five-year follow-up of total disc replacement compared to fusion: a randomized controlled trial. *European spine journal*, *22*(10), pp.2288-2295.

Smith, M., Davis, M.A., Stano, M. and Whedon, J.M., 2013. Aging baby boomers and the rising cost of chronic back pain: secular trend analysis of longitudinal Medical Expenditures Panel Survey data for years 2000 to 2007.*Journal of manipulative and physiological therapeutics*, *36*(1), pp.2-11.

Smoger, L.M., Fitzpatrick, C.K., Clary, C.W., Cyr, A.J., Maletsky, L.P., Rullkoetter, P.J. and Laz, P.J., 2015. Statistical modeling to characterize relationships between knee anatomy and kinematics. *Journal of Orthopaedic Research*, *33*(11), pp.1620-1630.

Steurer, J., Roner, S., Gnannt, R. and Hodler, J., 2011. Quantitative radiologic criteria for the diagnosis of lumbar spinal stenosis: a systematic literature review. *BMC musculoskeletal disorders*, *12*(1), p.1.

Strube, P., Hoff, E.K., Schmidt, H., Dreischarf, M., Rohlmann, A. and Putzier, M., 2013. Parameters influencing the outcome after total disc replacement at the lumbosacral junction. Part 2: distraction and posterior translation lead to clinical failure after a mean follow-up of 5 years. *European Spine Journal*, *22*(10), pp.2279-2287.

Tan, S.H., Teo, E.C. and Chua, H.C., 2004. Quantitative three-dimensional anatomy of cervical, thoracic and lumbar vertebrae of Chinese Singaporeans. *European Spine Journal*, *13*(2), pp.137-146.

Toosizadeh, N. and Haghpanahi, M., 2011. Generating a finite element model of the

cervical spine: Estimating muscle forces and internal loads. *Scientia Iranica*, *18*(6), pp.1237-1245.

Tropiano, P., Huang, R.C., Girardi, F.P., Cammisa, F.P. and Marnay, T., 2005. Lumbar total disc replacement. *J Bone Joint Surg Am*, *87*(3), pp.490-496.

Tsouknidas, A., Michailidis, N., Savvakis, S., Anagnostidis, K., Bouzakis, K.D. and Kapetanos, G., 2012. A finite element model technique to determine the mechanical response of a lumbar spine segment under complex loads. *J Appl Biomech*, *28*(4), pp.448-456.

UnitedHealthcare, 2012. Medical Policy of the Total Artificial Disc Replacement for the Spine. United HealthCare Services.

van den Bogert, A.J., Reinschmidt, C. and Lundberg, A., 2008. Helical axes of skeletal knee joint motion during running. *Journal of Biomechanics*, *41*(8), pp.1632-1638.

Velicer, W.F., 1976. Determining the number of components from the matrix of partial correlations. *Psychometrika*, *41*(3), pp.321-327.

Videbaek, T.S., Egund, N., Christensen, F.B., Jurik, A.G. and Bünger, C.E., 2010. Adjacent segment degeneration after lumbar spinal fusion: the impact of anterior column support: a randomized clinical trial with an eight-to thirteen-year magnetic resonance imaging follow-up. *Spine*, *35*(22), pp.1955-1964.

Videman, T., Battié, M.C., Gibbons, L.E., Maravilla, K., Manninen, H. and Kaprio, J., 2003. Associations between back pain history and lumbar MRI findings. *Spine*, *28*(6), pp.582-588.

Videman, T., Sarna, S., Battié, M.C., Koskinen, S., Gill, K., Paananen, H. and Gibbons, L., 1995. The long-term effects of physical loading and exercise lifestyles on back-related symptoms, disability, and spinal pathology among men. *Spine*, *20*(6), pp.699-709.

Wagner, D., Kamer, L., Rommens, P.M., Sawaguchi, T., Richards, R.G. and Noser, H., 2014. 3D statistical modeling techniques to investigate the anatomy of the sacrum, its bone mass distribution, and the trans-sacral corridors. *Journal of Orthopaedic Research*, *32*(11), pp.1543-1548.

Wang, W., Zhang, H., Sadeghipour, K. and Baran, G., 2013. Effect of posterolateral disc replacement on kinematics and stress distribution in the lumbar spine: A finite element study. *Medical engineering & physics*, *35*(3), pp.357-364.

Wang, Y., Battié, M.C. and Videman, T., 2012. A morphological study of lumbar vertebral endplates: radiographic, visual and digital measurements.*European Spine Journal*, *21*(11), pp.2316-2323.

Wang, Y., Wang, L., Du, C., Mo, Z. and Fan, Y., 2015. A comparative study on dynamic stiffness in typical finite element model and multi-body model of C6–C7 cervical spine segment. *International journal for numerical methods in biomedical engineering*.

Weinhoffer, S.L., Guyer, R.D., Herbert, M. and Griffith, S.L., 1995. Intradiscal Pressure Measurements Above an Instrumented Fusion: A Cadaveric Study.*Spine*, *20*(5), pp.526-531.

Willner, S. and Udén, A., 1982. A prospective prevalence study of scoliosis in Southern Sweden. *Acta Orthopaedica Scandinavica*, *53*(2), pp.233-237.

Wolf, A., Shoham, M., Michael, S. and Moshe, R., 2001. Morphometric Study of the Human Lumbar Spine for Operation–Workspace Specifications. Spine, 26(22), pp.2472-2477.
Vancouver

Womack, W., Leahy, P.D., Patel, V.V. and Puttlitz, C.M., 2011. Finite element modeling of kinematic and load transmission alterations due to cervical intervertebral disc replacement. *Spine*, *36*(17), pp.E1126-E1133.

Wu, G., Siegler, S., Allard, P., Kirtley, C., Leardini, A., Rosenbaum, D., Whittle, M., D D'Lima, D., Cristofolini, L., Witte, H. and Schmid, O., 2002. ISB recommendation on definitions of joint coordinate system of various joints for the reporting of human joint motion—part I: ankle, hip, and spine.*Journal of biomechanics*, *35*(4), pp.543-548.

Wu, Y., Wang, Y., Wu, J., Guan, J., Mao, N., Lu, C., Lv, R., Ding, M., Shi, Z. and Cai, B., 2015. Study of Double-level Degeneration of Lower Lumbar Spines by Finite Element Model. *World Neurosurgery*.

Yu, L.P., Qian, W.W., Yin, G.Y., Ren, Y.X. and Hu, Z.Y., 2012. MRI assessment of lumbar intervertebral disc degeneration with lumbar degenerative disease using the Pfirrmann grading systems. *PloS one*, *7*(12), p.e48074.

Yue, J.J. and Mo, F.F., 2010. Clinical study to evaluate the safety and effectiveness of the Aesculap Activ-L™ artificial disc in the treatment of degenerative disc disease. *BMC surgery*, *10*(1), p.1.

Zander, T., Rohlmann, A. and Bergmann, G., 2009. Influence of different artificial

disc kinematics on spine biomechanics. Clinical biomechanics, 24(2), pp.135-142.

Zeilstra, D.J., Miller, L.E. and Block, J.E., 2013. Axial lumbar interbody fusion: a 6-year single-center experience. *Clinical interventions in aging*, *8*, p.1063.

Zheng, J., Yang, Y., Lou, S., Zhang, D. and Liao, S., 2015. Construction and validation of a three-dimensional finite element model of degenerative scoliosis. *Journal of orthopaedic surgery and research*, *10*(1), p.1.

Zigler, J.E., Glenn, J. and Delamarter, R.B., 2012. Five-year adjacent-level degenerative changes in patients with single-level disease treated using lumbar total disc replacement with ProDisc-L versus circumferential fusion: Clinical article. *Journal of Neurosurgery: Spine*, *17*(6), pp.504-511.

APPENDICES

Appendix A: Associated Publications

Hollenbeck J.F.M., Cain, C.M., Fattor J., Patel, V., Burger, E., Rullkoetter, P.J., 2016. "Pre-operative Templating for TDR Predicts Post-Operative ROM and Could Improve Clinical Outcomes," *Orthopaedic Research Society Meeting*, Orlando, FL.

Cain, C.M., Hollenbeck J.F.M., Fattor J.A., Patel, V., Burger, E., Laz, P.J., Rullkoetter, P.J., 2016. "Patient-specific templating for ADR identifies factors that influence clinical outcomes," *International Society for the Advancement of Spinal Mechanics,* San Diego, CA.

Hollenbeck, J.F.M., Cain, C.M., Fattor J.A., Fitzpatrick C.K., Rullkoetter P.J., Laz, P.J., 2015. "Variation in Lumbar Anatomy for Healthy and Disc Degenerated Populations," *Orthopaedic Research Society Meeting,* Las Vegas, NV.

Hollenbeck, J.F.M., Cain, C, Fattor, J, Fitzpatrick, C.K, Rullkoetter, P.J, Laz, P.J., 2014, "Statistical Shape and Alignment Modeling to Characterize Disc Degeneration in the Lumbar Spine," *7th World Congress of Biomechanics 2014*, Boston, MA.

Hollenbeck, J.F.M., Rullkoetter, P.J., Fitzpatrick, C.K., Cain, C., Laz, P.J., 2014. "Statistical shape and alignment modeling of the lumbar spine," *ASME Summer Bioengineering Conference*, Sunriver, OR.

Hollenbeck, J.F.M., Laz, P.J., Cain, C.M., Fitzpatrick, C.K., Rullkoetter, P.J., 2013. "Statistical shape and alignment modeling of the lumbar spine," *Rocky Mountain American Society of Biomechanics Regional Meeting*, Estes Park, CO.